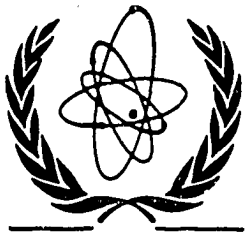

International Atomic Energy Agency

INDC(NDS)-355
Distr. R+G

INDC INTERNATIONAL NUCLEAR DATA COMMITTEE

International Benchmark Calculations of Radioactive Inventory for Fission Reactor Decommissioning

Edited by

N.P. Kocherov
IAEA Nuclear Data Section

April 1996

IAEA NUCLEAR DATA SECTION, WAGRAMERSTRASSE 5, A-1400 VIENNA

Printed by the IAEA in Austria
April 1996

INDC(NDS)-355
Distr. R+G

International Benchmark Calculations of Radioactive Inventory for Fission Reactor Decommissioning

Edited by

N.P. Kocherov
IAEA Nuclear Data Section

April 1996

Contents

Foreword 7

1. Decommissioning Calculations for IAEA Benchmark (JPDR), Phase 2
S.J. Wall, N.J. France, M.H. Dean 9

2. Results for Revised Biological Shield Configuration
B.L. Broadhead, R.L. Childs 47

3. UMass-Lowell Results of the IAEA Bechmark Calculation of Radioactive Inventory for Fission Reactor Decommissioning
John R. White, Andrew P. Fyfe 53

4. The Code System COROUT: Radioactive Inventory Calculations for Decommissioning Studies
A.A. Rimski-Korsakov, A.S. Roschin, S.G. Yavshits 89

Foreword

The worldwide statistics in the IAEA Nuclear Power and Research Reactors databases indicate that there is a large number of commercial and research reactors nearing the end of their service life and a significant number of them were already shutdown. Of the total 420 nuclear power reactors operating in the world, 28% have been supplying commercial power for 20 years and more and 51% for 15 years and more. As of April 1994 there were 68 nuclear power reactors in shutdown status worldwide. Only in the period from 1990 to 1995 42 research reactors were shutdown in the IAEA Member States. These statistics of ageing and shutdown commercial and research reactors indicate that decommissioning methodologies need to be developed and applied in the near future.

The IAEA considers this problem as being of high priority and is pursuing a number of projects in this field. The IAEA Advisory Group Meeting on Nuclear Data Requirements for Fission Reactor Decommissioning in 1992, in Vienna, was one of them. The meeting participants have discussed the problem of radioactive inventory evaluation for power and research reactor decommissioning and recommended to test the methods and nuclear databases used for that purpose by running an international intercomparison of calculations for a real decommissioning project comparing calculated results with the measured values. Following these recommendations the Nuclear Data Section has requested the measured activation data for the decommissioned JPDR reactor from the Japan Atomic Energy Research Institute (JAERI). Drs. K. Fujiki, N. Sasamoto and T. Sukegawa have kindly collected the necessary data and it was published as an IAEA report, INDC(JPN)-164, 1993. This report contained numerical data on geometry, composition of materials, reactor campaign, neutron flux in the core and the measured activation values for a number of nuclides in the pressure vessel and the biological shield. The data included measurements of ^{60}Co, ^{134}Cs, ^{152}Eu and ^{154}Eu in the bioshield and of ^{60}Co, ^{54}Mn, ^{55}Fe and ^{63}Ni in the reactor vessel.

The following laboratories have taken part in the intercomparison:

* AEA Technology, Technical Services Division, UK
* Oak Ridge National Laboratory, Reactor and Fuel Cycle Analyses, USA
* University of Massachusetts-Lowell, Chemical and Nuclear Engineering Dept., USA
* V.G. Khlopin Radium Institute, St. Petersburg, Russia

The first results of this exercise were discussed at the Consultants' Meeting in December 1994 at the IAEA Headquarters in Vienna. It was found that the agreement between calculated and measured JPDR values was quite satisfactory for the reactor core and the pressure vessel but the calculations for the bioshield overpredicted the measured values by a factor of 5 to 10.

It was decided to take into account the configuration of the re-bar structure in the bioshield more accurately and to run the exercise for the second time. This document summarizes the results of the second phase of the Intercomparison Benchmark Calculations of Radioactive Inventory for Fission Reactor Decommissioning.

N.P. Kocherov

AEA-TSD-0650
NCS/R(94)49

Decommissioning Calculations for IAEA Benchmark (JPDR)

Phase 2

S. J. Wall, N. J. France, M.H. Dean
AEA Technology
Technical Services Division

Summary

A Benchmark Inter-comparison Exercise on Radioactive Inventory Calculations for Fission Reactor Decommissioning was set up on the recommendation of the IAEA Advisory Group Meeting on Nuclear Data Requirements for Fission Reactor Decommissioning. The aim of the project is to derive likely calculational uncertainties in such calculations, and also to validate different methods against both measurement and each other.

A previous paper described benchmark calculations performed in the United Kingdom, using the codes ANISN, MCBEND and DORT. The data for this benchmark was derived from the actual project to decommission the Japanese reactor JPDR. ANISN, MCBEND and DORT results compared well with each other and agreement in the shroud and reactor vessel was good compared to experiment. However, calculated activities were found to be up to a factor of 5 to 10 times higher in the bio-shield, although this was in line with calculations carried out elsewhere. This paper investigates the origins of this discrepancy, within the limitations of data available.

The main sources of uncertainty are identified, and recommendations made for future work.

1.0 Introduction

The first phase of the benchmark Inter-comparison Exercise on Radioactive Inventory Calculations was set up on the recommendation of the IAEA Advisory Group Meeting on Nuclear Data Requirements for Fission Reactor Decommissioning (Ref 1). An earlier paper discussing the results of the first phase (Ref 2) describes one-dimensional calculations performed in the United Kingdom using the ANISN code, the two dimensional calculations for the region around the core using MCBEND and the full two dimensional analysis using DORT. The data for the benchmark was derived from the actual project to decommission the Japanese reactor JPDR (Ref 3). These calculations were all based on the same 'benchmark' data so that the different methods could be compared.

Comparisons between the various codes and the experimental data were good, except for deep penetrations into the bioshield. The present work, specified in Refs 4 and 5, attempts to identify where this discrepancy may derive from.

2.0 Method

In this study MCBEND (Ref 6) was used to determine all neutron fluxes. Activations were required for various radial scans in the bioshield. These were calculated by the FLUX4 code (Ref 7), which was modified both to accept MCBEND data, and also to accept input of stepped irradiation histories.

2.1 MCBEND

MCBEND is a Monte Carlo code using point energy data sets (8000 groups). Because of this, acceleration techniques are required whereby a neutron which crosses from a region of low importance to one of higher importance is preferentially tracked to one going in the other direction. This means that for large models, separate cases must be run for each region of interest. The method used to accelerate the calculations was the MAGIC module (within MCBEND) which runs an adjoint diffusion calculation and then uses this to generate an importance map for the Monte Carlo calculation.

The 8000 group neutron cross-section data set was derived from UKNDL (Ref 8), although results may be output in any group scheme required. Activation cross-sections were also available within the code, so as to make full use of the flux data available. These are derived from various sources, IRDF-85 (Ref 9) for $^{59}Co(n,\gamma)$, and $^{54}Fe(n,\gamma)$, and JEF-1 (Ref 10) for the remaining reactions of interest in this study.

More recent JEF-2 data cross-section was also used, together with IRDF-90 response data for the Co59(n,γ) reaction.

2.2 ACTIVATION CALCULATIONS

FLUX4 is based on the standard textbook equation (see Ref 11, for example) below. Cross-section data is largely taken from Ref 12 and is the 22-group CASK (Ref 13) scheme.

$$Activity = \frac{\lambda\phi\sigma(N_p)_0}{\lambda-\phi\sigma}(e^{-\phi\sigma T_I}-e^{-\lambda T_I})e^{-\lambda T_C}$$

No allowance is made for burn-up of the daughter during irradiation, or for the effect of burnup of the parent due to alternative irradiation processes. The calculation may incorporate the stepped power history of the reactor. The amount of daughter and parent is calculated for each of the decay/irradiation steps and the totals then incremented.

For the more complex europium isotopes, a different technique is used. The 22-group neutron fluxes were coarsely regrouped into fast, resonance and thermal groups by FLUX4. The resulting spectra and total fluxes, for each measured position, were then used to perform a FISPIN calculation (Ref 14) (including input of the reactor operating history).

3.0 Assumptions

Material specifications are given in Tables 1a and 1b. Half lives (see Table 2) were also taken from the original specification (Ref 3). The source spectrum was described in Ref 3, in terms of the equation below:

$$Source=0.484*e^{-E}*\sinh(\sqrt{(2E)})$$

The equation was integrated into the required group scheme by use of simple programs using Simpson's formula with automatic subdivision. The actual values used in MCBEND are shown in Table 4. The radial and axial source variations, derived from Ref 3, are shown in Tables 5 and 6 respectively. The number of neutrons emitted per fission, ν was assumed to have a typical value of 2.47 for a thermal reactor.

4.0 Model

The reactor model used was in RZ geometry. This means that the model varies radially and vertically, but not with angle. A vertical section through the model (based on Ref 3) including the whole height of the core, plus some additional regions above is shown in Figure 1.

Calculations were only performed for two heights, as details of reinforcements and cooling pipes were only available for the central portion of the bioshield. This meant that there was little point in extending the model below the bottom of the core supports (the only effect would have been to increase calculation times).

Material specifications were, unless stated, taken from Table A.2 of Ref 3 (see Table 1). Re-bars and cooling pipes were smeared with the concrete, over the diameter of the component. The outer, emergency cooling pipes were modelled as being empty.

5.0 Results

5.1 SENSITIVITY STUDIES

Assessments were carried out to determine the effect of uncertainties in fuel composition, sample position, bioshield water content, the inclusion of re-bars, and changes in coolant water density. MCBEND 7B and MCBEND 9A were compared for identical cases, and no significant differences were found. MCBEND 7B was used in the previous study, but MCBEND 9A includes the fractal geometry option, where repeated geometries, such as fuel elements, may be copied to different parts of the model. This would be particularly useful for creating an accurate model of the core region (should more detailed information become available).

No rigorous study was made of the actual value of ν as data was scarce concerning the fuel. Uncertainties in the measured activities were not available, and no information concerning the precise arrangement of the fuel region (other than fuel pin pitch, number of assemblies, and overall dimensions) were available. It is not thought that the precise variation of power history within each of the irradiation 'steps' would have much effect on overall activities, as only relatively long-lived nuclides have been considered.

It is hoped that should more complete data become available for a reactor, a more exhaustive analysis may be performed.

5.1.1 BIOSHIELD WATER CONTENT

Cases were run for two separate water content, 5.1% and 6.6%. The former is the measured amount of water in the concrete (as far as may be determined from the data provided), whilst the latter is derived from Ref 15, and represents a typical value for concrete from the literature. The actual water content of the concrete will vary with time, as it dries out. It is therefore, expected that a measured value at the end of the reactor's life will be lower than values quoted for new concrete. (This was in fact assumed in the original benchmark case (Ref 3), where a water content of 7% was assumed, despite the measured value of 5.1%). The significant value is the water content at the time of major irradiation, which in this case is toward the beginning of the reactor's operating life.

Reaction rates are shown in Figures 3-6. The two models, top2ld and top2o, are identical apart from the change in water content. The $^{59}Co(n,\gamma)$ reaction rate is 32% lower with the increased water content at a radius of 215 cm (Figures 3-6). Whilst this is obviously significant, it does not solely explain the larger discrepancies between calculation and measurement in the previous study.

5.1.2 BIOSHIELD DENSITY

Two different densities have been applied for the bioshield, 2.3 g/cc and 2.33 g/cc (a variation of about 1%). The effect of this appears small on the graphs, although it amounts to a decrease of about 8% at a radius of 215 cm, and will increase with depth into the bioshield. The uncertainty in density is assumed to be about 1%, as this corresponds to a change of water content from 6.6% to 5.1%.

5.1.3 FISSION SPECTRUM

Three different fission spectra were used. The original specification used the Watt-Cranberg expression (described in Section 3.0) for ^{235}U fission. To check that this had been done accurately the MCBEND library ^{235}U fission spectrum was also used (it is based upon the Watt-Cranberg expression too). Results confirmed that there was little difference (less than the uncertainty in the calculational statistics) between the two sets of results. The effect of fissions in plutonium was also considered, by including a limiting case with 50% of fissions occurring in plutonium. Reaction rates were still within the statistical uncertainties of the calculation. This was because none of the responses are threshold reactions, critically depending on high energy neutrons.

5.1.4 BIOSHIELD RE-BARS AND COOLING PIPES

Two cases, top2 and top2ref, were run with the only difference being the

omission of the re-bars and cooling pipes. Calculated ^{60}Co activities are higher by about 33% at a radius of 215 cm.

5.1.5 COOLING WATER DENSITY

JPDR is a boiling water reactor, with a lower layer of water (water(1) in Figure 1) surmounted by a layer of steam. The density specified (in Ref 3) for this material is about 0.76 g/cc. This is presumably including allowance for bubbles in the water, as water is largely incompressible and its density does not vary much with temperature either. It is assumed that the actual density in this region varies considerably, being denser at the bottom than at the top. A calculation was performed with the water(1) density 10% higher, so as to determine the effect of this uncertainty. It can be seen that the effect is quite considerable (Figures 3-6) (31% at a radius of 215 cm) (cases top2 and top2w).

5.1.6 GEOMETRY

One of the main requirements of this project was to consider three dimensional effects. Unfortunately, no additional information became available concerning the core arrangement, or the direction in which the samples were taken.

Two models were set up, based on the information already available in Ref 3, both with slab geometry cores, but one with scoring zones opposite the corner of the core top3ref45r), and the other opposite the flat facing of the core (top3refr) (Fig 2). Activations are shown in Figure 11 for the $^{59}Co(n,\gamma)$ response. It is seen that there is little difference between them and the results for the two dimensional case. This is largely because any part of the core further than 60 cm from the core centre-line was set to a relative power level of 0.944. A previous model using a distribution based on multiplying the radial distributions together resulted in a very strange source distribution, because the highest power is achieved at some distance from the core centre-line.

5.1.7 NUCLEAR DATA

Two dimensional calculations were repeated using the most recent JEF2 (Ref 17) cross-section data and IRDF-90 (Ref 18) responses (Table 7), which are just becoming available. Virtually no difference resulted in changing from IRDF-85 to IRDF-90 data for the $^{59}Co(n,\gamma)$ reaction. Using JEF2 data reduced reaction rates by about 5% at all positions considered in the bioshield.

5.1.8 RESONANCES

The original funding did not allow for an assessment of resonances on reaction rates and so it was not possible to address them here. This could be investigated

in later work, but is unlikely to affect results by factors of two or more.

6.0 Conclusions

The main sources of uncertainty in calculating bioshield activation have been assessed. It is concluded that the most important of these are (i) accurate modelling of the re-bars and cooling pipes, (ii) using a realistic water content during irradiation early in the reactor's life (not 15 years after shutdown), and (iii) accurate knowledge of the coolant density. Each of these is of approximately equal importance at a radius of 215 cm, although item (ii) will increase in importance with further depth in the shield, whereas the other two will have the same importance. These sources of uncertainty go some way to resolving the differences between calculation and measurement reported in Ref 2, but a discrepancy does still exist.

From comparison of the activation gradients deep into the bioshield, a concrete water content of about 6.6% seems reasonable. Unfortunately no firm conclusions can be made as to whether this is appropriate, due to the large uncertainties in coolant density and the lack of detailed information about the reactor.

The main discrepancy is in the prediction of the width of the thermal peak at the inner surface of the bioshield. Results are good up to this point, and activation gradients further out for the 'top2' cases are similar to those for the measured values. This suggests that there is a parameter to which responses are sensitive 10 cm into the bioshield (Ref 16). The cause may be investigated by a three group (thermal, epi-thermal and fast fluxes) sensitivity study of parameters thought likely to be responsible. These should include hydrogen content in both the coolant and the bioshield, iron content in the reactor vessel, liner, re-bars, bioshield, and core geometry/composition. Calculations should be performed for the reactor vessel outer wall, bioshield inner face, and for 10 cm into the bioshield. In particular the modelling of the re-bar may not be sufficiently detailed.

This study has concentrated on just one reactor. From the results of that study, it is not evident whether the concrete problem lies with the basic data derived for this reactor. A similar exercise for another reactor (or two), as long as they are well characterised, would help considerably in isolating the precise source of the problem. It is essential to have a validated calculational method (and associated uncertainties) for the assessment of reactor bioshield (etc) inventory in order to reduce the need for experimental sampling and in order to reduce overall costs.

7.0 References

1. Specification for IAEA Benchmark Intercomparison for Inventory Calculations for Fission Reactor Decommissioning. M T Cross, TSAF/WL/S(94)22, April 1994.
2. Current Status of Decommissioning Calculations for IAEA Benchmark (JPDR). M H Dean, N J France, S J Wall, AEA-TSD-0259, September 1994.
3. Accuracy Verification for Calculation of Inventory in JPDR due to Neutron Activation. T Sukegawa, N Sasamoto, and K Fujiku, INDC(JPN)-164, March 1993.
4. IAEA Consultants Meeting on Nuclear Data for the Calculations of Radioactive Inventory for Fission Reactor Decommissioning, IAEA 5-7 December 1994, M H Dean et al.
5. Task Agreement D1190, Plant Radioactivity Estimation Milestone 5.1 - IAEA Consultants Meeting, December 1994. Letter from M T Cross to T Kyffin.
6. MCBEND - User Guide to Version 7. Internal AEA Report.
7. User Guide: FLUX4 Version 6:- A program to calculate nuclide inventories from multigroup neutron fluxes. S J Wall, N J France. Internal AEA Report.
8. UKNDL, UK Nuclear Data Library
9. The International Reactor Dosimetry File (IRDF-85). D E Cullen and P K McLaughlin, IAEA-NDS-41.
10. Table of the main Radioactive Decay Data Parameters from JEF-1, ENDF/B-V, ENSDF, French, Japanese and UK Libraries. JEF report 9, NEA Data Bank, July 1987.
11. Nuclear Engineering Handbook. H Etherington, 1958.
12. Some coarse group activation cross-sections. S W Power, T J Whitehead. Internal AEA Report.
13. CASK coupled data libraries. Unpublished.
14. FISPIN A Computer Code for Nuclide Inventory Calculations. R F Burstall, ND-R-328(R), October 1979.
15. Progress Report on Literature Review to Assess Water Content of Bioshield Concrete. D Fisher, DDPM/P(95)279.
16. Private Communication. S J Chucas to S J Wall, 5 April 1995.
17. The 1994 Dice Nuclear Library. C J Dean, C R Eaton, AEA-RS-5697.
18. The International Reactor Dosimetry File (IRDF90). N Kocherov, P K McLaughlin, IAEA-NDS-141 Rev 2.

8.0 Key to Symbols used

E	Energy (MeV)
λ	Decay constant (s^{-1})
$\Sigma\phi\sigma$	Reaction rate (reactions per second)
T_i	Irradiation time (seconds)
T_c	Cooling time (seconds)
Np_o	Parent element concentration (atoms per gram)
ν	Number of neutrons released per fission

9.0 List of Tables

1. Material compositions
2. Half lives used in activation calculations
3. Comparison of FISPIN against FLUX4
4. Source spectrum and group scheme for MCBEND calculations
5. Radial source distribution
6. Axial source distribution
7. Variation of $^{59}Co(n,\gamma)$ reaction rate in radial bioshield
8. Variation of $^{133}Cs(n,\gamma)$ reaction rate in radial bioshield
9. Variation of $^{151}Eu(n,\gamma)$ total reaction rate in radial bioshield
10. Variation of $^{153}Eu(n,\gamma)$ reaction rate in radial bioshield
11. Variation of ^{60}Co activations for three-dimensional models
12. Variation of ^{134}Cs activations for three-dimensional models
13. Variation of ^{60}Co activity in radial bioshield
14. Variation of ^{134}Cs activity in radial bioshield
15. Variation of ^{152}Eu activity in radial bioshield
16. Variation of ^{154}Eu activity in radial bioshield

10. List of Figures

1. Two dimensional model of JPDR used in MCBEND
2. Section through three dimensional model
3. $^{59}Co(n,\gamma)$ reaction rates
4. $^{133}Cs(n,\gamma)$ reaction rates
5. $^{151}Eu(n,\gamma)$ total reaction rates
6. $^{153}Eu(n,\gamma)$ reaction rates
7. ^{60}Co activation in bioshield
8. ^{134}Cs activation in bioshield
9. ^{152}Eu activation in bioshield
10. ^{154}Eu activation in bioshield
11. ^{60}Co activation in bioshield for 3D model
12. ^{134}Cs activation in bioshield for 3D model
13. ^{60}Co activation in bioshield (2D model, z=475 cm)

Table 1a Material compositions: Structural materials (by weight)

Item	Core internals	Reactor Vessel		Bioshield
	Core Shroud	Clad	Basic Material	Concrete
Density (g/cc)	7.9	7.9	7.85	2.3
H %				0.59
Na %				1.4
Mg %				0.6
Al %	0.05	0.02		5.1
Si %	0.83	0.88	0.29	32.6
S %	0.006	0.005		0.13
K %				1.6
Ca %				7.2
Ti %				0.14
Cr %	19.3	18.6	0.074	0.015
Mn %	1.6	1.2	1.3	0.041
Fe %	70.7	71.4	97.4	1.9
Ni %	9.2	9.8	0.55	0.0013
Cu %	0.11	0.09	0.16	0.0016
O %				48.63
Co ppm	1300	1200	200	6.2
Nb ppm				12
Mo ppm	1900	2800	1200	2
Sn ppm	50	30	180	2
Eu ppm				0.59
Hf ppm				2.5

Table 1b Material compositions: Remaining materials (atoms/cm^3 *10^{-24})

Element	Fuel region (2)	Water (1)	Chimney, core supp.	Fuel region (3)	Fuel region (1)
H	2.4110E-2	5.0548E-2		2.1414E-2	2.7795E-2
C			3.1729E-4		
O	2.3493E-2	2.5274E-2		2.1694E-2	2.4885E-2
Si			1.8100E-3		
Cr	1.8999E-4		1.7408E-2	1.8999E-4	1.8999E-4
Mn			1.7343E-3		
Fe	7.3243E-4		5.7872E-2	7.3243E-4	7.3243E-4
Ni	8.2869E-5		8.1116E-3	8.2869E-5	8.2869E-5
Zr	5.0663E-3			5.0663E-3	5.0663E-3
^{235}U	1.4459E-4			1.4459E-4	1.4459E-4
^{238}U	5.3489E-3			5.3489E-3	5.3489E-3

Element	Air	Up plenum region	Up grid region	Water(2)	Steam
H		2.1918E-2	2.6419E-2	2.9662E-2	2.1068E-3
N	3.9099E-5				
O	1.0538E-5	1.0959E-2	1.3210E-2	1.4831E-2	1.0534E-3
Si			3.3582E-4		
Mn			2.7964E-4		
Fe			1.3451E-2		
Ni		2.5658E-3			
Zr		5.2307E-3	1.0223E-3		

Table 1b (cont.)

Element	Low plenum region	Fuel base region	Low plate region	Low grid region	Shielding region	Steel liner
H	3.0575E-2	3.6770E-2	1.9500E-2	3.8870E-2		
C	3.5386E-4	8.4909E-4	5.3076E-4	4.0917E-4		8.2658E-4
O	1.5287E-2	1.8385E-2	9.7501E-3	1.9811E-2		
Si			1.0794E-3			1.1468E-4
Cr			1.0381E-3			
Mn		4.1377E-4	1.0342E-3	3.6966E-4		9.8102E-4
Fe	3.9230E-3	1.9899E-2	3.9349E-2	1.7774E-2	8.4755E-2	8.4296E-2
Zr	4.2649E-3	6.8496E-4				

Table 2. Half lives used in activation calculations

Isotope	Half-life (days)
^{60}Co	1925.2
^{55}Fe	999
^{54}Mn	312.3
^{134}Cs	754.28
^{152}Eu	4933
^{154}Eu	3136.8

Table 3 Comparison of FISPIN and FLUX4

Radius	^{60}Co activity for top2 model		
	FLUX4	FISPIN	FLUX4/FISPIN
151.5	2.5536E2	2.7780E2	0.9192
155.5	2.2461E2	2.4226E2	0.9271
157.5	2.0223E2	2.1741E2	0.9302
159.5	1.7925E2	1.9169E2	0.9351
161.5	1.5411E2	1.6503E2	0.9338
169.5	7.9192E1	8.4527E1	0.9369
173.5	5.778E1	6.1059E1	0.9463
179.5	2.9362E1	3.1207E1	0.9409
207.5	2.3333E0	2.4295E0	0.9604
215.5	1.1012E0	1.1493E0	0.9581

Table 4. Source spectrum and group scheme for MCBEND calculations

Upper Energy (eV)	Source fraction
1.46e+07	4.36e-05
1.35e+07	9.20e-05
1.25e+07	2.87e-04
1.13e+07	7.68e-04
10.00e+06	2.71e-03
8.50e+06	8.42e-03
7.00e+06	1.24e-02
6.07e+06	4.09e-02
4.72e+06	6.94e-02
3.68e+06	9.60e-02
2.87e+06	2.32e-01
1.74e+06	3.70e-01
6.00e+05	7.21e-02
3.90e+05	7.92e-02
1.10e+05	8.16e-03
6.74e+04	6.01e-03
2.48e+04	1.37e-03
9.12e+03	3.23e-04
2.95e+03	5.94e-05
9.61e+02	1.06e-05
3.54e+02	2.06e-06
1.66e+02	8.24e-07
4.81e+01	1.23e-07
1.60e+01	2.56e-08
4.00e+00	2.81e-09
1.50e+00	6.52e-10
5.50e-01	1.78e-10
7.09e-02	8.61e-12

Table 5. Radial Source Distribution

Outer Radius (cm)	Source Factor
10	0.983
20	0.992
23	1.005
27	1.014
30	1.022
35	1.042
40	1.045
43	1.038
47	1.027
50	1.013
53	0.998
57	0.982
60	0.962
65.4	0.944

Table 6. Axial source distribution

Axial Height (cm)	Source Factor
232 - 240	0.55
240 - 250	0.7
250 - 260	0.85
260 - 270	1.02
270 - 280	1.12
280 - 290	1.19
290 - 300	1.24
300 - 320	1.25
320 - 330	1.23
330 - 340	1.17
340 - 350	1.07
350 - 360	0.95
360 - 370	0.76
370 - 379	0.53

Table 7 Variation of $^{59}Co(n,\gamma)$ reaction rate in radial bioshield

Radius	top2	top2ld	top2o	top2w	top2ref	top2j2(90)	top2j2(85)	top2oref
151.5	1.03e+10	1.01e+10	9.54e+09	6.56e+09	1.29e+10	1.01e+10	1.01e+10	1.43e+10
153.5	9.69e+09	9.62e+09	9.26e+09	6.31e+09	1.19e+10	9.45e+09	9.44e+09	1.30e+10
155.5	9.04e+09	8.96e+09	8.93e+09	5.89e+09	1.07e+10	8.56e+09	8.55e+09	1.18e+10
157.5	8.14e+09	8.10e+09	8.28e+09	5.33e+09	9.47e+09	7.75e+09	7.74e+09	1.06e+10
159.5	7.22e+09	7.22e+09	7.56e+09	4.72e+09	8.41e+09	6.78e+09	6.77e+09	9.47e+09
161.5	6.20e+09	6.26e+09	6.67e+09	4.09e+09	7.40e+09	5.90e+09	5.90e+09	8.24e+09
169.5	3.19e+09	3.24e+09	3.84e+09	2.10e+09	4.05e+09	2.98e+09	2.98e+09	4.60e+09
171.5	2.77e+09	2.79e+09	3.38e+09	1.83e+09	3.42e+09	2.59e+09	2.59e+09	3.86e+09
173.5	2.33e+09	2.35e+09	2.93e+09	1.55e+09	2.84e+09	2.20e+09	2.20e+09	3.26e+09
175.6	1.91e+09	1.94e+09	2.48e+09	1.29e+09	2.38e+09	1.81e+09	1.81e+09	2.75e+09
277.6	1.54e+09	1.58e+09	2.05e+09	1.04e+09	2.00e+09	1.46e+09	1.45e+09	2.32e+09
179.6	1.18e+09	1.22e+09	1.62e+09	7.89e+08	1.66e+09	1.11e+09	1.11e+09	1.95e+09
199.5	1.83e+08	1.98e+08	3.12e+08	1.25e+08	2.58e+08	1.69e+08	1.69e+08	3.14e+08
201.5	1.56e+08	1.69e+08	2.70e+08	1.05e+08	2.12e+08	1.44e+08	1.44e+08	2.60e+08
203.5	1.32e+08	1.44e+08	2.32e+08	8.92e+07	1.76e+08	1.22e+08	1.22e+08	2.16e+08
205.5	1.12e+08	1.21e+08	1.98e+08	7.55e+07	1.46e+08	1.05e+08	1.05e+08	1.81e+08
207.5	9.39e+07	1.01e+08	1.69e+08	6.36e+07	1.21e+08	8.71e+07	8.71e+07	1.49e+08
209.5	7.90e+07	8.48e+07	1.44e+08	5.30e+07	9.92e+07	7.49e+07	7.49e+07	1.24e+08
211.5	6.57e+07	7.06e+07	1.20e+08	4.37e+07	8.31e+07	6.35e+07	6.35e+07	1.02e+08
213.5	5.43e+07	5.95e+07	1.01e+08	3.68e+07	6.81e+07	5.27e+07	5.27e+07	8.45e+07
215.5	4.43e+07	4.99e+07	8.47e+07	3.05e+07	5.68e+07	4.22e+07	4.21e+07	6.97e+07

Table 8 Variation of $^{133}Cs(n,\gamma)$ reaction rate in radial bioshield

Radius	top2	top2ld	top2o	top2w	top2ref	top2oref	top2j2
151.5	1.45e+10	1.50e+10	1.53e+10	8.97e+09	1.68e+10	1.79e+10	1.42e+10
153.5	1.31e+10	1.34e+10	1.43e+10	8.58e+09	1.47e+10	1.55e+10	1.31e+10
155.5	1.19e+10	1.19e+10	1.31e+10	7.89e+09	1.29e+10	1.38e+10	1.15e+10
157.5	1.02e+10	1.05e+10	1.18e+10	6.80+09	1.11e+10	1.20e+10	9.87e+09
159.5	8.81e+09	8.84e+09	1.05e+10	6.07e+09	9.73e+09	1.03e+10	8.44e+09
161.5	7.61e+09	7.67e+09	9.08e+09	5.07e+09	8.36e+09	8.91e+09	7.10e+09
169.5	3.75e+09	3.79e+09	4.87e+09	2.41e+09	4.25e+09	4.65e+09	3.50e+09
171.5	3.16e+09	3.19e+09	4.16e+09	2.06e+09	3.56e+09	3.88e+09	3.02e+09
173.5	2.60e+09	2.65e+09	3.56e+09	1.70e+09	2.96e+09	3.22e+09	2.44e+09
175.5	2.12e+09	2.15e+09	3.03e+09	1.44e+09	2.47e+09	2.71e+09	2.00e+09
177.6	1.72e+09	1.75e+09	2.52e+09	1.15e+09	2.06e+09	2.26e+09	1.62e+09
179.6	1.38e+09	1.38e+09	2.05e+09	9.05e+08	1.67e+09	1.89e+09	1.26e+09
199.5	1.96e+08	2.04e+08	3.46e+08	1.33e+08	2.53e+08	2.95e+08	1.77e+08
210.5	1.66e+08	1.79e+08	2.91e+08	1.10e+08	2.13e+08	2.44e+08	1.51e+08
203.5	1.38e+08	1.48e+08	2.51e+08	9.35e+07	1.72e+08	2.06e+08	1.33e+08
205.5	1.17e+08	1.23e+08	2.12e+08	7.68e+07	1.43e+08	1.67e+08	1.09e+08
207.5	9.70e+07	1.02e+08	1.78e+08	6.58e+07	1.18e+08	1.39e+08	8.92e+07
209.5	8.12e+07	8.51e+07	1.48e+08	5.53e+07	9.52e+07	1.17e+08	7.61e+07
211.5	6.70e+07	7.09e+07	1.26e+08	4.57e+07	8.28e+07	9.38e+07	6.66e+07
213.5	5.60e+07	5.96e+07	1.01e+08	3.80e+07	6.61e+07	7.81e+07	5.32e+07
215.5	4.43e+07	5.03e+07	8.52e+07	3.08e+07	5.29e+07	6.42e+07	4.33e+07

Table 9 Variation of $^{151}Eu(n,\gamma)$ total reaction rate in radial bioshield

Radius	top2	top2ld	top2o	top2ref	top2w	top2oref	top2j2
151.5	2.12e+12	2.07e+12	1.89e+12	2.69e+12	1.34e+12	3.03e+12	2.03e+12
153.5	2.03e+12	1.99e+12	1.88e+12	2.50e+12	1.31e+12	2.77e+12	1.94e+12
155.5	1.90e+12	1.87e+12	1.83e+12	2.27e+12	1.23e+12	2.51e+12	1.79e+12
157.5	1.71e+12	1.70e+12	1.71e+12	2.01e+12	1.12e+12	2.28e+12	1.62e+12
159.5	1.53e+12	1.52e+12	1.57e+12	1.79e+12	1.00e+12	2.04e+12	1.43e+12
161.5	1.32e+12	1.32e+12	1.39e+12	1.58e+12	8.71e+11	1.78e+12	1.24e+12
169.5	6.82e+11	6.94e+11	8.07e+11	8.79e+11	4.47e+11	9.99e+11	6.33e+11
171.5	5.93e+11	5.98e+11	7.16e+11	7.40e+11	3.92e+11	8.40e+11	5.52e+11
173.6	5.00e+11	5.05e+11	6.22e+11	6.14e+11	3.33e+11	7.09e+11	4.69e+11
175.6	4.12e+11	4.19e+11	5.26e+11	5.17e+11	2.78e+11	5.99e+11	3.89e+11
177.6	3.30e+11	3.40e+11	4.36e+11	4.34e+11	2.24e+11	5.06e+11	3.10e+11
179.6	2.52e+11	2.61e+11	3.44e+11	3.62e+11	1.70e+11	4.26e+11	2.33e+11
199.5	3.94e+10	4.26e+10	6.73e+10	5.60e+10	2.68e+10	6.88e+10	3.60e+10
201.5	3.37e+10	3.64e+10	5.83e+10	4.61e+10	2.27e+10	5.69e+10	3.07e+10
203.5	2.85e+10	3.12e+10	5.01e+10	3.85e+10	1.93e+10	4.72e+10	2.62e+10
205.5	2.43e+10	2.61e+10	4.28e+10	3.18e+10	1.63e+10	3.96e+10	2.23e+10
207.5	2.04e+10	2.18e+10	3.65e+10	2.62e+10	1.38e+10	3.26e+10	1.87e+10
209.5	1.71e+10	1.84e+10	3.12e+10	2.15e+10	1.15e+10	2.71e+10	1.61e+10
211.5	1.42e+10	1.53e+10	2.60e+10	1.81e+10	9.44e+09	2.22e+10	1.37e+10
213.5	1.18e+10	1.29e+10	2.19e+10	1.49e+10	7.95e+09	1.85e+10	1.13e+10
215.5	9.53e+09	1.08e+10	1.83e+10	1.25e+10	6.60e+09	1.53e+10	8.96e+09

Table 10 Variation of $^{153}Eu(n,\gamma)$ reaction rate in radial bioshield

Radius	top2	top2ld	top2ref	top2w	top2o	top2oref	top2j2
151.5	9.48e+10	9.29e+10	1.15e+11	6.10e+10	9.11e+10	1.26e+11	9.11e+10
153.5	8.87e+10	8.78e+10	1.05e+11	5.72e+10	8.79e+10	1.13e+11	8.53e+10
155.5	8.13e+10	8.06e+10	9.37e+10	5.27e+10	8.30e+10	1.01e+11	7.68e+10
157.5	7.24e+10	7.23e+10	8.24e+10	4.77e+10	7.66e+10	9.09e+10	6.85e+10
159.5	6.34e+10	6.38e+10	7.24e+10	4.20e+10	6.91e+10	8.05e+10	5.97e+10
161.5	5.45e+10	5.50e+10	6.34e+10	3.62e+10	6.07e+10	6.98e+10	5.17e+10
169.5	2.77e+10	2.81e+10	3.40e+10	1.81e+10	3.42e+10	3.81e+10	2.59e+10
171.5	2.37e+10	2.40e+10	2.86e+10	1.57e+10	3.00e+10	3.20e+10	2.23e+10
173.5	1.99e+10	2.01e+10	2.37e+10	1.33e+10	2.58e+10	2.69e+10	1.87e+10
175.6	1.64e+10	1.66e+10	1.99e+10	1.10e+10	2.17e+10	2.26e+10	1.54e+10
177.6	1.32e+10	1.34e+10	1.66e+10	8.88e+09	1.80e+10	1.90e+10	1.23e+10
179.6	1.01e+10	1.04e+10	1.38e+10	6.82e+09	1.43e+10	1.60e+10	9.44e+09
199.5	1.55e+09	1.65e+09	2.11e+09	1.04e+09	2.65e+09	2.54e+09	1.41e+09
201.5	1.32e+09	1.40e+09	1.74e+09	8.81e+08	2.28e+09	2.11e+09	1.20e+09
203.5	1.11e+09	1.20e+09	1.45e+09	7.52e+08	1.96e+09	1.76e+09	1.03e+09
205.5	9.33e+08	1.01e+09	1.20e+09	6.30e+08	1.67e+09	1.47e+09	8.70e+08
207.5	7.82e+08	8.38e+08	9.88e+08	5.30e+08	1.42e+09	1.21e+09	7.31e+08
209.5	6.56e+08	7.05e+08	8.16e+08	4.42e+08	1.21e+09	1.00e+09	6.19e+08
211.5	5.46e+08	5.89e+08	6.81e+08	3.64e+08	1.01e+09	8.25e+08	5.24e+08
213.5	4.50e+08	4.92e+08	5.62e+08	3.05e+08	8.49e+08	6.85e+08	4.38e+08
215.5	3.65e+08	4.14e+08	4.69e+08	2.52e+08	7.08e+08	5.67e+08	3.52e+08

Table 11 Variation of ^{60}Co activations for three-dimensional models

Radius	Measurement	top2	top3refr	top3ref45r
169.5	21.2	79.192	79.59	82.099
171.5	19.8	68.859	69.38	70.995
173.6	15.1	57.78	58.252	59.991
175.6	11	47.521	47.943	49.657
177.6	10.9	38.255	38.752	39.969
179.6	9.08	29.362	29.71	30.529
199.5	0.99	4.5359	4.4142	4.8589
201.5	0.797	3.8851	3.7858	4.0143
203.5	0.638	3.2864	3.2045	3.4156
205.5	0.899	2.7871	2.6878	2.8368
207.5	0.448	2.3333	2.2645	2.3887
209.5	0.382	1.9624	1.9279	2.0176
211.5	0.362	1.6308	1.605	1.7125
213.5	0.359	1.3496	1.3563	1.4249
215.5	0.221	1.1012	1.3938	1.4226

Table 12 Variation of ^{134}Cs activations for three-dimensional models

Radius	Experiment	top2	top3refr	top3ref45r
169.5	0.226	0.59172	0.57846	0.62329
171.5	0.11	0.4986	0.50902	0.51359
173.6	0.111	0.41005	0.42615	0.42458
175.6	0.0985	0.33445	0.32624	0.34929
177.6	0.113	0.27069	0.26721	0.28789
179.6	0.0645	0.2175	0.2126	0.22349
199.5	0.00724	0.030967	0.028458	0.032451
201.5	0.00886	0.026201	0.024354	0.02639
203.5	0.00496	0.021844	0.021229	0.022065
205.5	0.00422	0.018388	0.016904	0.018546
207.5	0.0049	0.015308	0.014533	0.015894
209.5	0.00419	0.012818	0.012054	0.012575
211.5	0.00317	0.010578	0.010775	0.010708
213.5		0.0088404	0.0087267	0.0091134
215.5	0.00196	0.0069968	0.0087898	0.0094512

Table 13 Variation of ^{60}Co activity in the radial bioshield

Radius	Measurement	top2	top2oref (previous)	top2w
151.5	90.7	255.36	355.96	163.03
153.5	93	240.8	323.92	156.82
155.5	82.3	224.61	291.88	146.36
157.5	65.6	202.23	264.06	132.28
159.5	58.5	179.25	235.27	117.32
161.5	60.2	154.11	204.74	101.7
169.5	21.2	79.192	114.37	52.042
171.5	19.8	68.859	95.96	45.533
173.6	15.1	57.78	81.031	38.528
175.6	11	47.521	68.362	32.02
177.6	10.9	38.255	57.656	25.81
179.6	9.08	29.362	48.34	19.602
199.5	0.99	4.5359	7.7975	3.0927
201.5	0.797	3.8851	6.4686	2.6182
203.5	0.638	3.2864	5.3756	2.2156
205.5	0.899	2.7871	4.5061	1.8747
207.5	0.448	2.3333	3.7063	1.5801
209.5	0.382	1.9624	3.0728	1.3163
211.5	0.362	1.6308	2.5263	1.0858
213.5	0.359	1.3496	2.0991	0.91489
215.5	0.221	1.1012	1.7319	0.7564

Table 14 Variation of Cs^{134} activity in radial bioshield

Radius	Measurement	top2	top2oref (Previous)	top2w
151.5	0.787	2.2917	2.8189	1.4156
153.5	0.79	2.0613	2.4464	1.3547
155.5	0.97	1.8703	2.1844	1.2451
157.5	0.571	1.6131	1.8956	1.0723
159.5	0.544	1.391	1.6273	0.95742
161.5	0.376	1.2005	1.406	0.80053
169.5	0.226	0.59172	0.73424	0.3807
171.5	0.11	0.4986	0.61192	0.32435
173.6	0.111	0.41005	0.50854	0.26895
175.6	0.0985	0.33445	0.42789	0.22665
177.6	0.113	0.27069	0.35734	0.18135
179.6	0.0645	0.2175	0.29799	0.14278
199.5	0.00724	0.030967	0.046546	0.020976
201.5	0.00886	0.026201	0.038464	0.017315
203.5	0.00496	0.021844	0.032467	0.014761
205.5	0.00422	0.018388	0.026374	0.01212
207.5	0.0049	0.015308	0.021876	0.010378
209.5	0.00419	0.012818	0.01853	0.0087236
211.5	0.00317	0.010578	0.014799	0.0072162
213.5		0.0088404	0.012321	0.0059898
215.5	0.00196	0.0069968	0.010133	0.0048676

Table 15 Variation of ^{152}Eu activity in radial bioshield

Radius	top2	Measured
151.5	2.58e+03	6.80e+02
153.5		8.15e+02
155.5	2.29e+03	6.11e+02
158	2.07e+03	5.40e+02
159.5	1.84e+03	4.96e+02
161.5	1.59e+03	4.44e+02
169.5	8.24e+02	1.88e+02
171.5	7.15e+02	1.60e+02
173.6	5.99e+02	1.42e+02
175.6	4.93e+02	1.06e+02
177.6	3.96e+02	8.44e+01
179.6	3.06e+02	6.60e+01
199.5	4.71e+01	7.07e+00
201.5		7.34e+00
203.5	3.40e+01	5.32e+00
205.5		4.83e+00
207.5	2.41e+01	4.05e+00
209.5		3.17e+00
211.5	1.69e+01	2.72e+00
213.5		2.85e+00
215.5	1.14e+01	1.75e+00

Table 16 Variation of ^{154}Eu activity in radial bioshield

Radius	top2	Measured
151.5	9.43e+01	4.18e+01
153.5		4.61e+01
155.5	7.96e+01	4.08e+01
157.5	7.07e+01	2.66e+01
159.5	6.18e+01	2.34e+01
161.5	5.29e+01	2.21e+01
169.5	2.67e+01	8.93e+00
171.5	2.29e+01	6.96e+00
173.6	1.91e+01	8.12e+00
175.6	1.57e+01	5.34e+00
177.6	1.26e+01	4.24e+00
179.6	9.79e+00	3.66e+00
199.5	1.47e+00	3.74e-01
201.5		3.59e-01
203.5	1.05e+00	2.60e-01
205.5		2.58e-01
207.5	7.45e-01	2.09e-01
209.5		1.56e-01
211.5	5.19e-01	1.37e-01
213.5		1.46e-01
215.5	3.52e-01	7.05e-02

Figure 1 Two dimensional model of JPDR used in MCBEND

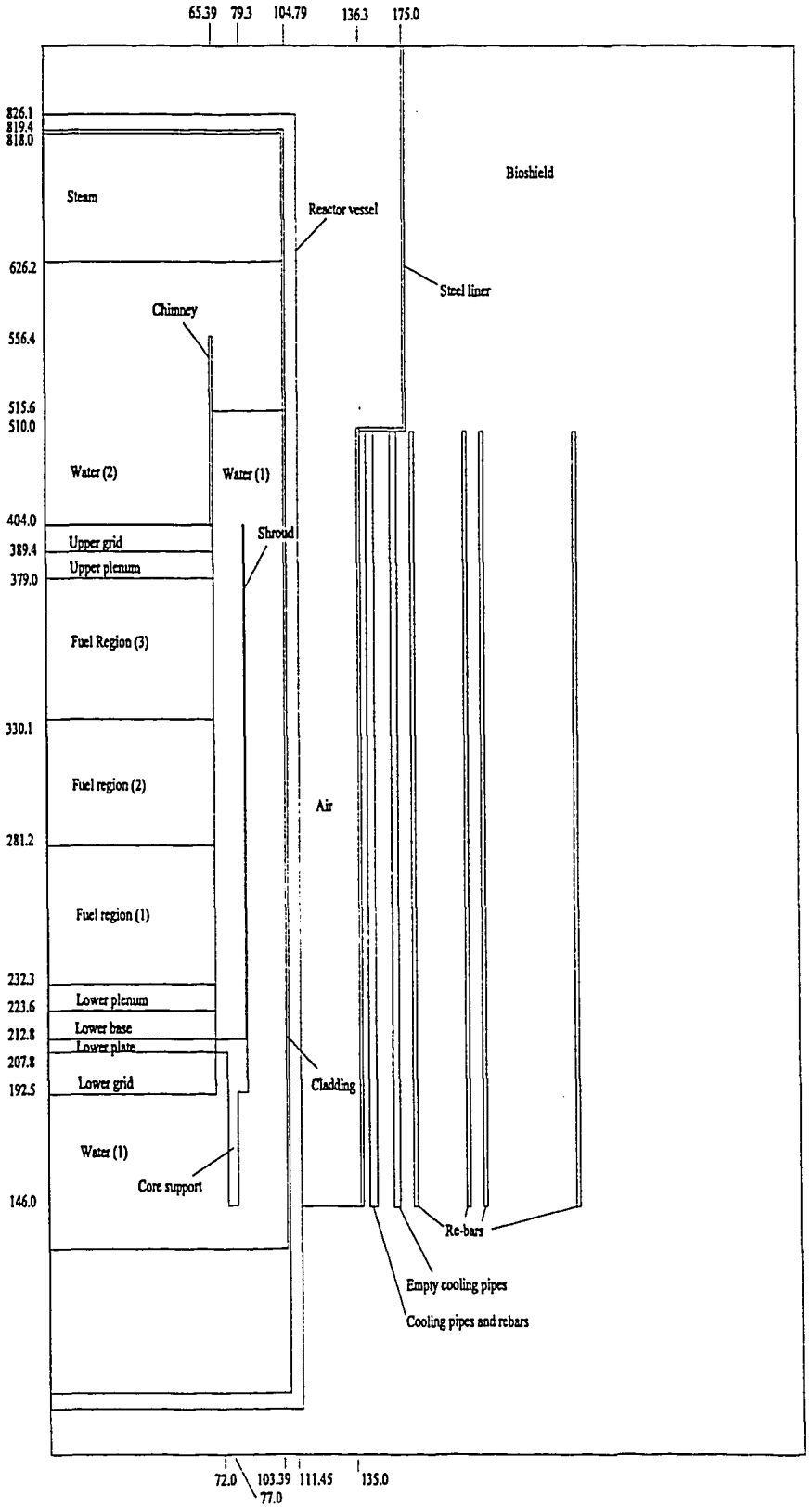

Figure 2 Section through three dimensional model

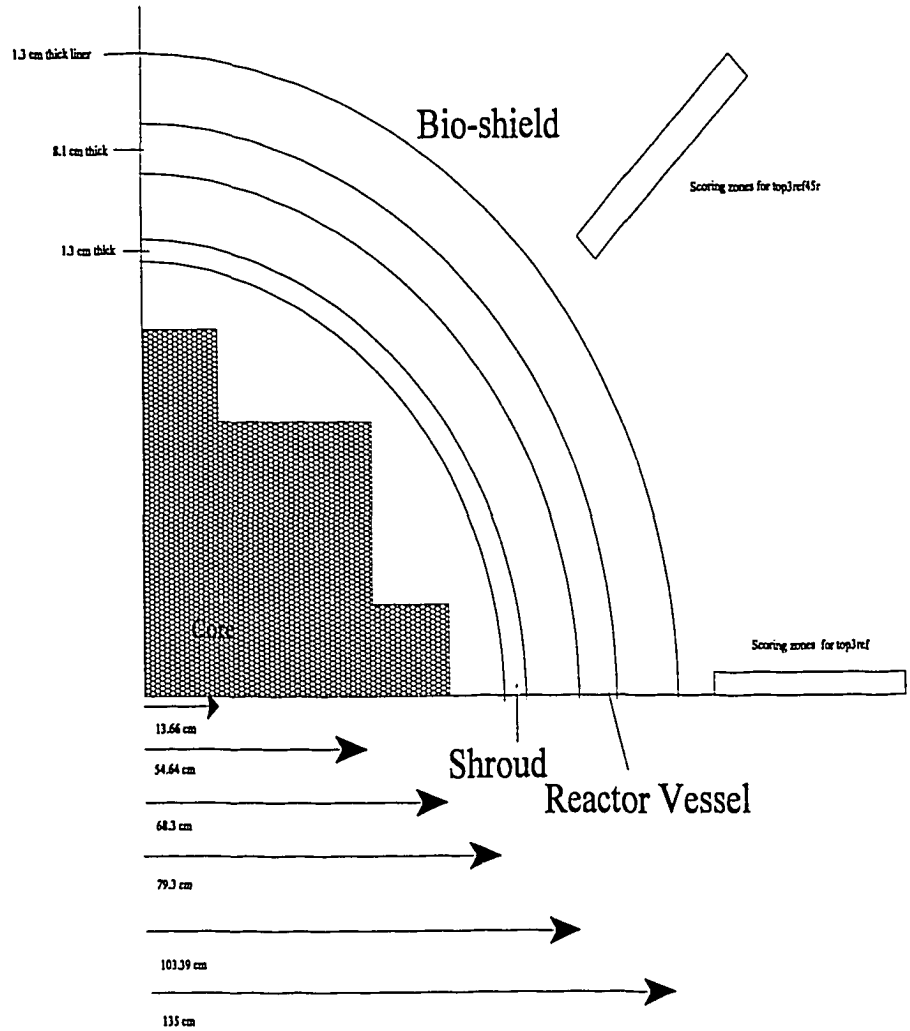

Figure 3 $^{59}Co(n,\gamma)$ reaction rates

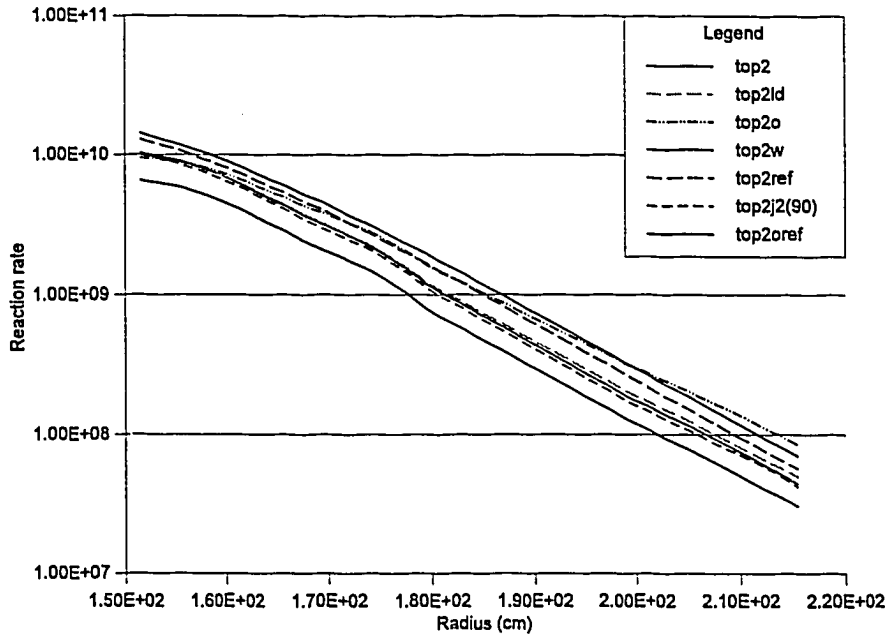

All cases include re-bars (unless stated)

top2 -	6.6% water content, concrete density of 2.33 g/cc, and Watt-Cranberg source.
top2ld -	As top2 but concrete density of 2.3 g/cc.
top2o -	5.1% water content, concrete density 2.3 g/cc.
top2w -	As top2, but water(1) density increased by 10%.
top2ref -	As top2, but no rebars etc.
top2j2(90) -	As top2, but with JEF2 material cross-sections, and IRDF90 response data.
top2oref -	As previous model described in Ref 2.

Figure 4 $^{133}Cs(n,\gamma)$ reaction rates

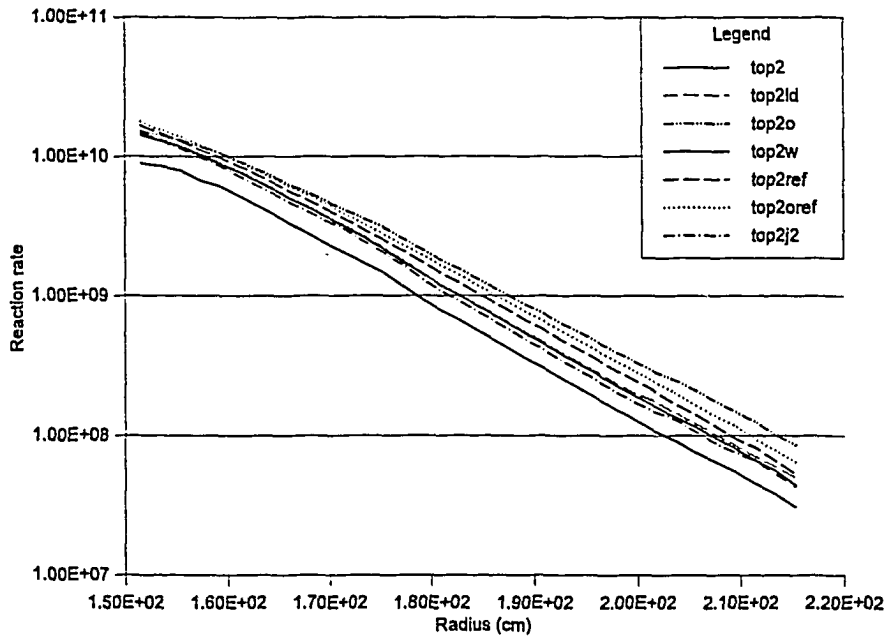

All cases include re-bars (unless stated)

top2 -	6.6% water content, concrete density of 2.33 g/cc, and Watt-Cranberg source.
top2ld -	As top2 but concrete density of 2.3 g/cc.
top2o -	5.1% water content, concrete density 2.3 g/cc.
top2w -	As top2, but water(1) density increased by 10%.
top2ref -	As top2, but no rebars etc.
top2j2 -	As top2, but with JEF2 material cross-sections, and IRDF90 response data.
top2oref -	As previous model described in Ref 2.

Figure 7 ^{60}Co activation in bioshield

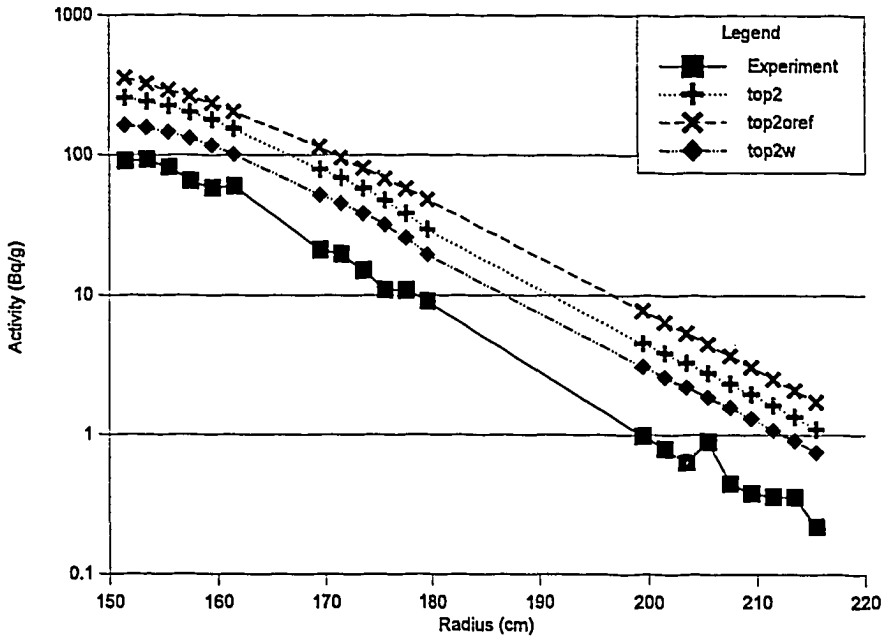

Figure 8 ^{134}Cs activation in bioshield

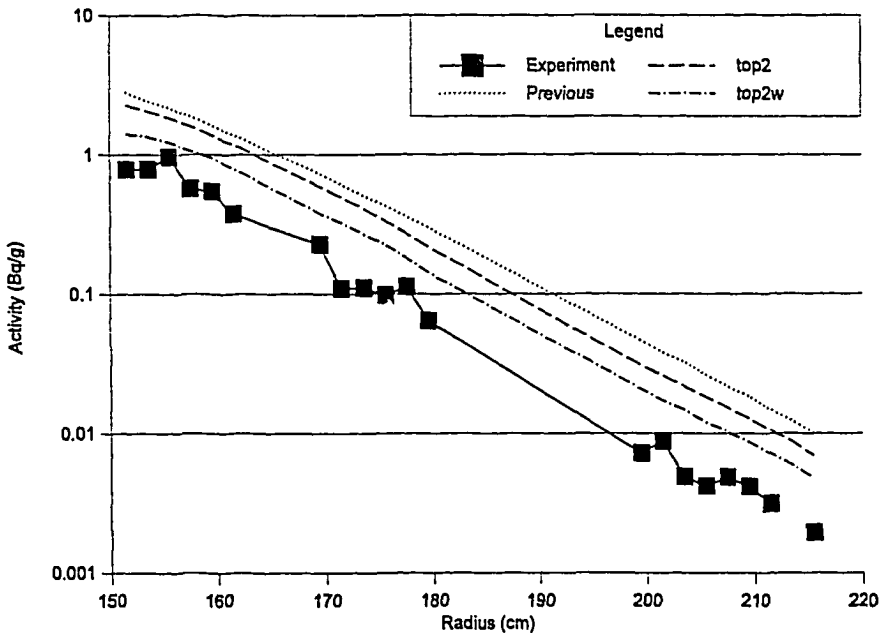

Figure 11 ^{60}Co activation in bioshield for 3D models

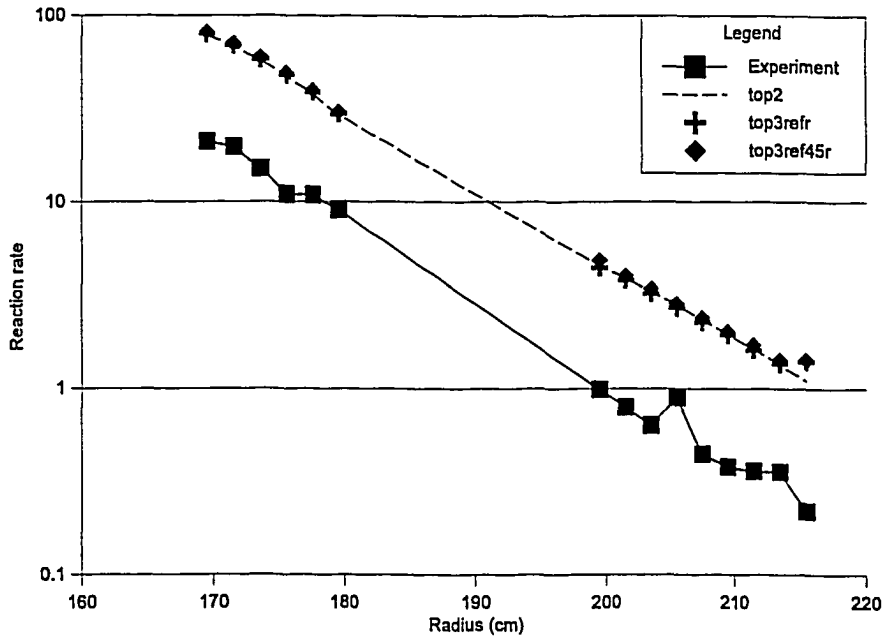

All cases include re-bars

top2 - 6.6% water content, concrete density of 2.33 g/cc, and Watt-Cranberg source.

top3ref - As top2, but 3-D source, samples opposite flat side of core.

top3ref45 - As top3ref, but samples opposite corner of core.

Figure 12 ^{134}Cs activation in bioshield for 3D models (z=340 cm)

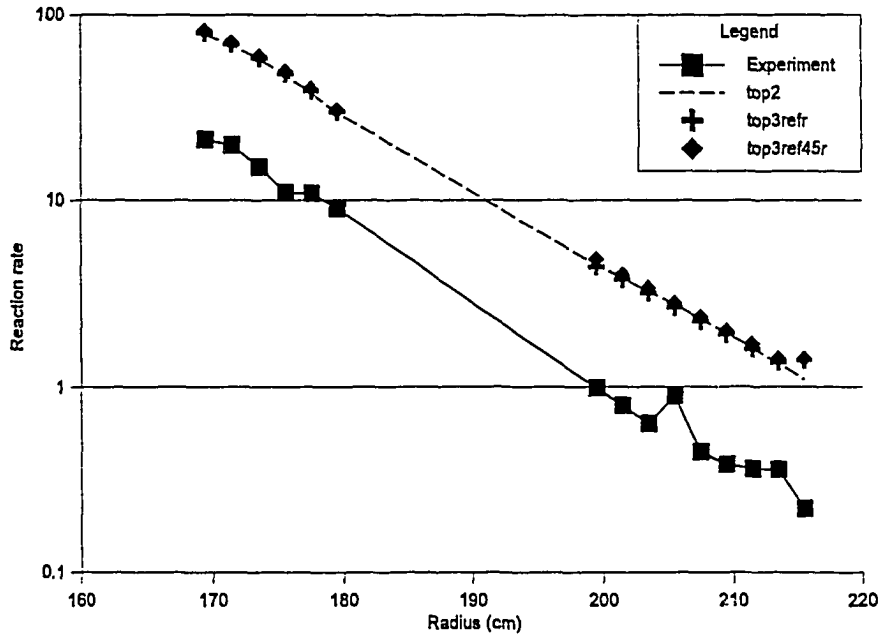

Figure 13 ^{60}Co activation in bioshield (2D model, z=475 cm)

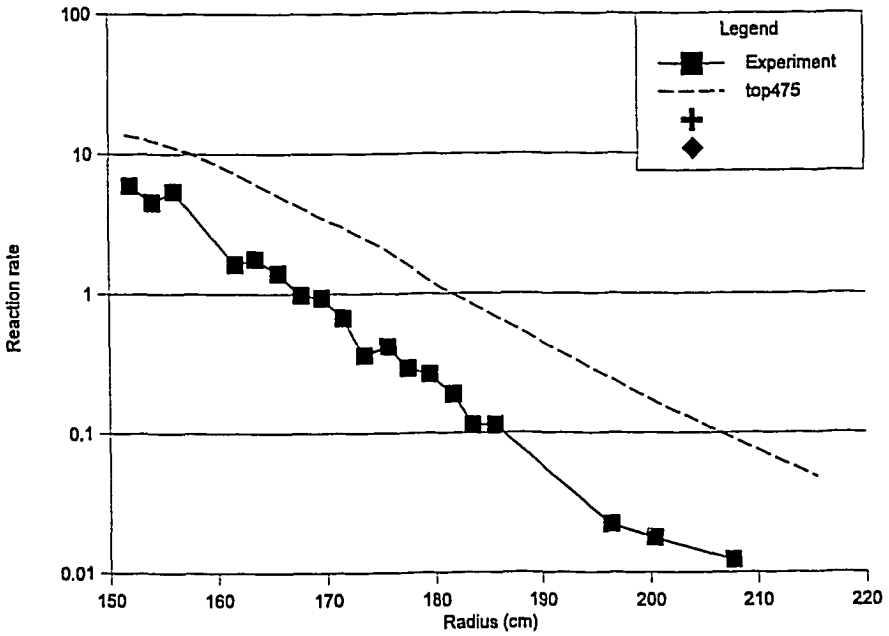

Results for Revised Biological Shield Configuration

B. L. Broadhead, R. L. Childs

Oak Ridge National Laboratory, USA

This paper updates previous work [1] and reports the approach and results for the revised JPDR biological shield.

APPROACH

A modified approach was taken in these updated analyses over the previous study. The previous approach to solving the reactor material activation problem was utilization of several SCALE[2] utility modules (MALOCS, NITAWL, WINE, and COUPLE) to effectively allow the creation of specific cross section libraries for arbitrary spatial points, each of which can then be analyzed using the point depletion code ORIGEN-S[2]. This approach allowed the study of one-dimensional (1-D) versus two-dimensional (2-D) neutron flux representations. The primary cross section libraries utilized in the previous study were the SCALE 27-neutron-group[2] set based on ENDF/B-IV data, and the VITAMIN-B6 library[3] in 199-neutron groups based on ENDF/B-VI. Due to size of this problem, only 27-group solutions were attempted in 2-D. In 1-D, both 27-group and 199-group solutions were obtained. While the 2-D results were in general agreement with other solutions, the 1-D broad-group and fine-group results differed by up to a factor of 2 from each other, indicating possible group structure effects for the discrepancies seen.

The current results are again based on the utilization of the same SCALE utility modules, however, the new procedure first determines a 1-D based spectrum in 199-groups then collapses the cross section library to 67-groups (effectively the BUGLE-93[3] structure with 20 additional thermal groups) and then performs a 2-D calculation in 67 groups. These 2-D fluxes are then used in the activation calculations for both the pressure vessel and biological shield.

RESULTS

Although only the biological shield configuration was updated, calculations were performed for both the pressure vessel and biological shield to incorporate both the new biological shield specifications and the updated calculational procedure described above. The latest results are presented in Figs. 1 and 2 for the pressure vessel and biological shield, respectively. These results are based on 2-D discrete ordinates calculations and are in general closer to the measurements than the previous results. The pressure vessel results in Fig. 1 match the measurements very closely at the front and near the back of the pressure vessel, while somewhat underpredicting the measurements in the middle of the vessel.

The biological shield predicted results in Fig. 2 are also closer to the measurements than the previous results, for the worst case approximately a factor of 4-5 higher as opposed to about a factor of 10 previously. Near the front of the biological shield the agreement between the calculations and measurements is quite good. As the distance into the shield increases, the predictions increase relative to the measurements. The improvement in the results while accounting for the rebar structure in the biological shield is encouraging, however, the agreement is still not very good near the outside of the shield.

RECOMMENDATIONS

Clearly, the effect of the rebar should have been taken into account in the original analyses, and the additional phase of this work was beneficial. There are definitely group structure effects in this problem, and it appears that all participants have sufficiently accounted for these effects. Perhaps a Monte Carlo analysis with point data would settle this for good, but I'm not completely convinced at this point that it is necessary. Based on the relatively good agreement in the pressure vessel and near the front of the biological shield, the calculational methods and models should be reasonably accurate. I believe that the source of this discrepancy must be in either the concrete/water densities or possibly a discrepant cross section in the concrete/water. The biological shield decreases the activities some 6 orders of magnitude, and hence a 10% change in a cross section can produce approximately a factor of 4 change in the activation near the back of the biological shield. A sensitivity analysis should allow for identification of possible primary contributors to the discrepancy, along with a combination with cross section or density uncertainty information to estimate the uncertainties in the calculated activities in the shield.

At the same time, it would be very useful to look at another facility to see if the trends noted in this study are common in other decommissioned plants. The U.S. has several decommissioned plants, but I do not know the availability of this data. In summary, my recommendations for further work in this area are as

follows:

(1) investigate sensitivity/uncertainties in the JPDR biological shield for possible explanations of the observed discrepancies.

(2) study another plant to see if the JPDR trends are observed elsewhere.

Thanks for inviting our participation in this IAEA activity. I look forward to continued discussions with you regarding this activity, either by electronic means or a meeting if you deem it necessary.

REFERENCES

1. Letter from B. L. Broadhead to N. Kocherov, December 2, 1994.

2. "*SCALE*: A Modular Code System for Performing Standardized Computer Analyses for Licensing Evaluation," NUREG/CR-0200, Rev. 4 (ORNL/NUREG/CSD-2/R4), Vols. 1-3, draft February 1990. Available from Radiation Shielding Information Center as CCC-545.

3. D. T. Ingersoll, et al., "Production and Testing of the VITAMIN-B6 Fine-Group and the BUGLE-93 Broad-Group Neutron/Photon Cross-Section Libraries Derived form ENDF/B-VI Nuclear Data," Oak Ridge National Laboratory, ORNL-6795 (1994).

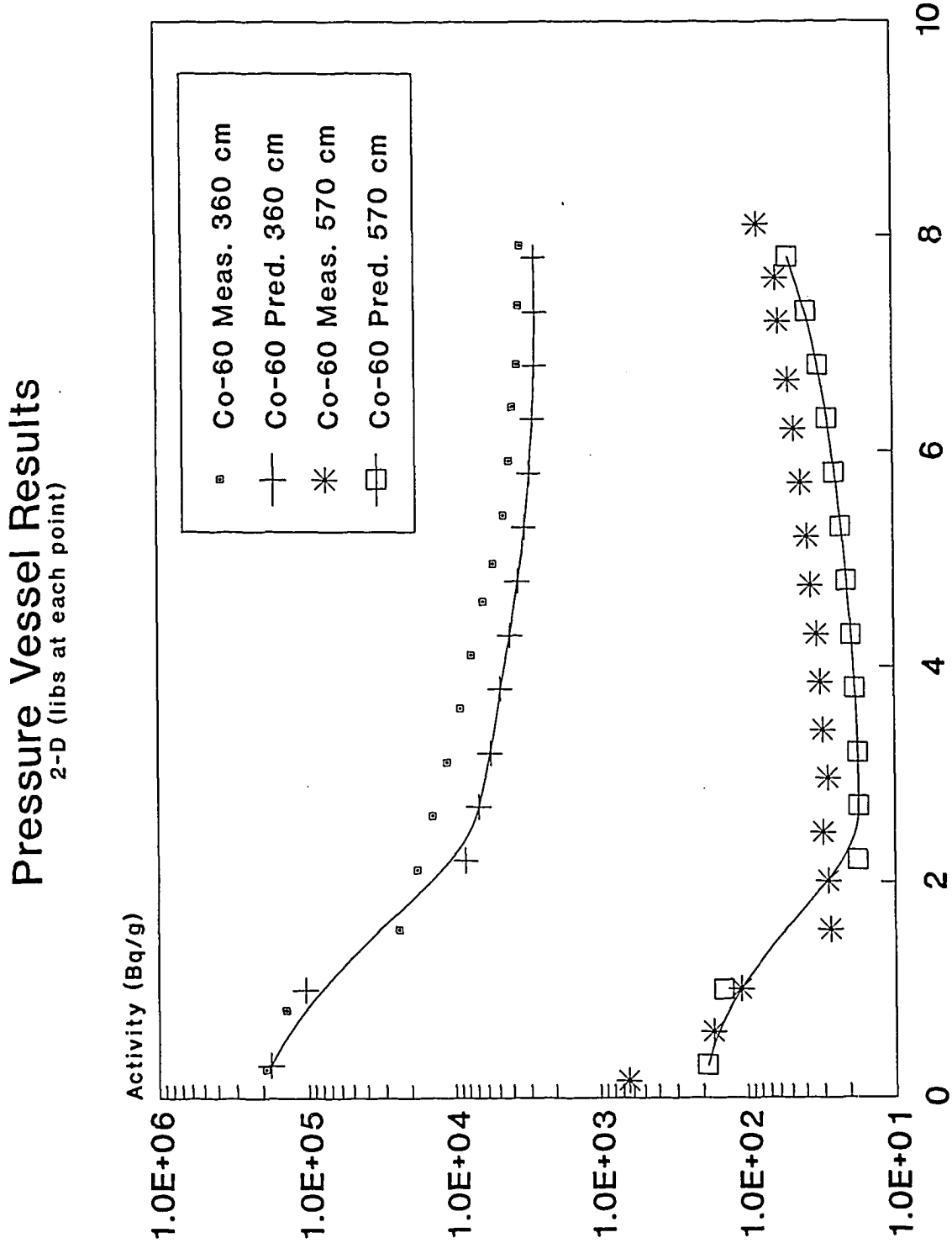

Figure 1: Two-dimensional ^{60}Co activation predictions in the JPDR pressure vessel

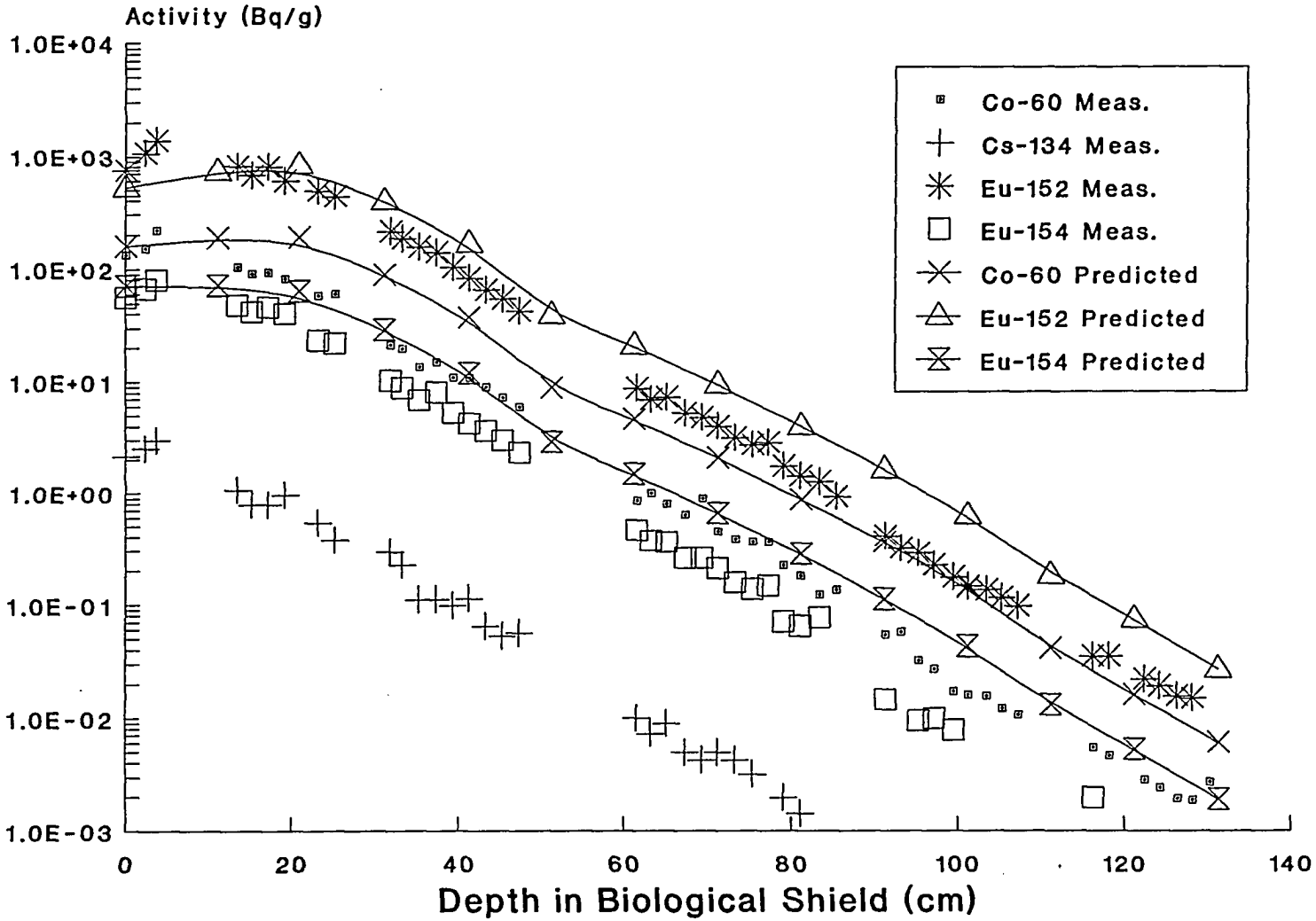

Figure 2: Two-dimensional activation predictions in the JPDR biological shield

XA9642548

UMass-Lowell Results of the IAEA Benchmark Calculation of Radioactive Inventory for Fission Reactor Decommissioning

Dr. John R. White and Mr. Andrew P. Fyfe
Chemical and Nuclear Engineering Department
University of Massachusetts-Lowell, Lowell, Massachusetts 01854

July 7, 1995

Introduction/Overview

In January 1994, the University of Massachusetts Lowell (UMass-Lowell) was invited by the International Atomic Energy Agency (IAEA) to participate in an international benchmark exercise to address the adequacy of current cross section data and computational methods for quantifying neutron activation in the excore regions of commercial power reactors.[1] The ability to accurately predict the inventory of several relatively long-lived radioactive isotopes that result from years of exposure to a neutron environment is of critical concern for planning and executing a rational, safe, and economical decommissioning strategy.

The central focus of the benchmark exercise involved comparison of calculated results to measured activation data from the Japan Power Demonstration Reactor (JPDR).[2] The available experimental data include radial and axial activity profiles at various locations in the excore structure and bioshield materials for several important radioactive isotopes (^{60}Co, ^{54}Mn, ^{55}Fe, etc.). The benchmark exercise required the development of detailed computational models of the JPDR based on the geometry, material, and operational data supplied in Refs. 2 and 3, and the calculation of the space and energy dependent neutron flux throughout the model (using discrete ordinates transport theory). The induced activities at several desired locations were then computed with a newly-developed space-energy activation analysis code called ACTIV. This code uses the power history of the JPDR to normalize the pointwise multigroup neutron fluxes from the transport calculations to compute the time-dependent inventory of the important activation products in any desired location outside the active core region. ACTIV uses an ENDF/B-VI multigroup activation cross section library that is fully compatible with the group structure used within the transport calculations. The results from the ACTIV code were then compared to measured activation data from the JPDR decommissioning program.

The purpose of this report is to document the UMass-Lowell results for the JPDR activation analysis benchmark. The report first documents the data and methods incorporated within the actual codes utilized in the analysis, highlighting, of course, the new ACTIV code and its integration within an existing code system for performing excore and ex-vessel transport theory computations.[4] The details of our specific RZ geometric models of the JPDR configuration within the context of the DORT discrete ordinates transport code[5] are also reviewed, as well as the development of the absolute

normalization of the neutron source distribution used to drive the DORT fixed-source computations.

Important neutron flux data from the DORT analyses are summarized into three groups (fast, epi-thermal, and thermal) for efficient presentation of these data. However, the full multigroup fluxes (47 groups for the DORT 2-D analyses) were utilized with a compatible activation cross section library within ACTIV to produce activities for several key isotopes. The computed activities are compared directly with the JPDR measured data given in Ref. 2. These calculated-to-experimental comparisons are made at various radial and axial locations within the excore regions of the JPDR, and they show relatively good agreement for all the measured isotopes out through the pressure vessel region. Some significant discrepancies, however, are observed at relatively large distances within the concrete bioshield.

Preliminary results from this benchmark exercise were reviewed at an IAEA Consultant's Meeting in December 1994. All participants had roughly similar results, especially with the generally poor agreement between measured and computed activities in the bioshield region. Several questions were raised concerning the simplified bioshield geometry data given in Ref. 2, and subsequent correspondence[3] has identified additional geometry details, including the location and number of cooling tubes and rebar structural reinforcements within the bioshield region.

Based on data from Ref. 3, a new bioshield model was constructed and the results from this model (which is referred to as the Case B model) are given here as the best UMass-Lowell results to date for the JPDR activation benchmark. Some comparisons to the results from the original model (referred to as the Case A model), which was based entirely on Ref. 2, are also included to highlight the improvement obtained with the more detailed bioshield representation. However, although significant improvements were achieved, some large discrepancies are still apparent within the concrete bioshield.

Several sensitivity studies have been initiated in a continuing attempt to resolve the bioshield discrepancies. At present, it appears that much of the observed error may be due to poor energy detail at low energies in the current computations. Some 1-D fine group calculations (with several thermal groups) have been performed and they suggest that the 47-group BUGLE-93 library[6] is simply not adequate for accurately determining the thermal flux in the vessel-cavity-bioshield regions. Preliminary results from this work are briefly summarized at the end of this report, with a focus on the future work that is clearly needed to resolve this issue.

Data, Methods, and Codes

The nuclear data needed for neutron activation studies fall into two general categories:

1. multigroup neutron cross sections for use in the transport calculations to compute the space and energy dependence of the neutron flux, and

2. multigroup activation cross sections (n,γ, n,p, n,2n, etc.) and decay data (natural abundances, halflifes, branching fractions, etc.) for all the important parent and daughter isotopes that can be generated via neutron activation.

If possible, the transport calculation and the activation analysis should be done with a consistent set of multigroup data. However, in practice, the two calculations are often done independently and are only loosely connected via a set of collapsed neutron flux information from the transport calculation that is used in zero-dimensional few-group codes that model and simulate the isotope transmutation schemes. Usually significant detail is lost in this space and energy collapsing process, which can lead to large uncertainties in the computed activities. This is especially true in regions where rapid changes in the neutron spectra cannot be treated adequately in a zero-dimensional model. In addition, the coupling process is often somewhat cumbersome, since it usually requires a fair amount of manual intervention.

The new ACTIV code, which was developed recently at UMass-Lowell, eliminates this separate coupling and collapsing process by simply performing the activation calculations with the full space and energy dependent fluxes from the transport code. The same geometry is modeled and the user can select any number of pointwise radial and axial traverses or zone average activations that he or she desires. Thus, all of the space-energy detail from the original transport calculation is preserved and included within the activation calculation – thereby, essentially removing all the uncertainty that is introduced in the traditional two-step process. Now, the only uncertainties remaining are those associated with the computed neutron fluxes, the base activation data used within the ACTIV code, and, of course, the initial impurity concentrations present in the unirradiated structural materials.

The UMass-Lowell JPDR benchmark computations used the DORT code[5] for the transport calculations and the ACTIV code for the activity computations. The BUGLE-93 library[6] was used for all the 2-D transport calculations within DORT. The BUGLE-93 data include information for 120 isotopes/materials in 47 neutron groups and 20 gamma groups. This broad-group data set was collapsed from the VITAMIN-B6 fine-group library which contains 199 neutron group and 42 gamma group information derived from the ENDF/B-VI nuclear data files.[6] The BUGLE-93 library was designed specifically for shielding applications focusing on fast neutron and gamma transport analyses, vessel damage studies, excore dosimetry evaluations, etc., and it is not considered a very reliable data base for determining thermal fluxes, thermal reaction rates, and thermal neutron activation – since there are only two energy groups below 0.4 eV. However it has several positive attributes including the fact that it contains the latest ENDF data, it is readily available to the user community, and it already has a wide user base. In addition, the generation of a new multigroup library, that includes all the features of BUGLE-93 with greater thermal energy detail, was well beyond the scope of work for performing this benchmark analysis. Thus, it was decided that BUGLE-93 would be used exclusively for the 2-D DORT computations – and that the results of this exercise would be a good test of the utility of the BUGLE-93 library for general activation studies.

UMass-Lowell Results for JPDR Activation Benchmark

For full consistency, the activation cross sections used within ACTIV were also derived from VITAMIN-B6. The 199-group neutron data from the fine-group library were collapsed to the BUGLE-93 47-group structure using the same concrete weighting spectrum utilized in the generation of BUGLE-93 from VITAMIN-B6. Eight separate reaction cross sections were extracted from the collapsed library and stored in a format suitable for use in ACTIV. The specific reactions and the associated ENDF MT numbers that are included in the ACTIV activation library are listed below:

ENDF MT No.	102	107	103	16	104	105	18	27
Reaction	n,γ	n,α	n,p	n,2n	n,d	n,t	n,f	n,abs

For the activation calculations, in addition to the neutron cross sections, natural isotopic abundances, decay data, and appropriate branching fractions are also needed. These data were obtained from the ENDF/B-VI version of the ORIGEN data libraries that are distributed as part of the SCALE 4.2 package.[7] The necessary data were extracted from the ORIGEN data files and incorporated into the activation library used within ACTIV.

The final activation library, called VB6ACTXS.LIB, has all the required nuclear data for subsequent activation analyses within ACTIV. This library contains base information for approximately 800 isotopes (nuclides from the ORIGEN data files), but it only has activity cross sections for about 100 isotopes (nuclides from the VITAMIN-B6 library). However, as new cross section information for additional isotopes becomes available (in the VITAMIN-B6 master library format), it can be incorporated within VB6ACTXS.LIB quite easily.

A simplified schematic that illustrates the development of the activation library used within ACTIV is shown in Fig. 1. This figure summarizes the various steps involved in the generation of VB6ACTXS.LIB. Most of the codes mentioned (MALOCS, NITAWL-II, ALPO, and ORIGEN) are part of the SCALE 4.2 package.[7] ACTXS, the last code in the sequence, was written at UMass-Lowell to integrate all the necessary nuclear data into a single file, VB6ACTXS.LIB, for use in ACTIV.

The ACTIV code itself uses the traditional matrix exponential technique for solution of the nuclide transmutation equations. The primary computational algorithms for the matrix exponential method were taken from the DEPTH-CHARGE modules of the VENTURE code system.[8-9] The ACTIV code simply reads the appropriate nuclide chain information, geometry data, initial isotope densities, and operational power versus time data and, using the precomputed space-energy fluxes from DORT and the nuclear data from VB6ACTXS.LIB, computes the time-dependent isotope inventories for each spatial point or zone of interest. The data flow and interaction between DORT and ACTIV are illustrated in Fig. 2. The summary edit from ACTIV gives the activity in Bq/g for the desired isotopes, spatial locations, and time points. These data can then be plotted or tabulated for further analyses – which, in the present JPDR benchmark study, involves direct comparison to the measured data from Ref. 2.

UMass-Lowell Results for JPDR Activation Benchmark

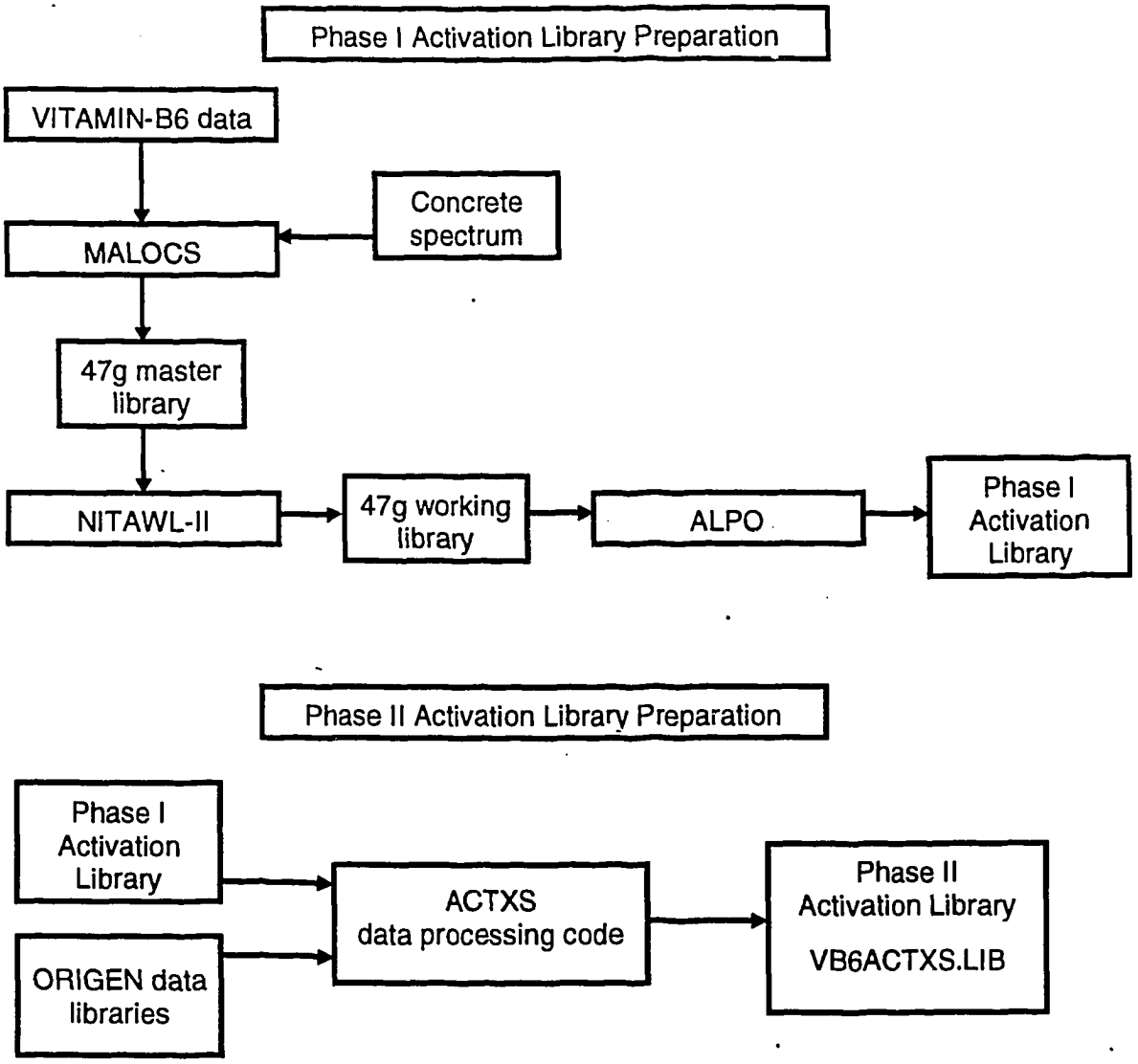

Fig. 1. Simplified schematic showing the development of VB6ACTXS.LIB.

JPDR Modeling Within DORT

The bulk of the effort needed for performing the JPDR benchmark analyses was related to the development and execution of the DORT models that were used to compute the space-energy distribution of the flux throughout the system. The Japan Power Demonstration Reactor (JPDR) was a direct-cycle BWR with dimensions that spanned over 12 m axially and 4 m radially. The reactor operated intermittently with varying power level over a period of about 13 years, from 1963 to 1976, with a total reactor thermal output of 21,500 MWD.

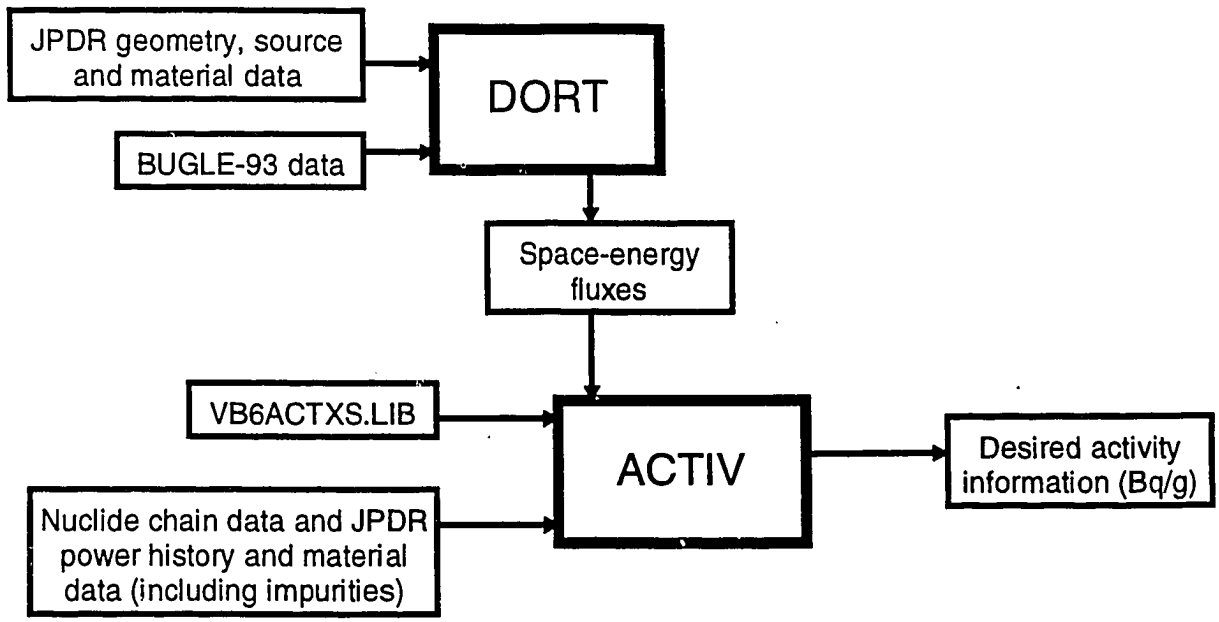

Fig. 2. Data flow and interaction between DORT and ACTIV.

After making a series of drawings of the reactor based on data from Ref. 2, it was apparent that the overall computational model would have to be broken into multiple sections axially, since a single DORT calculation with sufficient detail would be totally impractical. Therefore, the 12.2 m axial dimension was broken into three regions and labeled accordingly, with Region 1 at the bottom and Region 3 at the top. A bootstrapping technique, which couples one axial region to another via a saved internal boundary source is envisioned as a mechanism to complete the full benchmark computation.

An overall radial dimension of 3 m was used in the DORT models, with the radial fine mesh layout remaining the same in each axial model so as to maintain spatial continuity from one axial region to the next. This continuity is required for proper alignment of the saved boundary sources that couple the axial models. The axial locations of the saved boundary sources are in relatively homogeneous regions well above and below the active core zones. These locations seem very reasonable, since they allow regions of practical size to be modeled while, at the same time, placing the boundary sources in regions relatively far away from structural materials where backscatter may be important.

Modeling of the JPDR started at Region 2 which contains the core, and hence, the neutron source which drives the entire model. This is the only computation that has been completed at present. However, internal sources were saved at an axial distance of about 100 cm from the top and bottom boundaries of the model. These sources can

be used to continue computations into the upper and lower structural regions of the JPDR configuration, if desired.

The Region 2 RZ geometric models in DORT spanned a radial distance of 300 cm and an axial dimension of about 410 cm. As mentioned earlier, two separate cases have been treated:

Case A – has a simple bioshield geometry consisting of only the homogeneous concrete region as given in Ref. 2 (has a 109 x 123 mesh grid).

Case B – has a concrete bioshield containing explicit zones that account for several cooling tubes and structural rebar reinforcements (has a 118 x 123 mesh grid).

The Case B model represents a better model of the actual JPDR configuration (with bioshield data from Ref. 3).

The DORT mesh layouts for the two cases are shown in Figs. 3 and 4, respectively for Cases A and B, where the dark heavy lines represent major material or component boundaries and the two horizontal dark dashed lines identify where the internal boundary sources were saved for subsequent computations above and below Region 2. Notice that the boundary source locations were chosen about 100 cm from the physical model boundaries so that the choice of boundary conditions on the top and bottom surfaces in the central model have little effect on subsequent calculations. Reflected boundary conditions were employed on the left and right and vacuum conditions were imposed on the top and bottom of the Region 2 RZ models.

The material compositions for the various regions highlighted in Fig. 3 for the Case A model were taken directly from Table A.2 in Ref. 2. Identical composition data were used for the Case B model, except for the more explicit modeling in the bioshield region. Table I shows the concrete, steel, and water volume fractions used in the Case B bioshield model (derived from Ref. 3). The Zone 1 - 9 designations in the table map to the nine explicit regions identified in Fig. 4 within the bioshield. These are the single-mesh zones within the heavy lines and they are numbered from left to right, not counting the concrete liner. The 10th zone in Table I is pure concrete and this material occupies all the remaining bioshield regions (with multiple mesh per region). The concrete compositions are identical for Cases A and B, with material densities obtained from Ref. 2.

The material composition data for the various regions and the material IDs from the BUGLE-93 library were used as part of the mixing table within GIP[5] to create a set of 47-group macroscopic cross sections for use within the DORT transport calculations. Although scattering expansions up to 5th order are available within the BUGLE-93 library, only P_3 data were used in these benchmark calculations.

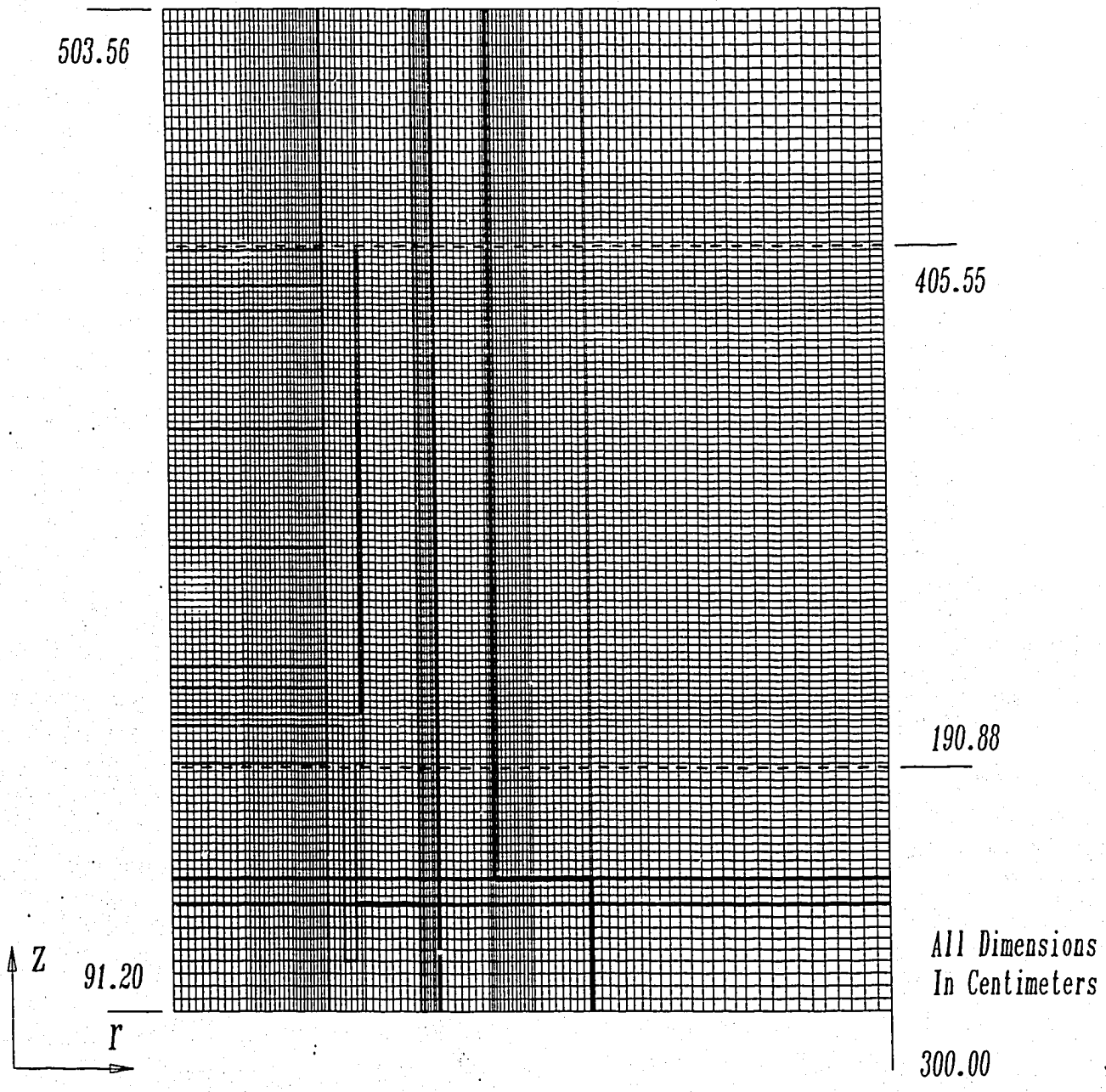

Fig. 3. DORT mesh structure for the JPDR Case A model.

UMass-Lowell Results for JPDR Activation Benchmark

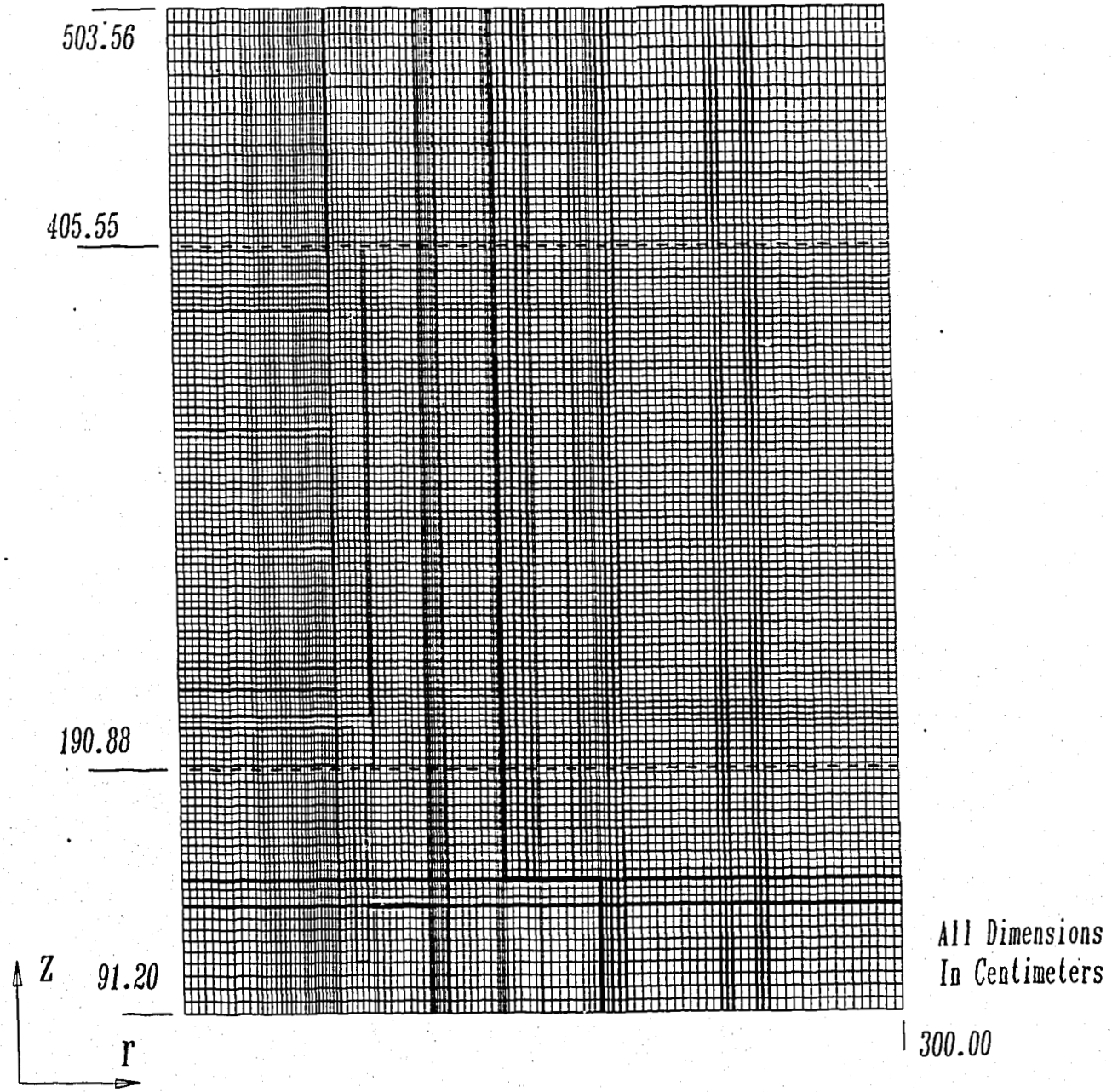

Fig. 4. DORT mesh structure for the JPDR Case B model.

UMass-Lowell Results for JPDR Activation Benchmark

Table I. Volume fractions for Case B bioshield model.

		Volume Fractions		
Zone #	Description	Concrete	Steel	Water
1	vertical rebar & cooling pipes w/o water*	0.6928	0.1138	0.0000
2	horizontal rebar	0.8482	0.1518	0.0000
3	vertical cooling pipes with water	0.8466	0.0552	0.0982
4	vertical rebar	0.8841	0.1159	0.0000
5	horizontal rebar	0.8482	0.1518	0.0000
6	vertical rebar	0.9337	0.0663	0.0000
7	horizontal rebar	0.9346	0.0654	0.0000
8	horizontal rebar	0.9346	0.0654	0.0000
9	vertical rebar	0.9333	0.0667	0.0000
10	concrete regions	1.0000	0.0000	0.0000

*Since there is no water within the pipes, the volume fractions sum to less than unity.

Because of the size of the computational model, a variable quadrature scheme within DORT was adopted to help cut back on the overall computational time. An S_{16} symmetric quadrature was maintained on both sides of the internal boundary source locations for fine angular detail in these regions. The S_{16} set was also used near the core periphery and radially outward through the cavity to a short distance in the bioshield. These are the zones of most interest in the Region 2 model. In particular, the angular discretization approximation in the cavity region is especially important since axial streaming up and down the voided cavity becomes the dominant source of neutrons to all regions adjacent to the cavity. All remaining areas in the model used a symmetric S_8 quadrature set – including the central core, outer bioshield, and regions well above (top) and below (bottom) the internal boundary source lines. Preliminary calculations with a single S_{16} quadrature throughout the full model verified the validity of the variable quadrature approximation. Therefore, all calculations reported herein used the variable quadrature option within DORT, with about a 20% reduction in run time relative to the full S_{16} case.

The final information necessary to run DORT was the space-energy source distribution within the core region of the JPDR models. Numerical estimates of the spatial source distribution were obtained from Figs. A.2 and A.3 in Ref. 2. A spline fit to the discrete radial and axial profiles produced a continuous distribution and, with this information, the relative source strength associated with the specific mesh spacing

utilized in the UMass-Lowell JPDR models was obtained. The RZ spatial source distribution is then simply the product of the radial and axial profiles, S(r,z) = S(r)*S(z).

The source energy spectrum for the 47-group computations was obtained by integrating the Watt fission spectrum over the appropriate 47-group energy grid. Finally, the total source was normalized such that 1 MW of thermal power is generated within the core. Using typical values for the energy per fission (κ = 200 MeV/fiss) and average number of neutrons per fission (ν = 2.5 n/fiss), the source normalization factor in DORT for a power of 1 MW is

$$XNF = \frac{\nu}{\kappa}P = \left(\frac{2.5\ n/fiss}{3.204\times10^{-11}W-s/fiss}\right)\left(10^{6}W\right) = 7.803\times10^{16}n/s$$

Note that the actual power level at any specific time is handled within ACTIV via a simple time-dependent normalization of the absolute flux for the 1 MW power case.

With all the necessary data defined, the DORT calculations were made with a pointwise convergence criterion in the important regions of 0.001. The full space and energy dependent scalar flux data were saved for subsequent use in ACTIV. In addition, some post-processing of the multigroup data – collapsing of the data to three broad groups – was performed for summary presentation of key radial and axial flux profiles. Of particular interest were the profiles in the locations where measured activity data are available.

Figures 5 and 6 show typical radial and axial broad-group flux profiles obtained from the JPDR Region 2 Case B computational model. Group 1 represents fast neutrons above 0.1 MeV, Group 3 is the thermal group with energies below 0.4 eV, and Group 2 covers all energies between these limits. The radial profiles in Fig. 5 are for a height of 360 cm, which corresponds to the location where the measured horizontal distribution of the ^{60}Co activity within the pressure vessel is available. The axial profiles in Fig. 6 are taken at the radial location corresponding to the first mesh point in the concrete bioshield.

Although the profiles in Figs. 5 and 6 behave qualitatively as expected, they also illustrate, quite nicely, the rapid change in neutron spectrum that occurs at various locations throughout the excore regions. The most dramatic example, of course, is the very large attenuation of the thermal flux in the vessel – which has a significant impact on the effective activation cross section versus distance within the vessel. A similar rapid change in the flux spectrum occurs within 20-30 cm of the bioshield, but , in this case, the thermal flux is increasing, rather than decreasing, relative to the epithermal and fast fluxes. These spectral shifts are also seen in the axial direction, although the observed changes are certainly not as severe as in the radial direction.

The impact of these spectral shifts can be illustrated by computing the effective activation cross sections versus position, taking into account the explicit change in the multigroup weight function at each spatial point. A good example is given in Fig. 7

UMass-Lowell Results for JPDR Activation Benchmark

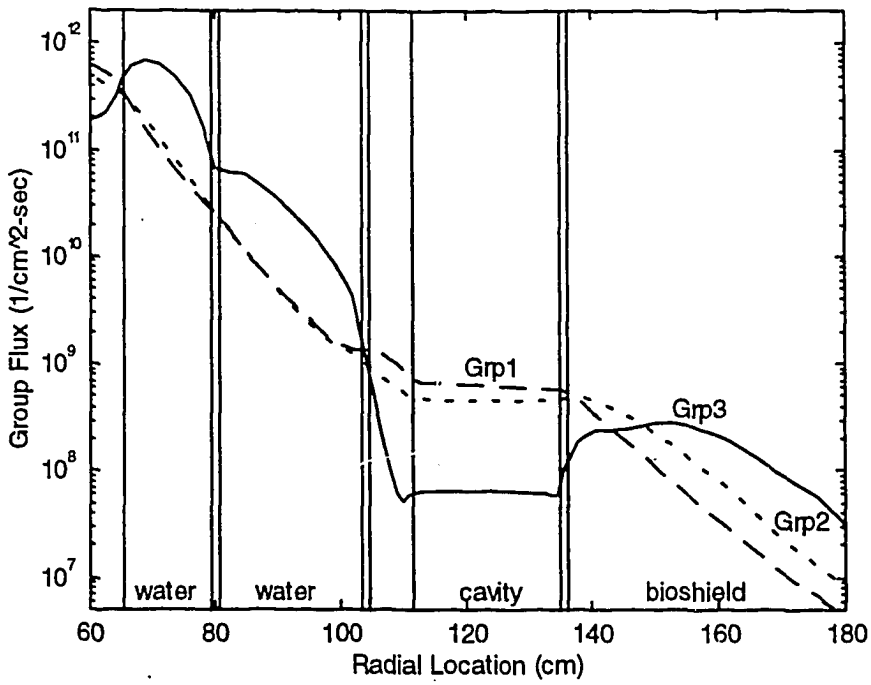

Fig. 5. JPDR broad-group radial flux profiles at H = 360 cm.

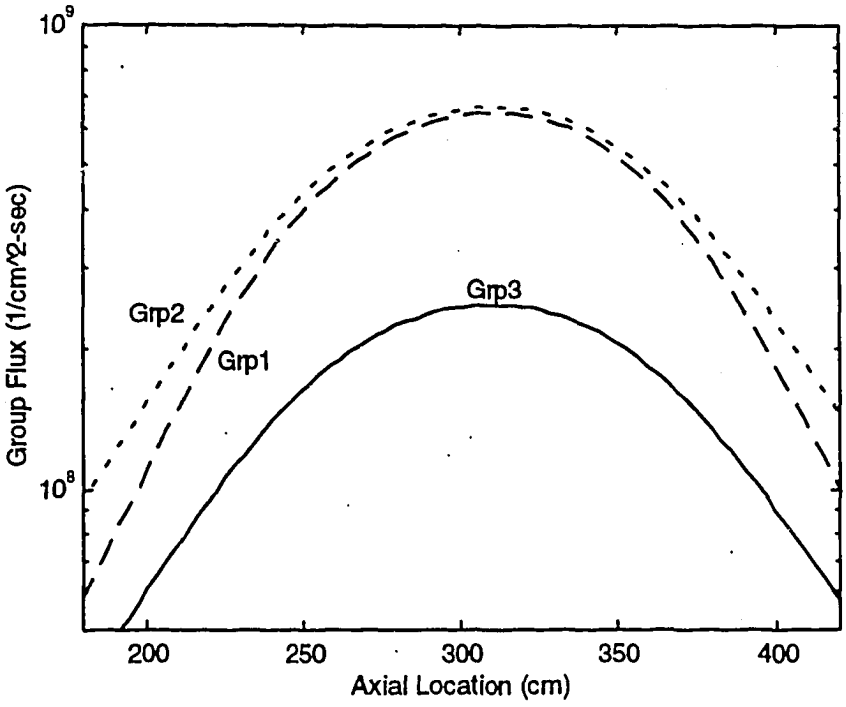

Fig. 6. JPDR broad-group axial flux profiles at inner surface of bioshield.

which shows the effective ^{59}Co n,γ cross section versus radial position at an axial height of 360 cm in the Case B JPDR model. Note that the 1-group average cross section varies by about a factor of 4-5 in the two regions shown in Fig. 7 (pressure vessel and bioshield regions). This phenomenon is certainly significant and it must be treated with reasonable care if reliable activation calculations are desired. Since the ACTIV code models this space-energy coupling in full detail, all the uncertainty related to the use of zone and energy averaged cross sections in the usual zero-dimensional activation analysis is eliminated completely.

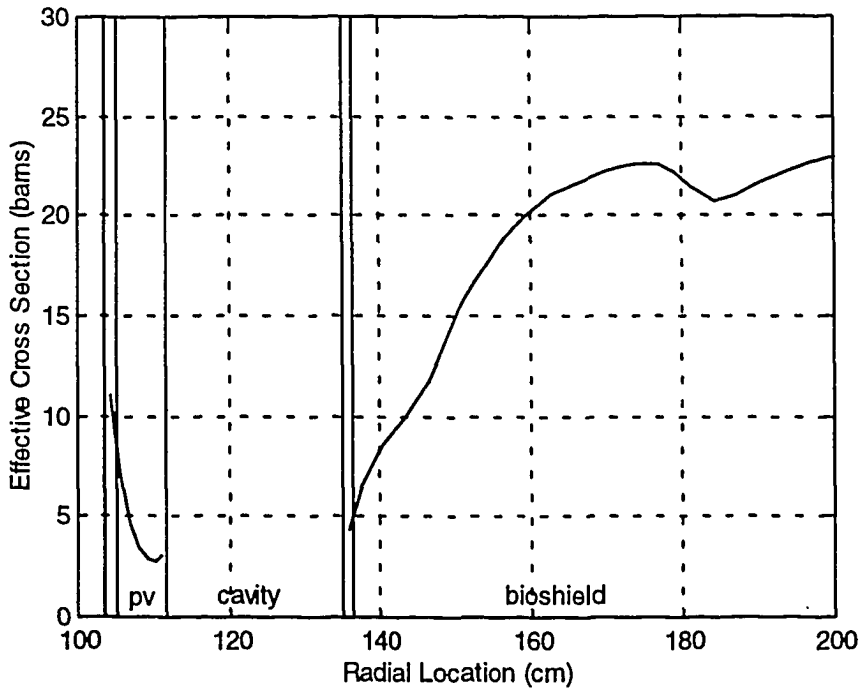

Fig. 7. ^{59}Co 1-group n,γ cross section at H = 360 cm in JPDR.

Activation Analysis Results

Using the 47-group fluxes from the DORT cases and the 47-group activation cross sections in VB6ACTXS.LIB, ACTIV was run using the chain and decay data given in Table II and the initial parent densities given in Table III. Note that the current calculations focus on the activities associated with ^{54}Mn, ^{55}Fe, ^{60}Co, ^{63}Ni, ^{152}Eu, and ^{154}Eu because these were measured as part of the experimental program in the JPDR. The activity of ^{134}Cs was also measured at selected locations within the bioshield, however, its parent isotope, ^{133}Cs, is not available in the current VITAMIN-B6 library. Therefore, the activity associated with ^{134}Cs could not be included in this study.

UMass-Lowell Results for JPDR Activation Benchmark

Table II. Nuclide chain and decay data used in ACTIV.

Parent Isotope	Abundance (a/o)	Daughter Isotope	Halflife (days)	Process
^{54}Fe	5.81	^{54}Mn	3.1215+2	n,p
^{54}Fe	5.81	^{55}Fe	9.9711+2	n,γ
^{59}Co	100	^{60}Co	1.9248+3	n,γ
^{62}Ni	3.59	^{63}Ni	3.6562+4	n,γ
^{151}Eu	47.9	^{152}Eu	4.8680+3	n,γ
^{153}Eu	52.1	^{154}Eu	3.1377+3	n,γ

Table III. Initial parent densities for various activation materials in the JPDR.

Parent Isotope	SUS27 Core Shroud		ASTM-A167 Vessel Clad		ASTM-A302B Pressure Vessel		Bioshield Concrete	
	7.90 g/cc		7.90 g/cc		7.85 g/cc		2.30 g/cc	
	w/o or ppm	atom density	w/o or ppm	atom density	w/o or ppm	atom density	w/o or ppm	atom density
^{54}Fe	70.7*	3.495-3	71.4*	3.530-3	97.4*	4.785-3	1.9*	2.735-5
^{59}Co	1300	1.048-4	1200	9.677-5	200	1.603-5	6.2	1.456-7
^{62}Ni	9.2*	2.675-4	9.8*	2.849-4	0.55*	1.589-5	.0013*	1.100-8
^{151}Eu							0.59	2.575-9
^{153}Eu							0.59	2.801-9

* These entries represent weight percent and the remaining (unstarred) values in this list have units of parts per million (ppm), where both the w/o and ppm values refer to the naturally occurring material (not the specific isotope). Also, the atom densities are in atoms/b-cm.

The abundances and decay data in Table II came directly from the ORIGEN data libraries from SCALE 4.2.[7] The initial parent concentrations in Table III were taken from Table 2 of Ref. 2. These data were then converted to atom densities (atoms/b-cm) for use in ACTIV. For example, if the base information is given in weight percent, one has

$$N_{ij} = \rho_j \times \frac{w_{kj}}{100} \times \left(\frac{a_i}{100} \times \frac{MW_i}{MW_k} \right) \times \frac{.60225}{MW_i}$$

where

N_{ij} = atom density (atoms/b-cm) of isotope i in material j
ρ_j = mass density (g/cm^3) of material j
a_i = atom percent abundance of isotope i in element k
w_{kj} = weight percent of natural element k in material j
MW_i = molecular weight of isotope i (g)
MW_k = molecular weight of isotope k (g)

If parts per million (ppm) is given instead of weight percent (w/o), one simply replaces (w_{kj}/100) with ($ppm_{kj}/10^6$) in the above equation.

The power versus time history for the ACTIV calculation was taken from Fig. A.4 of Ref. 2. There were ten alternating periods of constant power operation and full shutdown, with the last shutdown period lasting 15 years. This latter time interval represents the time from when the reactor was shutdown permanently to when the activation measurements were made. The total simulation time, from initial startup of the JPDR to the measurement time, was 10011.8 days. Thus, all subsequent activation results are reported for this point in time (relative to startup at time zero).

With all this background to establish some specificity to the actual computations that were performed, we can now finally show some of the calculated activities, with a direct comparison to the data measured in the JPDR decommissioning program. The comparisons are broken into two parts:

Radial Profiles

Fig. 8 ^{60}Co activity in pressure vessel at H = 360 cm for Case A
Fig. 9 ^{60}Co activity in pressure vessel at H = 360 cm for Case B
Fig. 10 ^{60}Co activity in bioshield at H = 340 cm for Case A
Fig. 11 ^{60}Co activity in bioshield at H = 340 cm for Case B
Fig. 12 ^{152}Eu activity in bioshield at H = 340 cm for Case B
Fig. 13 ^{154}Eu activity in bioshield at H = 340 cm for Case B

Each figure comparing the calculated and experimental radial activities has two components. The first part shows a plot of the absolute activities, with the circles representing the measured values and the solid line giving the computed values. The second figure in each set displays the behavior of the ratio of the calculated-to-experimental value (C/E value) with the asterisks showing the actual C/E value at each measurement location and the solid line representing a low-order best fit to these individual points. For the pressure vessel (see Figs. 8 and 9), a quadratic fit was used and, in the bioshield (see Figs. 10-13), a simple linear fit was used for all three cases shown (^{60}Co, ^{152}Eu, and ^{154}Eu).

Axial Profiles for Case B

Fig. 14 ^{60}Co activity at inner surface of core shroud and reactor vessel
Fig. 15 ^{55}Fe activity at inner surface of core shroud and reactor vessel

UMass-Lowell Results for JPDR Activation Benchmark

For the axial comparisons, the plots are also grouped in pairs; this time according to specific isotope. In particular, Figs. 14a and 14b look at the absolute ^{60}Co activities at the inner surface of the core shroud and the inner surface of the pressure vessel liner, respectively. Figure 15a and 15b show similar comparisons for the ^{55}Fe activity profiles. Note that, for the axial profiles in the Region 2 model of the JPDR, only a few measured data points are available. For this reason, only absolute activities are plotted, since there are not enough points to give informative C/E profiles in the axial direction.

The computed numerical data used in these comparisons are also included in tabular form in the Appendix. For completeness, the data in the Appendix include activities for all the radioactive isotopes computed for the JPDR Case B Region 2 model, not just those presented graphically in the figures.

Concerning the plots, one can easily argue that very good results were obtained for all points through the pressure vessel in both Models A and B. For example, Fig. 8b for Case A shows that the C/E values range from a minimum around 0.80 to a maximum near 1.10. The C/E values for the Case B model (see Fig. 9b) have a similar range, varying from about 0.80 to slightly less than unity. The small differences near the outer periphery of the pressure vessel are due to the differences in the bioshield models for Cases A and B, since some of the neutron population in this region of the vessel is due to backscatter from the bioshield.

The good agreement up through the vessel is also apparent in the axial activity profiles given in Figs. 14 and 15, with a maximum error of about ±25% for the worst locations in the shroud and pressure vessel liner. Thus, the overall accuracy of the calculations, up to and including the vessel, is on the order of ±25%. This is a very impressive finding, especially considering the complexity of the calculations required to produce these comparisons. In addition, although not explicitly stated, it is expected that the experimental data and the initial impurity concentrations in the structural materials have uncertainties approaching, or possibly exceeding, the range of C/E values determined within the vessel of the JPDR configuration.

Figures 10-13, however, show that this same level of accuracy is not achieved in the exvessel bioshield region. In fact, the relative error starts out at roughly 50-100% too high, and the error tends to grow with distance into the shield, approaching factors of about 10 and 6, respectively, for Cases A and B at approximately 100 cm into the shield. This behavior is consistent for all the isotopes and the error trend is roughly linear with distance into the concrete region.

Clearly there is a problem in the prediction of the bioshield activities. In fact, it was the large discrepancies in the preliminary results from the Case A model with the simple bioshield geometry that prompted further investigation into the details of the bioshield configuration. The new information from Ref. 3 led to the more detailed Case B bioshield configuration and, as shown in Figs. 10 and 11, the new model did indeed improve the C/E values, both at the surface and at larger distances into the bioshield.

UMass-Lowell Results for JPDR Activation Benchmark

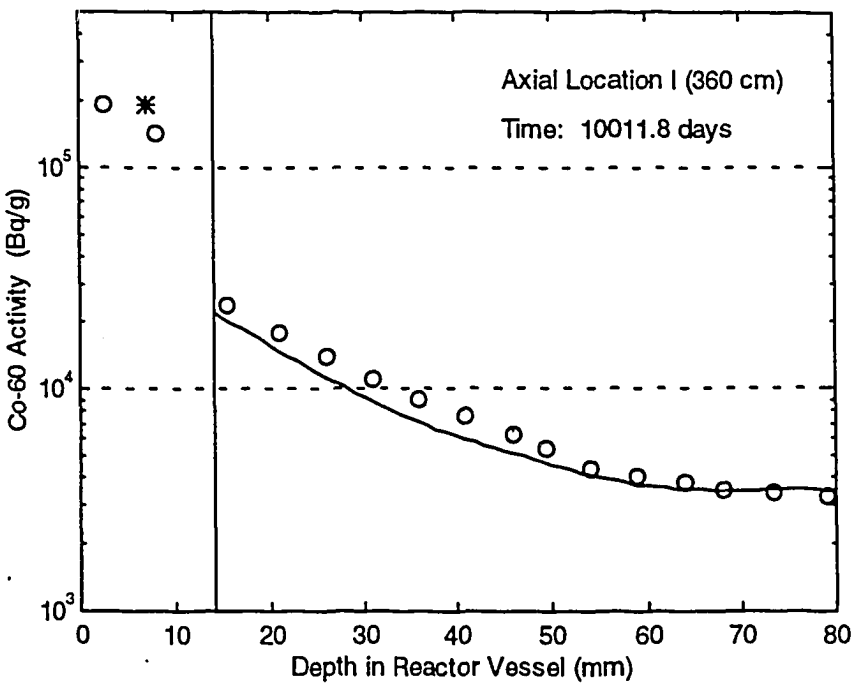

Fig. 8a. Absolute ^{60}Co activity profile within the reactor vessel for Case A.

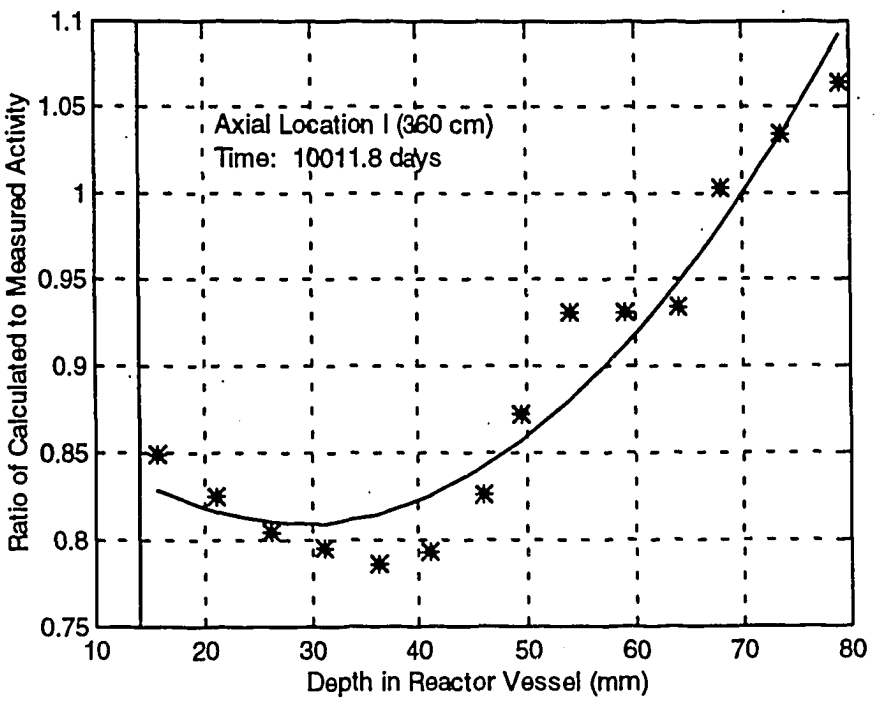

Fig. 8b. C/E profile for the ^{60}Co activity within the reactor vessel for Case A.

UMass-Lowell Results for JPDR Activation Benchmark

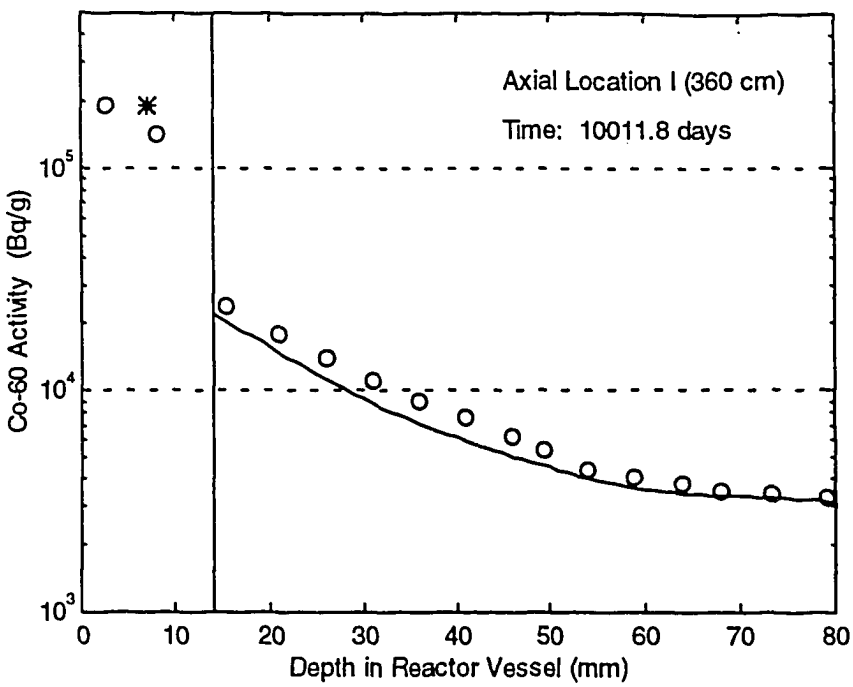

Fig. 9a. Absolute ^{60}Co activity profile within the reactor vessel for Case B.

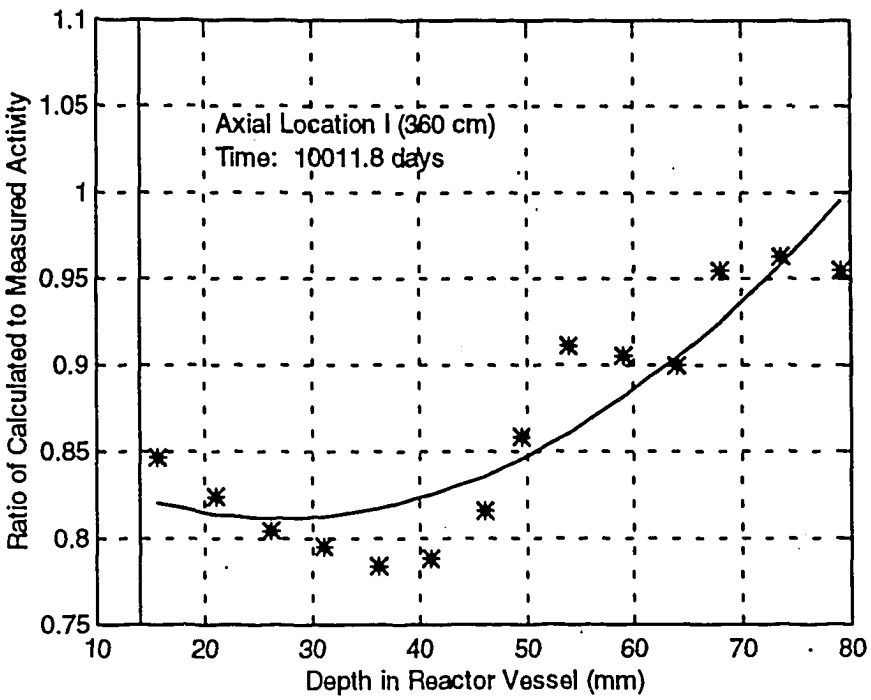

Fig. 9b. C/E profile for the ^{60}Co activity within the reactor vessel for Case B.

UMass-Lowell Results for JPDR Activation Benchmark

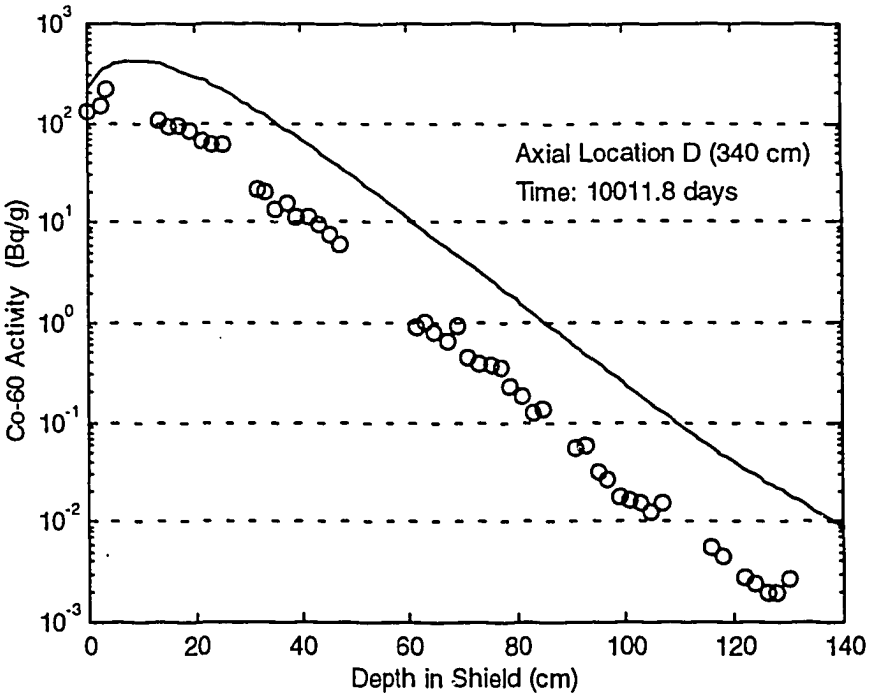

Fig. 10a. Absolute ^{60}Co activity profile within the bioshield for Case A.

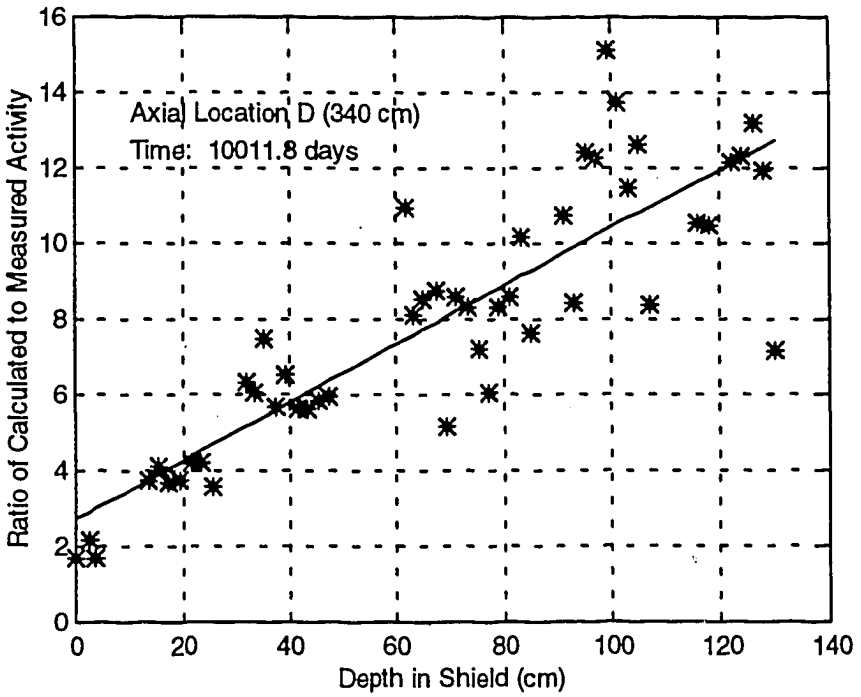

Fig. 10b. C/E profile for the ^{60}Co activity within the bioshield for Case A.

UMass-Lowell Results for JPDR Activation Benchmark

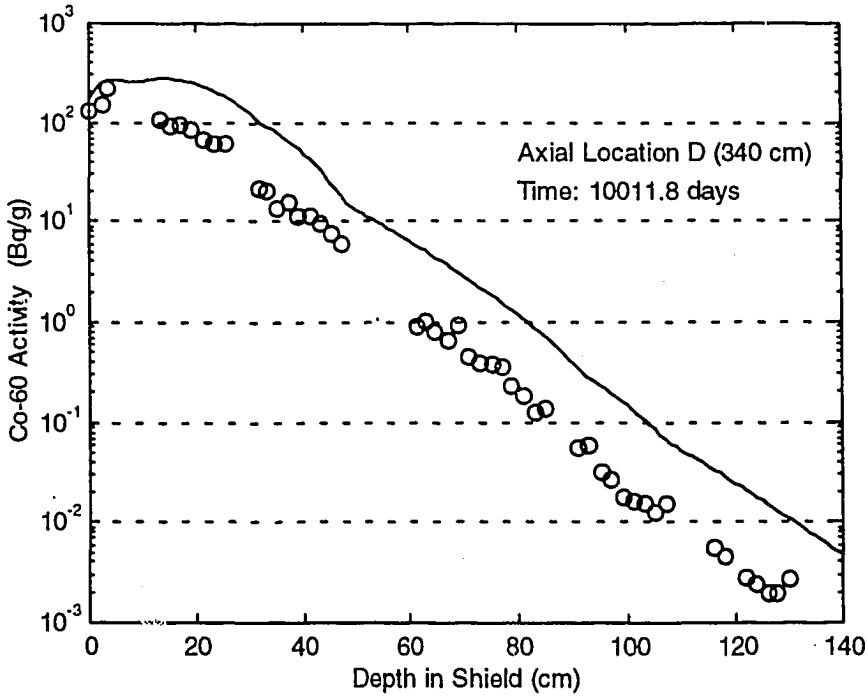

Fig. 11a. Absolute ^{60}Co activity profile within the bioshield for Case B.

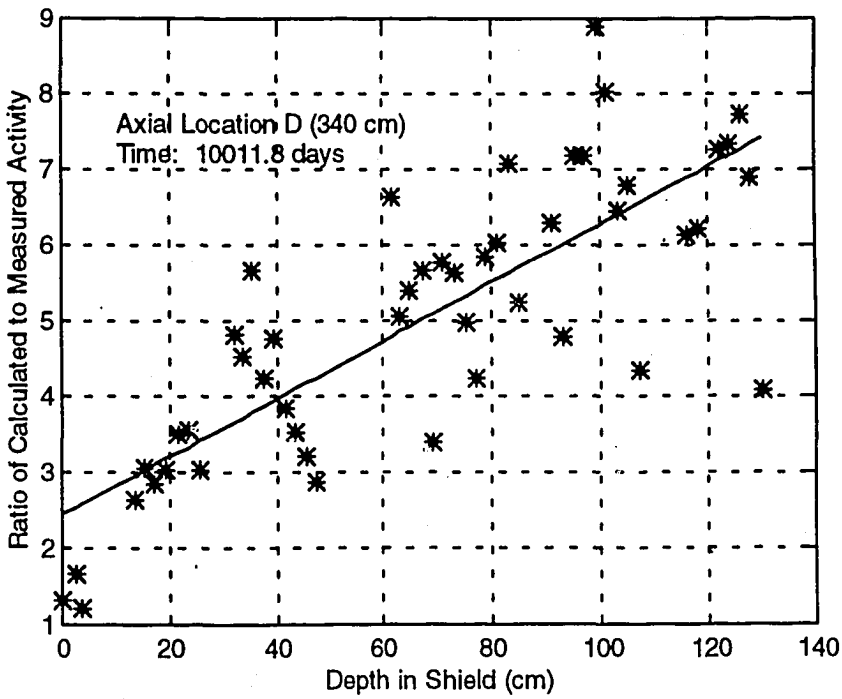

Fig. 11b. C/E profile for the ^{60}Co activity within the bioshield for Case B.

UMass-Lowell Results for JPDR Activation Benchmark

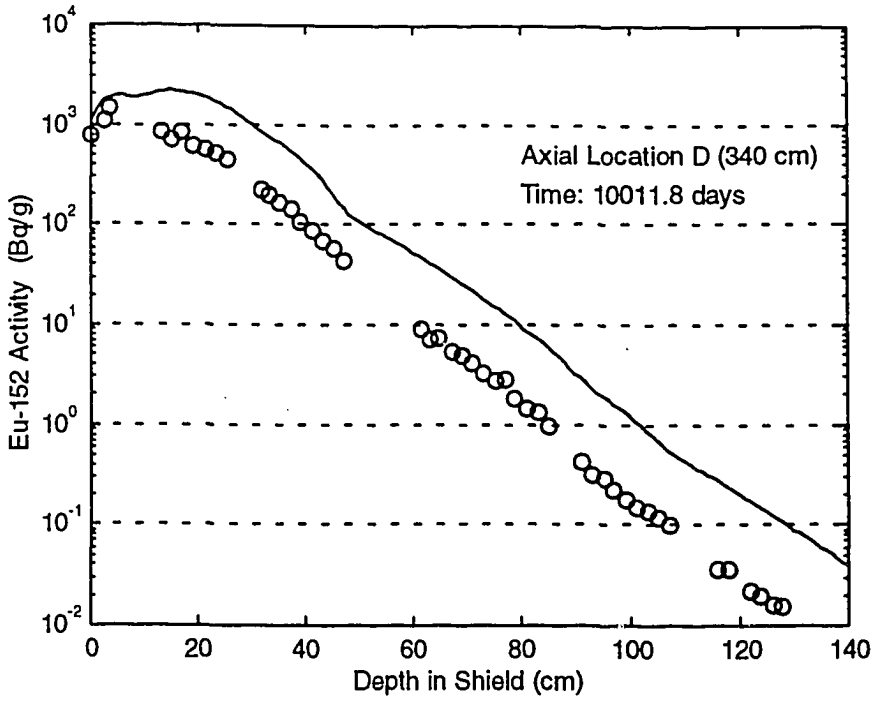

Fig. 12a. Absolute ^{152}Eu activity profile within the bioshield for Case B.

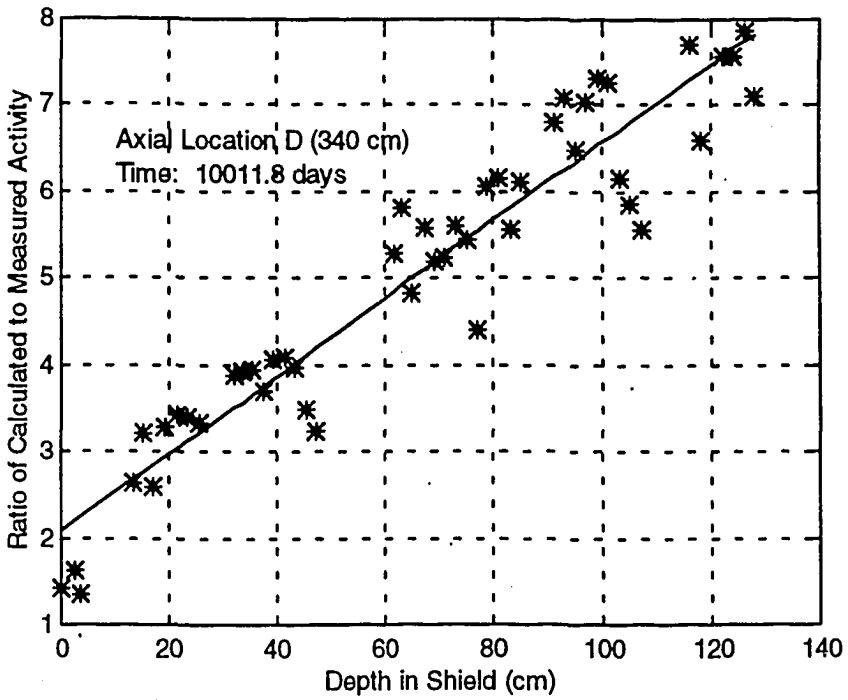

Fig. 12b. C/E profile for the ^{152}Eu activity within the bioshield for Case B.

UMass-Lowell Results for JPDR Activation Benchmark

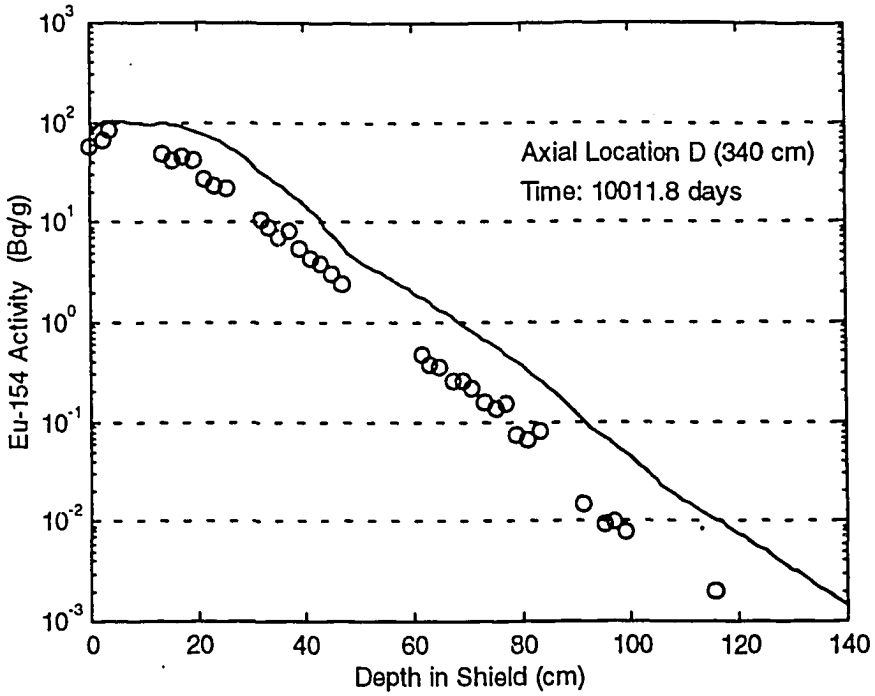

Fig. 13a. Absolute ^{154}Eu activity profile within the bioshield for Case B.

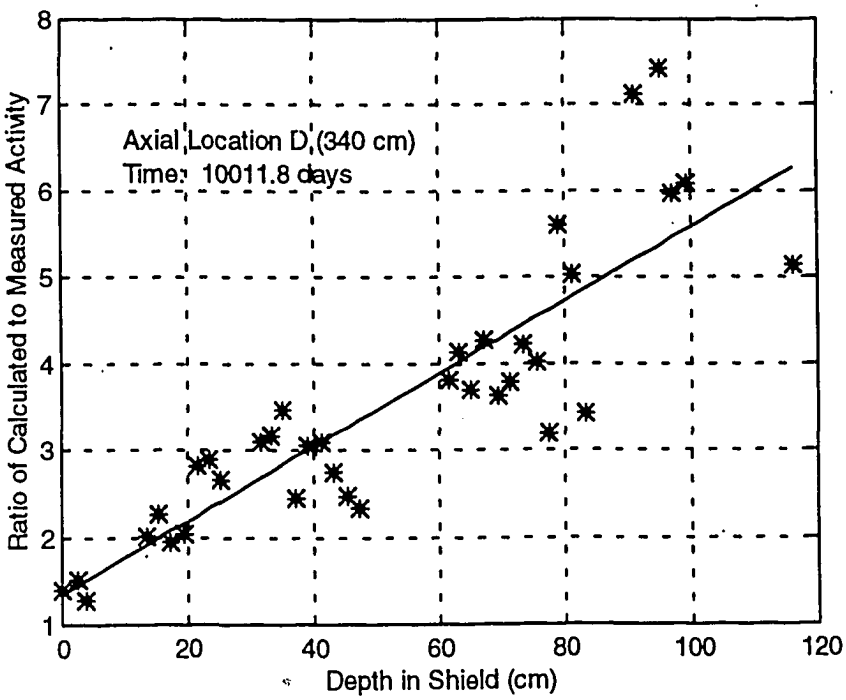

Fig. 13b. C/E profile for the ^{154}Eu activity within the bioshield for Case B.

UMass-Lowell Results for JPDR Activation Benchmark

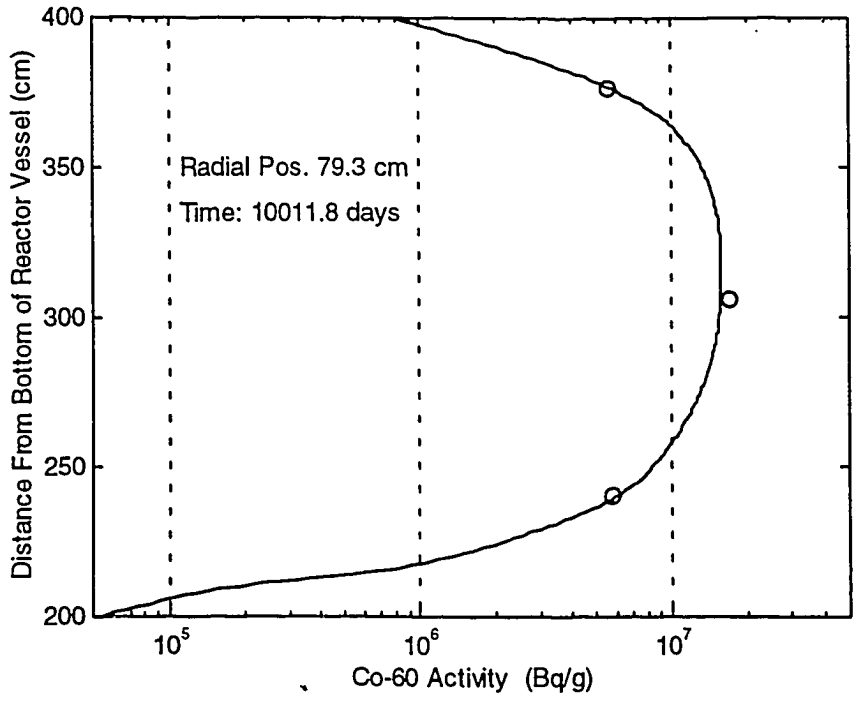

Fig. 14a. Absolute ^{60}Co activity profile along inner surface of shroud for Case B.

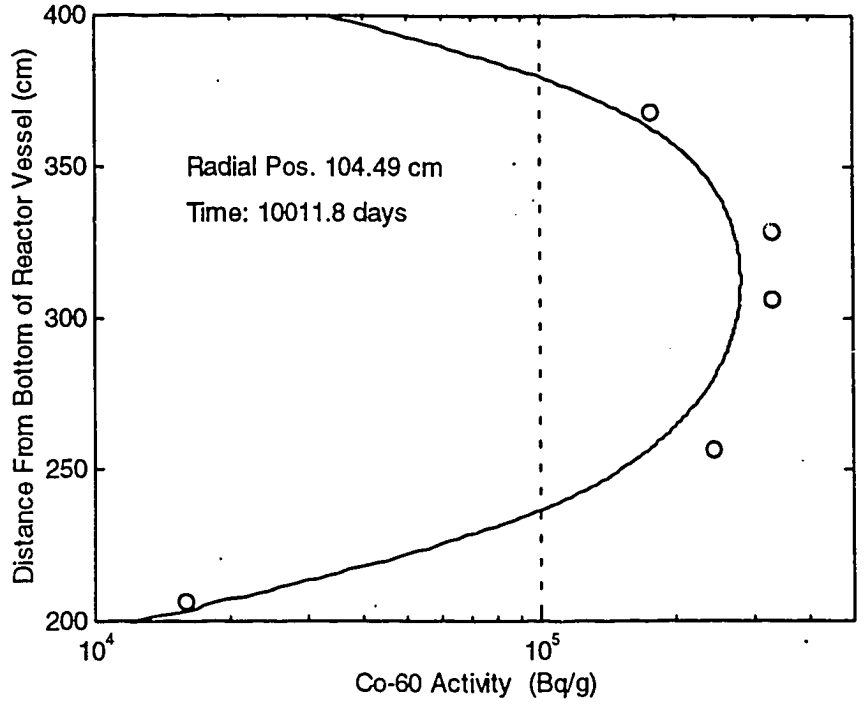

Fig. 14b. Absolute ^{60}Co activity profile along inner surface of vessel for Case B.

UMass-Lowell Results for JPDR Activation Benchmark

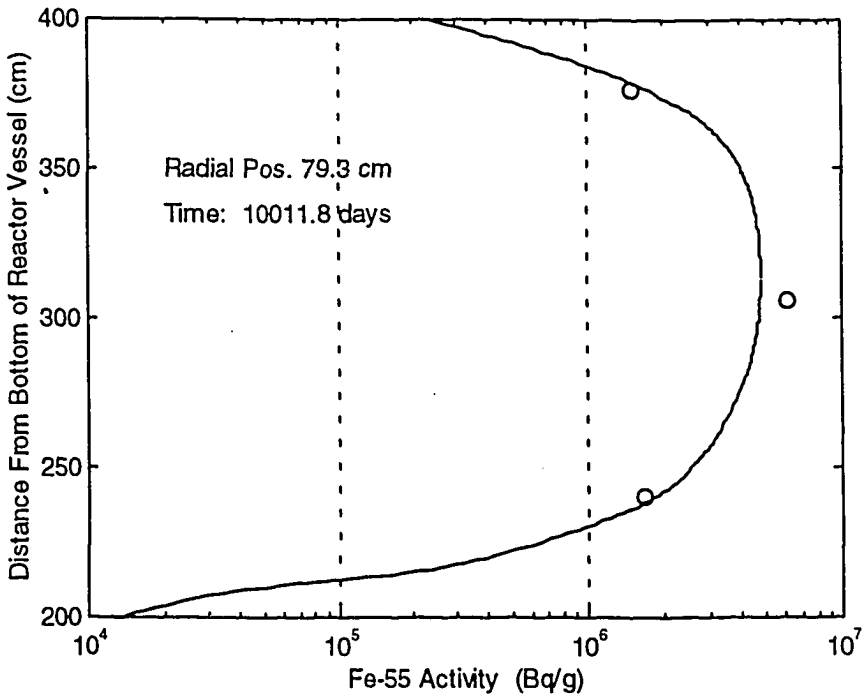

Fig. 15a. Absolute ^{55}Fe activity profile along inner surface of shroud for Case B.

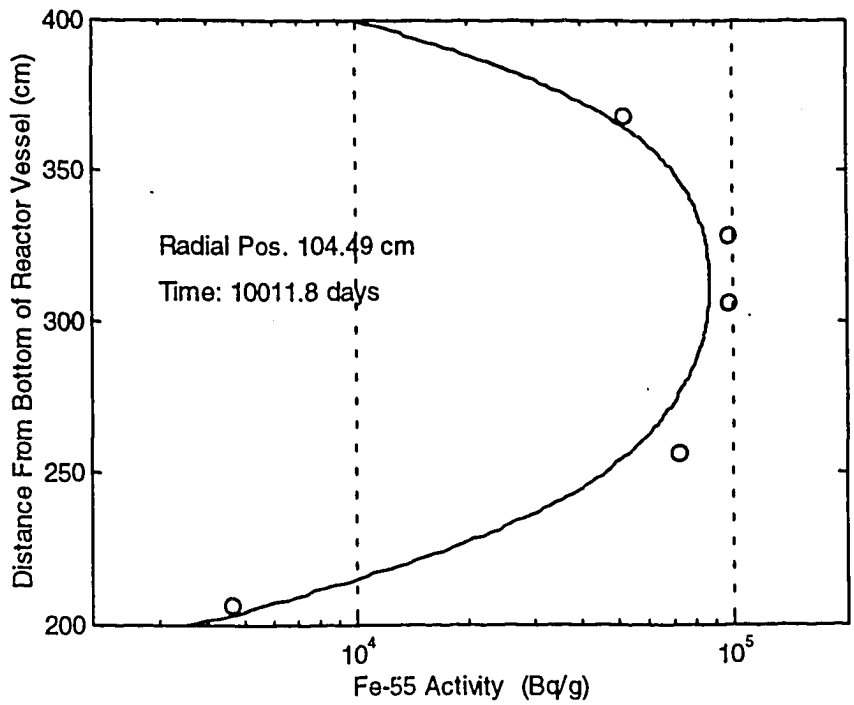

Fig. 15b. Absolute ^{55}Fe activity profile along inner surface of vessel for Case B.

The comparisons given in Figs. 10 and 11 focus on ^{60}Co, but the differences for the Case A and Case B activities were similar for all the isotopes addressed in this benchmark.

However, even with an improved geometric model, the discrepancies in the bioshield are still larger than desired. The root cause of these discrepancies has not been isolated explicitly, although a number of sensitivity studies (quadrature order, mesh spacing, concrete composition, energy resolution, etc.) has identified the relatively poor low-energy resolution in the BUGLE-93 library as a possible culprit. In fact, it is very probable that the 47 group BUGLE-93 library may have been a poor choice for performing this benchmark exercise. Further work is ongoing to address this concern (see below).

Finally, on a positive note, a larger uncertainty with distance into the bioshield, although worrisome from a modeling and analysis viewpoint, is probably not of real concern in practice, since the activity levels are so low anyway. The ^{60}Co activity, for example, is reduced by about 6 orders of magnitude at 100 cm into the shield relative to the magnitude at the inner surface of the pressure vessel. Thus, for disposal and general decommissioning concerns, the activity of the concrete beyond the first 100 cm is negligibly small compared to other components in the system. A factor of 5-10 error in a negligibly small activity may not be of practical concern – but it sure does leave room for some improvements in the data and methods.

Summary/Future Work

This paper summarizes the UMass-Lowell results of a benchmark exercise posed by the IAEA to test data and methods for computing the inventory of several radioactive isotopes that impact decisions concerning the decommissioning of fission reactors. The Japan Power Demonstration Reactor (JPDR) was chosen for this test because of an available data base of measured radial and axial activity profiles for several isotopes and locations in the excore structural regions of the reactor system.

In the UMass-Lowell benchmark tests, the DORT discrete ordinates transport code and the 47-group BUGLE-93 cross section library were used to compute the space and energy distribution of the neutron flux in the regions directly surrounding the core of the JPDR. In addition, a library of activation cross sections with the same group structure as BUGLE-93 was derived from the 199-group VITAMIN-B6 data set. Finally, the ACTIV code, along with the DORT multigroup fluxes and consistent multigroup activation cross sections, was used to compute the time dependent inventory of several isotopes produced via neutron activation over the life of the reactor.

The computed activities from ACTIV, when compared to the measured data from the JPDR decommissioning program, showed very good agreement in all cases for spatial points up to and including the reactor vessel. Calculational errors in these tests were typically less than ±25%. Similar comparisons in the bioshield regions, even with a relatively detailed geometric model, showed much larger differences – typically a factor of 50% or more too high initially, with the error increasing roughly linearly with distance into the bioshield.

UMass-Lowell Results for JPDR Activation Benchmark

The good comparisons that were observed in the pressure vessel regions are very encouraging and they suggest that the basic procedure used for these analyses (DORT, BUGLE-93, ACTIV, and a compatible multigroup activation library) are indeed adequate to the task at hand. These comparisons also serve as an independent validation of the recently developed ACTIV code.

The results in the bioshield, on the other hand, are quite disappointing. However, the consistent behavior that was observed for all the isotopes does suggest that much of the discrepancy is due to inadequate knowledge of the flux magnitude, spectrum, and overall attenuation characteristics, and not due to the activation cross sections and basic methodology. Thus, the search for the root cause of the observed errors should focus on the DORT computation of the space-energy fluxes in the JPDR bioshield.

In addressing this concern, preliminary sensitivity studies have identified the relatively poor thermal energy resolution within the BUGLE-93 library (recall that there are only two groups below 0.4 eV) as a possible source for the majority of the errors observed in the bioshield regions of the JPDR configuration. The relatively hard spectrum in the vessel reduces the importance of thermal activation in this region, but in the concrete bioshield, the much softer spectrum magnifies the need for a good computation of the thermal flux. Previous studies have noted the inadequacy of this particular 47 group structure for computing the thermal fluxes in the excore regions of large PWR systems.[10] Also, as part of the current project, some 1-D fine group calculations for the JPDR model using the XSDRN code[7] with the 199 neutron group VITAMIN-B6 library show significant differences from the thermal flux computed via consistent 47-group 1-D calculations with DORT using BUGLE-93. The full ramification of these differences has not been determined yet, but an ACTIV computation using the 199 group XSDRN fluxes collapsed to 47 groups shows that the new thermal fluxes produce significantly better comparisons with the JPDR experimental data. These studies are not complete, but they do suggest that the two thermal groups in the BUGLE-93 library are not sufficient to adequately represent the rapidly changing thermal flux spectrum in the first 20-30 cm of the JPDR bioshield.

Based on these conclusions, further studies needed to fully complete this benchmark exercise can be grouped into two categories:

1. Completion of the neutron transport and activation calculations for the regions above and below the central axial region that was modeled in the current work.
2. Investigation and resolution of the discrepancies observed in the bioshield region.

The first item, although straightforward, is a major effort simply because of the shear size of the reactor system being modeled. Recall that the full axial dimension of the JPDR is over 12 m, and that the plan is to break the full geometry into three boot-strapped models. Appropriate boundary sources from the centrally located Region 2 model have been saved so that neutron transport calculations, above and below Region 2, can be continued. The completion of these additional calculations will

provide activation information in areas far above and below the core region. This should be a good test of our ability to compute neutron transport into these remote regions. At present, these computations have relatively low priority – at least until the bioshield discrepancies are completely resolved.

The second area for future work is less well defined, since there could be several factors contributing to the discrepancies in the bioshield. It does appear, however, that the poor thermal energy resolution in the BUGLE-93 library is the dominant factor, but further work is needed to prove this theory. What is really needed to test this theory is a new library, similar in all respects to BUGLE-93, but with more thermal energy detail (possibly 7 or 8 thermal groups, instead of only two groups below 0.4 eV). Unfortunately, developing and testing a new multigroup library (say 53 groups) for general neutron and gamma transport analyses and shielding applications, as well as for excore activation computations, is a relatively major undertaking. Even so, we feel strongly that this is the direction to follow. If successful, the space-energy activation analysis methodology utilized in this work could become the definitive tool for performing accurate excore activation studies – studies that could provide the predictive support needed for the planning of safe and economical decommissioning strategies.

References

1. N. Kocherov, "Benchmark on Radioactive Inventory Calculations for Fission Reactor Decommissioning," letter to potential participants in benchmark exercise (1994).
2. T. Sukegawa, et. al., " Accuracy Verification for Calculation of Inventory in JPDR Due to Neutron Activation," International Atomic Energy Agency, INDC(JPN)-164 (1993).
3. Letter from N. Kocherov (IAEA) to J. R. White (UMass-Lowell) dated March 31, 1995 containing detailed drawings from JAERI describing the central part of the JPDR bioshield.
4. J. R. White, et. al., "Maine Yankee Dosimetry Capsule and Pressure Vessel Neutron Fluence Calculations," **Reactor Dosimetry ASTM STP 1228** (1994).
5. "TORT - A Three Dimensional Discrete Ordinates Transport Code," Radiation Shielding Information Center Computer Code Collection, CCC-543 (1990). This manual also contains the DORT code and document.
6. D. T. Ingersoll, et al., "Production and Testing of the VITAMIN-B6 Fine-Group and the BUGLE-93 Broad-Group Neutron/Photon Cross-Section Libraries Derived from ENDF/B-VI Nuclear Data," Oak Ridge National Laboratory, ORNL-6795 (1994).
7. "SCALE 4.2 - Modular Code System for Performing Standardized Computer Analyses for Licensing Evaluation," Radiation Shielding Information Center Computer Code Collection, CCC-545 (1993).
8. J. R. White, "The DEPTH-CHARGE Static and Time-Dependent Perturbation/ Sensitivity System for Nuclear Reactor Core Analysis, Revision I," Oak Ridge National Laboratory, ORNL/CSD-78R (1985).
9. D. R. Vondy, et. al., The BOLD VENTURE Computation System for Nuclear Reactor Core Analysis," Oak Ridge National Laboratory, ORNL-5711 (1981).
10. J. R. White, et. al., "Comparison of the BUGLE-80 and SAILOR Libraries for Coupled Neutron-Gamma Transport Applications," **Reactor Dosimetry ASTM STP 1228** (1994).

Appendix A

Numerical Data from ACTIV

Fig. A.1 Radial activities from ACTIV for JPDR Case B at H = 340 cm

			Nontrivial Activities (Bq/g)					
Zone #	matl #	location	mn 54	fe 55	co 60	ni 63	eu152	eu154
14	1	79.95	2.239E+01	4.405E+06	1.451E+07	1.185E+07	0.000E+00	0.000E+00
15	2	104.09	1.200E+00	7.812E+04	2.516E+05	2.204E+05	0.000E+00	0.000E+00
16	3	105.41	1.338E+00	4.683E+04	2.031E+04	5.373E+03	0.000E+00	0.000E+00
16	3	106.64	1.091E+00	2.072E+04	1.059E+04	2.323E+03	0.000E+00	0.000E+00
16	3	107.87	8.845E-01	1.117E+04	6.758E+03	1.214E+03	0.000E+00	0.000E+00
16	3	108.99	7.218E-01	6.688E+03	4.812E+03	6.984E+02	0.000E+00	0.000E+00
16	3	109.99	6.050E-01	5.603E+03	4.166E+03	5.787E+02	0.000E+00	0.000E+00
16	3	110.99	4.945E-01	5.616E+03	3.873E+03	5.895E+02	0.000E+00	0.000E+00
18	3	135.65	3.067E-01	8.633E+03	4.793E+03	9.496E+02	0.000E+00	0.000E+00
29	4	137.65	5.026E-03	3.003E+02	2.246E+02	4.113E+00	1.515E+03	9.317E+01
29	4	140.35	3.954E-03	3.784E+02	2.653E+02	5.240E+00	1.896E+03	1.041E+02
20	4	143.40	2.995E-03	3.805E+02	2.607E+02	5.295E+00	1.900E+03	1.002E+02
21	4	146.55	2.212E-03	3.935E+02	2.586E+02	5.507E+00	1.945E+03	9.572E+01
29	4	149.00	1.715E-03	4.316E+02	2.724E+02	6.070E+00	2.108E+03	9.653E+01
29	4	150.50	1.473E-03	4.496E+02	2.784E+02	6.335E+00	2.183E+03	9.657E+01
29	4	152.69	1.208E-03	4.434E+02	2.701E+02	6.259E+00	2.140E+03	9.176E+01
29	4	156.06	8.672E-04	4.105E+02	2.451E+02	5.805E+00	1.968E+03	8.115E+01
29	4	159.44	6.218E-04	3.533E+02	2.081E+02	5.002E+00	1.686E+03	6.764E+01
29	4	162.81	4.425E-04	2.857E+02	1.668E+02	4.048E+00	1.359E+03	5.349E+01
22	4	166.20	3.110E-04	2.125E+02	1.233E+02	3.014E+00	1.009E+03	3.917E+01
29	4	169.08	2.304E-04	1.610E+02	9.300E+01	2.284E+00	7.629E+02	2.931E+01
29	4	171.45	1.835E-04	1.340E+02	7.715E+01	1.901E+00	6.337E+02	2.418E+01
29	4	173.82	1.460E-04	1.087E+02	6.250E+01	1.542E+00	5.137E+02	1.952E+01
29	4	175.50	1.232E-04	9.204E+01	5.291E+01	1.306E+00	4.350E+02	1.651E+01
29	4	177.00	1.069E-04	7.818E+01	4.495E+01	1.109E+00	3.696E+02	1.403E+01
29	4	179.00	8.755E-05	6.053E+01	3.487E+01	8.586E-01	2.865E+02	1.093E+01
23	4	181.45	6.824E-05	4.134E+01	2.393E+01	5.862E-01	1.962E+02	7.571E+00
24	4	184.35	4.997E-05	2.661E+01	1.547E+01	3.771E-01	1.265E+02	4.928E+00
29	4	187.43	3.657E-05	2.038E+01	1.181E+01	2.890E-01	9.674E+01	3.738E+00
29	4	190.70	2.668E-05	1.658E+01	9.570E+00	2.351E-01	7.847E+01	3.001E+00
29	4	193.97	1.942E-05	1.319E+01	7.591E+00	1.871E-01	6.228E+01	2.366E+00
29	4	197.23	1.413E-05	1.037E+01	5.953E+00	1.472E-01	4.890E+01	1.846E+00
29	4	200.50	1.030E-05	8.062E+00	4.619E+00	1.144E-01	3.796E+01	1.427E+00
29	4	203.77	7.520E-06	6.223E+00	3.559E+00	8.833E-02	2.927E+01	1.095E+00
29	4	207.03	5.504E-06	4.706E+00	2.688E+00	6.680E-02	2.211E+01	8.252E-01
29	4	210.30	3.947E-06	3.559E+00	2.030E+00	5.053E-02	1.671E+01	6.217E-01
29	4	213.57	2.878E-06	2.682E+00	1.529E+00	3.809E-02	1.259E+01	4.676E-01
29	4	216.83	2.103E-06	1.978E+00	1.127E+00	2.808E-02	9.278E+00	3.442E-01
29	4	220.10	1.537E-06	1.446E+00	8.238E-01	2.053E-02	6.782E+00	2.517E-01
29	4	223.37	1.119E-06	1.009E+00	5.755E-01	1.432E-02	4.735E+00	1.763E-01
25	4	226.25	8.385E-07	6.999E-01	4.003E-01	9.935E-03	3.290E+00	1.232E-01
26	4	228.75	6.506E-07	5.150E-01	2.949E-01	7.309E-03	2.423E+00	9.096E-02
29	4	231.67	4.901E-07	3.934E-01	2.252E-01	5.584E-03	1.850E+00	6.937E-02
29	4	235.00	3.559E-07	2.903E-01	1.662E-01	4.121E-03	1.366E+00	5.122E-02
29	4	238.33	2.586E-07	2.072E-01	1.188E-01	2.940E-03	9.753E-01	3.668E-02
27	4	241.25	1.948E-07	1.477E-01	8.483E-02	2.095E-03	6.960E-01	2.631E-02
28	4	243.75	1.487E-07	1.117E-01	6.420E-02	1.585E-03	5.266E-01	1.994E-02
29	4	246.72	1.119E-07	8.825E-02	5.063E-02	1.252E-03	4.156E-01	1.567E-02
29	4	250.16	8.092E-08	6.856E-02	3.926E-02	9.730E-04	3.225E-01	1.211E-02
29	4	253.59	5.840E-08	5.294E-02	3.026E-02	7.514E-04	2.489E-01	9.303E-03
29	4	257.03	4.214E-08	4.040E-02	2.307E-02	5.735E-04	1.897E-01	7.078E-03
29	4	260.47	3.016E-08	3.084E-02	1.758E-02	4.378E-04	1.447E-01	5.377E-03
29	4	263.91	2.193E-08	2.332E-02	1.329E-02	3.312E-04	1.094E-01	4.059E-03
29	4	267.34	1.570E-08	1.765E-02	1.005E-02	2.507E-04	8.275E-02	3.061E-03
29	4	270.78	1.136E-08	1.331E-02	7.572E-03	1.891E-04	6.236E-02	2.304E-03
29	4	274.22	8.203E-09	1.003E-02	5.699E-03	1.425E-04	4.697E-02	1.730E-03
29	4	277.66	5.940E-09	7.586E-03	4.309E-03	1.077E-04	3.551E-02	1.307E-03
29	4	281.09	4.352E-09	5.756E-03	3.266E-03	8.176E-05	2.692E-02	9.895E-04
29	4	284.53	3.187E-09	4.415E-03	2.503E-03	6.271E-05	2.064E-02	7.572E-04
29	4	287.97	2.405E-09	3.492E-03	1.979E-03	4.960E-05	1.632E-02	5.980E-04
29	4	291.41	1.881E-09	2.856E-03	1.618E-03	4.058E-05	1.334E-02	4.878E-04
29	4	294.84	1.565E-09	2.486E-03	1.407E-03	3.532E-05	1.161E-02	4.240E-04
29	4	298.28	1.420E-09	2.304E-03	1.303E-03	3.273E-05	1.075E-02	3.922E-04

Fig. A.2 Radial activities from ACTIV for JPDR Case B at H = 360 cm

			Nontrivial Activities (Bq/g)					
Zone #	matl #	location	mn 54	fe 55	co 60	ni 63	eu152	eu154
14	1	79.95	1.722E+01	3.367E+06	1.110E+07	9.061E+06	0.000E+00	0.000E+00
15	2	104.09	9.023E-01	5.982E+04	1.928E+05	1.687E+05	0.000E+00	0.000E+00
16	3	105.41	1.011E+00	3.592E+04	1.561E+04	4.120E+03	0.000E+00	0.000E+00
16	3	106.64	8.260E-01	1.594E+04	8.198E+03	1.786E+03	0.000E+00	0.000E+00
16	3	107.87	6.705E-01	8.603E+03	5.265E+03	9.336E+02	0.000E+00	0.000E+00
16	3	108.99	5.512E-01	5.274E+03	3.835E+03	5.498E+02	0.000E+00	0.000E+00
16	3	109.99	4.612E-01	4.518E+03	3.377E+03	4.667E+02	0.000E+00	0.000E+00
16	3	110.99	3.787E-01	4.680E+03	3.234E+03	4.919E+02	0.000E+00	0.000E+00
18	3	135.65	2.456E-01	7.239E+03	4.030E+03	7.965E+02	0.000E+00	0.000E+00
29	4	137.65	4.015E-03	2.497E+02	1.867E+02	3.421E+00	1.261E+03	7.747E+01
29	4	140.35	3.150E-03	3.141E+02	2.200E+02	4.352E+00	1.575E+03	8.638E+01
20	4	143.40	2.381E-03	3.150E+02	2.155E+02	4.386E+00	1.575E+03	8.283E+01
21	4	146.55	1.764E-03	3.249E+02	2.132E+02	4.549E+00	1.607E+03	7.888E+01
29	4	149.00	1.366E-03	3.557E+02	2.241E+02	5.003E+00	1.738E+03	7.937E+01
29	4	150.50	1.178E-03	3.703E+02	2.290E+02	5.218E+00	1.799E+03	7.936E+01
29	4	152.69	9.600E-04	3.648E+02	2.219E+02	5.150E+00	1.762E+03	7.533E+01
29	4	156.06	6.919E-04	3.374E+02	2.013E+02	4.773E+00	1.618E+03	6.658E+01
29	4	159.44	4.957E-04	2.901E+02	1.708E+02	4.109E+00	1.385E+03	5.546E+01
29	4	162.81	3.536E-04	2.345E+02	1.368E+02	3.323E+00	1.116E+03	4.385E+01
22	4	166.20	2.488E-04	1.743E+02	1.011E+02	2.472E+00	8.277E+02	3.209E+01
29	4	169.08	1.847E-04	1.321E+02	7.626E+01	1.874E+00	6.259E+02	2.402E+01
29	4	171.45	1.479E-04	1.099E+02	6.326E+01	1.559E+00	5.199E+02	1.981E+01
29	4	173.82	1.169E-04	8.918E+01	5.126E+01	1.265E+00	4.215E+02	1.600E+01
29	4	175.50	1.002E-04	7.554E+01	4.340E+01	1.072E+00	3.570E+02	1.353E+01
29	4	177.00	8.584E-05	6.414E+01	3.687E+01	9.101E-01	3.032E+02	1.150E+01
29	4	179.00	7.060E-05	4.969E+01	2.861E+01	7.049E-01	2.352E+02	8.960E+00
23	4	181.45	5.496E-05	3.391E+01	1.962E+01	4.809E-01	1.609E+02	6.204E+00
24	4	184.35	4.033E-05	2.186E+01	1.270E+01	3.098E-01	1.039E+02	4.043E+00
29	4	187.43	2.960E-05	1.673E+01	9.693E+00	2.372E-01	7.938E+01	3.064E+00
29	4	190.70	2.160E-05	1.365E+01	7.874E+00	1.935E-01	6.457E+01	2.467E+00
29	4	193.97	1.578E-05	1.083E+01	6.235E+00	1.537E-01	5.117E+01	1.942E+00
29	4	197.23	1.150E-05	8.550E+00	4.907E+00	1.213E-01	4.031E+01	1.521E+00
29	4	200.50	8.409E-06	6.626E+00	3.796E+00	9.404E-02	3.120E+01	1.172E+00
29	4	203.77	6.128E-06	5.126E+00	2.931E+00	7.275E-02	2.410E+01	9.018E-01
29	4	207.03	4.493E-06	3.873E+00	2.212E+00	5.498E-02	1.820E+01	6.787E-01
29	4	210.30	3.223E-06	2.929E+00	1.671E+00	4.158E-02	1.375E+01	5.114E-01
29	4	213.57	2.359E-06	2.205E+00	1.257E+00	3.131E-02	1.035E+01	3.842E-01
29	4	216.83	1.717E-06	1.627E+00	9.270E-01	2.311E-02	7.633E+00	2.831E-01
29	4	220.10	1.257E-06	1.191E+00	6.789E-01	1.692E-02	5.589E+00	2.074E-01
29	4	223.37	9.144E-07	8.328E-01	4.751E-01	1.182E-02	3.910E+00	1.455E-01
25	4	226.25	6.857E-07	5.820E-01	3.328E-01	8.261E-03	2.735E+00	1.023E-01
26	4	228.75	5.357E-07	4.290E-01	2.456E-01	6.089E-03	2.018E+00	7.571E-02
29	4	231.67	3.988E-07	3.292E-01	1.883E-01	4.672E-03	1.548E+00	5.795E-02
29	4	235.00	2.934E-07	2.447E-01	1.400E-01	3.473E-03	1.151E+00	4.311E-02
29	4	238.33	2.107E-07	1.750E-01	1.003E-01	2.484E-03	8.237E-01	3.093E-02
27	4	241.25	1.603E-07	1.251E-01	7.181E-02	1.775E-03	5.895E-01	2.227E-02
28	4	243.75	1.238E-07	9.397E-02	5.400E-02	1.333E-03	4.429E-01	1.676E-02
29	4	246.72	9.285E-08	7.440E-02	4.267E-02	1.056E-03	3.504E-01	1.321E-02
29	4	250.16	6.706E-08	5.789E-02	3.314E-02	8.217E-04	2.723E-01	1.021E-02
29	4	253.59	4.852E-08	4.486E-02	2.564E-02	6.369E-04	2.108E-01	7.877E-03
29	4	257.03	3.519E-08	3.434E-02	1.960E-02	4.875E-04	1.612E-01	6.006E-03
29	4	260.47	2.519E-08	2.631E-02	1.500E-02	3.736E-04	1.235E-01	4.584E-03
29	4	263.91	1.831E-08	1.993E-02	1.135E-02	2.830E-04	9.344E-02	3.461E-03
29	4	267.34	1.306E-08	1.514E-02	8.614E-03	2.150E-04	7.096E-02	2.622E-03
29	4	270.78	9.650E-09	1.140E-02	6.480E-03	1.619E-04	5.340E-02	1.969E-03
29	4	274.22	6.811E-09	8.631E-03	4.902E-03	1.226E-04	4.040E-02	1.487E-03
29	4	277.66	5.111E-09	6.480E-03	3.677E-03	9.204E-05	3.031E-02	1.114E-03
29	4	281.09	3.699E-09	4.961E-03	2.814E-03	7.047E-05	2.320E-02	8.511E-04
29	4	284.53	2.752E-09	3.799E-03	2.153E-03	5.397E-05	1.775E-02	6.503E-04
29	4	287.97	2.099E-09	3.019E-03	1.710E-03	4.289E-05	1.411E-02	5.159E-04
29	4	291.41	1.645E-09	2.465E-03	1.395E-03	3.502E-05	1.151E-02	4.203E-04
29	4	294.84	1.369E-09	2.145E-03	1.213E-03	3.048E-05	1.001E-02	3.650E-04
29	4	298.28	1.236E-09	1.984E-03	1.122E-03	2.819E-05	9.259E-03	3.375E-04

Fig. A.3 Axial activities from ACTIV for JPDR Case B at core shroud

			Nontrivial Activities (Bq/g)					
Zone #	matl #	location	mn 54	fe 55	co 60	ni 63	eu152	eu154
19	1	43.80	1.870E-04	2.059E+01	6.908E+01	5.535E+01	0.000E+00	0.000E+00
3	1	102.83	5.845E-02	9.928E+03	3.681E+04	2.640E+04	0.000E+00	0.000E+00
3	1	105.89	9.071E-02	9.946E+03	3.946E+04	2.622E+04	0.000E+00	0.000E+00
3	1	108.95	1.550E-01	1.397E+04	5.588E+04	3.679E+04	0.000E+00	0.000E+00
3	1	112.01	2.661E-01	1.909E+04	7.619E+04	5.027E+04	0.000E+00	0.000E+00
3	1	115.07	4.682E-01	2.666E+04	1.059E+05	7.025E+04	0.000E+00	0.000E+00
3	1	117.85	8.014E-01	4.139E+04	1.586E+05	1.096E+05	0.000E+00	0.000E+00
3	1	120.35	1.243E+00	7.778E+04	2.810E+05	2.074E+05	0.000E+00	0.000E+00
14	1	122.95	1.619E+00	1.618E+05	5.537E+05	4.341E+05	0.000E+00	0.000E+00
14	1	125.65	2.030E+00	2.714E+05	9.081E+05	7.297E+05	0.000E+00	0.000E+00
14	1	128.35	2.564E+00	3.795E+05	1.260E+06	1.021E+06	0.000E+00	0.000E+00
14	1	131.05	3.159E+00	5.008E+05	1.658E+06	1.348E+06	0.000E+00	0.000E+00
14	1	133.85	3.860E+00	6.505E+05	2.151E+06	1.751E+06	0.000E+00	0.000E+00
14	1	136.75	4.721E+00	8.357E+05	2.762E+06	2.250E+06	0.000E+00	0.000E+00
14	1	139.65	5.788E+00	1.046E+06	3.454E+06	2.815E+06	0.000E+00	0.000E+00
14	1	142.63	6.856E+00	1.285E+06	4.245E+06	3.460E+06	0.000E+00	0.000E+00
14	1	145.68	8.081E+00	1.541E+06	5.089E+06	4.149E+06	0.000E+00	0.000E+00
14	1	148.74	9.586E+00	1.803E+06	5.952E+06	4.852E+06	0.000E+00	0.000E+00
14	1	151.80	1.082E+01	2.056E+06	6.787E+06	5.533E+06	0.000E+00	0.000E+00
14	1	154.85	1.208E+01	2.297E+06	7.582E+06	6.182E+06	0.000E+00	0.000E+00
14	1	157.91	1.317E+01	2.486E+06	8.204E+06	6.690E+06	0.000E+00	0.000E+00
14	1	160.97	1.418E+01	2.687E+06	8.864E+06	7.231E+06	0.000E+00	0.000E+00
14	1	164.02	1.508E+01	2.892E+06	9.539E+06	7.782E+06	0.000E+00	0.000E+00
14	1	167.08	1.583E+01	3.062E+06	1.010E+07	8.240E+06	0.000E+00	0.000E+00
14	1	170.13	1.676E+01	3.247E+06	1.071E+07	8.738E+06	0.000E+00	0.000E+00
14	1	173.19	1.772E+01	3.403E+06	1.122E+07	9.158E+06	0.000E+00	0.000E+00
14	1	176.25	1.864E+01	3.571E+06	1.178E+07	9.610E+06	0.000E+00	0.000E+00
14	1	179.30	1.938E+01	3.719E+06	1.226E+07	1.001E+07	0.000E+00	0.000E+00
14	1	182.36	2.015E+01	3.872E+06	1.277E+07	1.042E+07	0.000E+00	0.000E+00
14	1	185.42	2.093E+01	4.010E+06	1.322E+07	1.079E+07	0.000E+00	0.000E+00
14	1	188.47	2.161E+01	4.147E+06	1.367E+07	1.116E+07	0.000E+00	0.000E+00
14	1	191.53	2.218E+01	4.269E+06	1.407E+07	1.149E+07	0.000E+00	0.000E+00
14	1	194.58	2.263E+01	4.381E+06	1.444E+07	1.179E+07	0.000E+00	0.000E+00
14	1	197.64	2.319E+01	4.476E+06	1.475E+07	1.204E+07	0.000E+00	0.000E+00
14	1	200.70	2.359E+01	4.557E+06	1.502E+07	1.226E+07	0.000E+00	0.000E+00
14	1	203.75	2.390E+01	4.621E+06	1.523E+07	1.243E+07	0.000E+00	0.000E+00
14	1	206.81	2.411E+01	4.672E+06	1.539E+07	1.257E+07	0.000E+00	0.000E+00
14	1	209.87	2.440E+01	4.711E+06	1.552E+07	1.267E+07	0.000E+00	0.000E+00
14	1	212.92	2.457E+01	4.740E+06	1.562E+07	1.275E+07	0.000E+00	0.000E+00
14	1	215.98	2.463E+01	4.760E+06	1.568E+07	1.281E+07	0.000E+00	0.000E+00
14	1	219.03	2.467E+01	4.773E+06	1.572E+07	1.284E+07	0.000E+00	0.000E+00
14	1	222.09	2.468E+01	4.778E+06	1.574E+07	1.285E+07	0.000E+00	0.000E+00
14	1	225.15	2.471E+01	4.776E+06	1.573E+07	1.285E+07	0.000E+00	0.000E+00
14	1	228.20	2.457E+01	4.767E+06	1.570E+07	1.282E+07	0.000E+00	0.000E+00
14	1	231.26	2.449E+01	4.749E+06	1.565E+07	1.278E+07	0.000E+00	0.000E+00
14	1	234.32	2.432E+01	4.726E+06	1.557E+07	1.271E+07	0.000E+00	0.000E+00
14	1	237.37	2.409E+01	4.689E+06	1.545E+07	1.262E+07	0.000E+00	0.000E+00
14	1	240.43	2.372E+01	4.646E+06	1.530E+07	1.250E+07	0.000E+00	0.000E+00
14	1	243.48	2.334E+01	4.581E+06	1.509E+07	1.233E+07	0.000E+00	0.000E+00
14	1	246.54	2.291E+01	4.508E+06	1.485E+07	1.213E+07	0.000E+00	0.000E+00
14	1	249.60	2.239E+01	4.405E+06	1.451E+07	1.185E+07	0.000E+00	0.000E+00
14	1	252.65	2.170E+01	4.296E+06	1.415E+07	1.156E+07	0.000E+00	0.000E+00
14	1	255.71	2.085E+01	4.147E+06	1.366E+07	1.116E+07	0.000E+00	0.000E+00
14	1	258.77	1.997E+01	3.999E+06	1.318E+07	1.076E+07	0.000E+00	0.000E+00
14	1	261.82	1.902E+01	3.802E+06	1.253E+07	1.023E+07	0.000E+00	0.000E+00
14	1	264.88	1.822E+01	3.612E+06	1.191E+07	9.720E+06	0.000E+00	0.000E+00
14	1	267.93	1.722E+01	3.367E+06	1.110E+07	9.061E+06	0.000E+00	0.000E+00
14	1	270.99	1.601E+01	3.120E+06	1.029E+07	8.396E+06	0.000E+00	0.000E+00
14	1	274.05	1.477E+01	2.883E+06	9.510E+06	7.758E+06	0.000E+00	0.000E+00
14	1	277.10	1.323E+01	2.578E+06	8.508E+06	6.940E+06	0.000E+00	0.000E+00
14	1	280.16	1.165E+01	2.260E+06	7.459E+06	6.084E+06	0.000E+00	0.000E+00
14	1	283.22	9.889E+00	1.935E+06	6.386E+06	5.208E+06	0.000E+00	0.000E+00
14	1	286.27	8.449E+00	1.620E+06	5.349E+06	4.361E+06	0.000E+00	0.000E+00
14	1	289.10	7.234E+00	1.343E+06	4.433E+06	3.615E+06	0.000E+00	0.000E+00
14	1	291.70	6.074E+00	1.113E+06	3.675E+06	2.996E+06	0.000E+00	0.000E+00
14	1	294.30	5.120E+00	9.065E+05	2.994E+06	2.440E+06	0.000E+00	0.000E+00
14	1	296.90	4.302E+00	7.288E+05	2.408E+06	1.962E+06	0.000E+00	0.000E+00
14	1	299.66	3.556E+00	5.713E+05	1.889E+06	1.538E+06	0.000E+00	0.000E+00
14	1	302.58	2.860E+00	4.355E+05	1.441E+06	1.172E+06	0.000E+00	0.000E+00
14	1	305.50	2.294E+00	3.304E+05	1.093E+06	8.892E+05	0.000E+00	0.000E+00
14	1	308.42	1.845E+00	2.487E+05	8.237E+05	6.695E+05	0.000E+00	0.000E+00
14	1	311.34	1.428E+00	2.266E+05	7.426E+05	6.106E+05	0.000E+00	0.000E+00

Fig. A.4 Axial activities from ACTIV for JPDR Case B at PV liner

			Nontrivial Activities (Bq/g)					
Zone #	matl #	location	mn 54	fe 55	co 60	ni 63	eu152	eu154
15	2	2.60	3.341E-05	1.824E+01	7.570E+01	4.955E+01	0.000E+00	0.000E+00
15	2	7.80	4.546E-05	4.340E+01	1.750E+02	1.190E+02	0.000E+00	0.000E+00
15	2	13.00	5.632E-05	6.023E+01	2.389E+02	1.656E+02	0.000E+00	0.000E+00
15	2	18.20	6.898E-05	7.423E+01	2.918E+02	2.043E+02	0.000E+00	0.000E+00
15	2	23.05	8.112E-05	8.637E+01	3.393E+02	2.378E+02	0.000E+00	0.000E+00
15	2	27.55	9.571E-05	9.989E+01	3.917E+02	2.750E+02	0.000E+00	0.000E+00
15	2	32.05	1.160E-04	1.167E+02	4.566E+02	3.213E+02	0.000E+00	0.000E+00
15	2	36.55	1.434E-04	1.325E+02	5.233E+02	3.645E+02	0.000E+00	0.000E+00
15	2	41.05	1.817E-04	1.270E+02	5.369E+02	3.462E+02	0.000E+00	0.000E+00
15	2	43.80	2.188E-04	1.220E+02	5.431E+02	3.298E+02	0.000E+00	0.000E+00
15	2	45.88	2.493E-04	1.470E+02	6.290E+02	4.000E+02	0.000E+00	0.000E+00
15	2	49.05	2.987E-04	2.026E+02	8.090E+02	5.569E+02	0.000E+00	0.000E+00
15	2	52.22	3.697E-04	2.334E+02	9.242E+02	6.422E+02	0.000E+00	0.000E+00
15	2	54.30	4.486E-04	2.626E+02	1.024E+03	7.240E+02	0.000E+00	0.000E+00
15	2	56.55	5.428E-04	2.698E+02	1.070E+03	7.424E+02	0.000E+00	0.000E+00
15	2	60.05	6.779E-04	3.220E+02	1.257E+03	8.882E+02	0.000E+00	0.000E+00
15	2	63.55	9.496E-04	3.436E+02	1.362E+03	9.458E+02	0.000E+00	0.000E+00
15	2	67.05	1.218E-03	4.150E+02	1.610E+03	1.145E+03	0.000E+00	0.000E+00
15	2	70.42	1.690E-03	4.377E+02	1.723E+03	1.206E+03	0.000E+00	0.000E+00
15	2	73.67	2.295E-03	5.333E+02	2.045E+03	1.474E+03	0.000E+00	0.000E+00
15	2	76.92	2.994E-03	5.592E+02	2.176E+03	1.543E+03	0.000E+00	0.000E+00
15	2	80.17	4.190E-03	7.007E+02	2.642E+03	1.941E+03	0.000E+00	0.000E+00
15	2	83.42	5.865E-03	7.422E+02	2.834E+03	2.052E+03	0.000E+00	0.000E+00
15	2	86.67	8.232E-03	9.589E+02	3.538E+03	2.662E+03	0.000E+00	0.000E+00
15	2	89.92	1.104E-02	1.036E+03	3.857E+03	2.872E+03	0.000E+00	0.000E+00
15	2	93.17	1.690E-02	1.377E+03	4.958E+03	3.834E+03	0.000E+00	0.000E+00
15	2	96.42	1.981E-02	1.524E+03	5.520E+03	4.239E+03	0.000E+00	0.000E+00
15	2	99.67	2.926E-02	2.072E+03	7.281E+03	5.787E+03	0.000E+00	0.000E+00
15	2	102.83	3.793E-02	2.333E+03	8.237E+03	6.512E+03	0.000E+00	0.000E+00
15	2	105.89	5.245E-02	3.156E+03	1.086E+04	8.833E+03	0.000E+00	0.000E+00
15	2	108.95	6.035E-02	3.593E+03	1.241E+04	1.005E+04	0.000E+00	0.000E+00
15	2	112.01	8.341E-02	4.767E+03	1.616E+04	1.337E+04	0.000E+00	0.000E+00
15	2	115.07	9.949E-02	5.516E+03	1.872E+04	1.547E+04	0.000E+00	0.000E+00
15	2	117.85	1.226E-01	6.935E+03	2.329E+04	1.947E+04	0.000E+00	0.000E+00
15	2	120.35	1.441E-01	7.898E+03	2.654E+04	2.217E+04	0.000E+00	0.000E+00
15	2	122.95	1.676E-01	9.533E+03	3.180E+04	2.678E+04	0.000E+00	0.000E+00
15	2	125.65	1.932E-01	1.107E+04	3.681E+04	3.111E+04	0.000E+00	0.000E+00
15	2	128.35	2.261E-01	1.333E+04	4.407E+04	3.750E+04	0.000E+00	0.000E+00
15	2	131.05	2.570E-01	1.532E+04	5.048E+04	4.311E+04	0.000E+00	0.000E+00
15	2	133.85	3.065E-01	1.803E+04	5.919E+04	5.075E+04	0.000E+00	0.000E+00
15	2	136.75	3.438E-01	2.074E+04	6.789E+04	5.841E+04	0.000E+00	0.000E+00
15	2	139.65	3.980E-01	2.409E+04	7.862E+04	6.786E+04	0.000E+00	0.000E+00
15	2	142.63	4.388E-01	2.752E+04	8.948E+04	7.755E+04	0.000E+00	0.000E+00
15	2	145.68	4.851E-01	3.134E+04	1.017E+05	8.832E+04	0.000E+00	0.000E+00
15	2	148.74	5.475E-01	3.491E+04	1.131E+05	9.842E+04	0.000E+00	0.000E+00
15	2	151.80	6.126E-01	3.872E+04	1.254E+05	1.092E+05	0.000E+00	0.000E+00
15	2	154.85	6.748E-01	4.246E+04	1.373E+05	1.197E+05	0.000E+00	0.000E+00
15	2	157.91	7.211E-01	4.598E+04	1.486E+05	1.296E+05	0.000E+00	0.000E+00
15	2	160.97	7.654E-01	4.957E+04	1.602E+05	1.398E+05	0.000E+00	0.000E+00
15	2	164.02	8.252E-01	5.303E+04	1.712E+05	1.495E+05	0.000E+00	0.000E+00
15	2	167.08	8.937E-01	5.622E+04	1.816E+05	1.585E+05	0.000E+00	0.000E+00
15	2	170.13	9.361E-01	5.947E+04	1.920E+05	1.677E+05	0.000E+00	0.000E+00
15	2	173.19	9.700E-01	6.249E+04	2.017E+05	1.762E+05	0.000E+00	0.000E+00
15	2	176.25	1.020E+00	6.545E+04	2.112E+05	1.846E+05	0.000E+00	0.000E+00
15	2	179.30	1.067E+00	6.827E+04	2.203E+05	1.925E+05	0.000E+00	0.000E+00
15	2	182.36	1.103E+00	7.092E+04	2.289E+05	2.000E+05	0.000E+00	0.000E+00
15	2	185.42	1.153E+00	7.345E+04	2.369E+05	2.072E+05	0.000E+00	0.000E+00
15	2	188.47	1.173E+00	7.574E+04	2.443E+05	2.136E+05	0.000E+00	0.000E+00
15	2	191.53	1.218E+00	7.797E+04	2.513E+05	2.199E+05	0.000E+00	0.000E+00
15	2	194.58	1.236E+00	7.986E+04	2.575E+05	2.252E+05	0.000E+00	0.000E+00
15	2	197.64	1.265E+00	8.159E+04	2.630E+05	2.301E+05	0.000E+00	0.000E+00
15	2	200.70	1.288E+00	8.308E+04	2.679E+05	2.343E+05	0.000E+00	0.000E+00
15	2	203.75	1.307E+00	8.434E+04	2.718E+05	2.379E+05	0.000E+00	0.000E+00
15	2	206.81	1.331E+00	8.538E+04	2.753E+05	2.408E+05	0.000E+00	0.000E+00
15	2	209.87	1.344E+00	8.619E+04	2.778E+05	2.431E+05	0.000E+00	0.000E+00
15	2	212.92	1.352E+00	8.682E+04	2.798E+05	2.449E+05	0.000E+00	0.000E+00
15	2	215.98	1.358E+00	8.722E+04	2.811E+05	2.460E+05	0.000E+00	0.000E+00
15	2	219.03	1.357E+00	8.748E+04	2.819E+05	2.468E+05	0.000E+00	0.000E+00
15	2	222.09	1.358E+00	8.751E+04	2.821E+05	2.468E+05	0.000E+00	0.000E+00
15	2	225.15	1.351E+00	8.740E+04	2.817E+05	2.465E+05	0.000E+00	0.000E+00
15	2	228.20	1.352E+00	8.702E+04	2.805E+05	2.454E+05	0.000E+00	0.000E+00
15	2	231.26	1.343E+00	8.650E+04	2.787E+05	2.440E+05	0.000E+00	0.000E+00
15	2	234.32	1.325E+00	8.567E+04	2.761E+05	2.416E+05	0.000E+00	0.000E+00
15	2	237.37	1.313E+00	8.468E+04	2.727E+05	2.389E+05	0.000E+00	0.000E+00

15	2	240.43	1.275E+00	8.345E+04	2.689E+05	2.354E+05	0.000E+00	0.000E+00
15	2	243.48	1.267E+00	8.195E+04	2.639E+05	2.312E+05	0.000E+00	0.000E+00
15	2	246.54	1.221E+00	8.014E+04	2.582E+05	2.261E+05	0.000E+00	0.000E+00
15	2	249.60	1.200E+00	7.812E+04	2.516E+05	2.204E+05	0.000E+00	0.000E+00
15	2	252.65	1.161E+00	7.576E+04	2.440E+05	2.137E+05	0.000E+00	0.000E+00
15	2	255.71	1.115E+00	7.313E+04	2.356E+05	2.063E+05	0.000E+00	0.000E+00
15	2	258.77	1.087E+00	7.025E+04	2.263E+05	1.982E+05	0.000E+00	0.000E+00
15	2	261.82	1.038E+00	6.698E+04	2.158E+05	1.889E+05	0.000E+00	0.000E+00
15	2	264.88	9.644E-01	6.359E+04	2.049E+05	1.794E+05	0.000E+00	0.000E+00
15	2	267.93	9.023E-01	5.982E+04	1.928E+05	1.687E+05	0.000E+00	0.000E+00
15	2	270.99	8.554E-01	5.568E+04	1.796E+05	1.570E+05	0.000E+00	0.000E+00
15	2	274.05	8.061E-01	5.150E+04	1.662E+05	1.452E+05	0.000E+00	0.000E+00
15	2	277.10	7.331E-01	4.702E+04	1.519E+05	1.326E+05	0.000E+00	0.000E+00
15	2	280.16	6.595E-01	4.261E+04	1.378E+05	1.201E+05	0.000E+00	0.000E+00
15	2	283.22	5.885E-01	3.829E+04	1.240E+05	1.079E+05	0.000E+00	0.000E+00
15	2	286.27	5.336E-01	3.376E+04	1.095E+05	9.515E+04	0.000E+00	0.000E+00
15	2	289.10	4.890E-01	2.987E+04	9.719E+04	8.416E+04	0.000E+00	0.000E+00
15	2	291.70	4.310E-01	2.621E+04	8.551E+04	7.381E+04	0.000E+00	0.000E+00
15	2	294.30	3.897E-01	2.309E+04	7.555E+04	6.500E+04	0.000E+00	0.000E+00
15	2	296.90	3.348E-01	1.992E+04	6.540E+04	5.607E+04	0.000E+00	0.000E+00
15		299.66	2.953E-01	1.735E+04	5.712E+04	4.882E+04	0.000E+00	0.000E+00
15		302.58	2.490E-01	1.447E+04	4.784E+04	4.069E+04	0.000E+00	0.000E+00
15		305.50	2.178E-01	1.237E+04	4.106E+04	3.477E+04	0.000E+00	0.000E+00
15		308.42	1.832E-01	1.019E+04	3.400E+04	2.861E+04	0.000E+00	0.000E+00
15		311.34	1.571E-01	8.748E+03	2.928E+04	2.457E+04	0.000E+00	0.000E+00
15		314.35	1.287E-01	7.158E+03	2.408E+04	2.009E+04	0.000E+00	0.000E+00
15		317.45	1.087E-01	6.112E+03	2.062E+04	1.715E+04	0.000E+00	0.000E+00
15		320.55	8.492E-02	4.865E+03	1.659E+04	1.363E+04	0.000E+00	0.000E+00
15		323.65	7.443E-02	4.251E+03	1.450E+04	1.191E+04	0.000E+00	0.000E+00
15		326.75	5.812E-02	3.381E+03	1.169E+04	9.460E+03	0.000E+00	0.000E+00
15		329.85	4.897E-02	3.029E+03	1.045E+04	8.478E+03	0.000E+00	0.000E+00
15		332.95	3.832E-02	2.388E+03	8.384E+03	6.670E+03	0.000E+00	0.000E+00
15		336.05	3.375E-02	2.194E+03	7.658E+03	6.130E+03	0.000E+00	0.000E+00
15		339.15	2.581E-02	1.713E+03	6.122E+03	4.773E+03	0.000E+00	0.000E+00
15		342.25	2.225E-02	1.606E+03	5.691E+03	4.482E+03	0.000E+00	0.000E+00
15		346.25	1.621E-02	1.167E+03	4.290E+03	3.242E+03	0.000E+00	0.000E+00
15		351.15	1.332E-02	1.084E+03	3.931E+03	3.017E+03	0.000E+00	0.000E+00
15	2	356.04	9.058E-03	7.863E+02	2.961E+03	2.178E+03	0.000E+00	0.000E+00
15	2	360.94	6.684E-03	7.563E+02	2.792E+03	2.101E+03	0.000E+00	0.000E+00
15	2	365.84	4.797E-03	5.569E+02	2.142E+03	1.539E+03	0.000E+00	0.000E+00
15	2	370.73	3.521E-03	5.457E+02	2.050E+03	1.513E+03	0.000E+00	0.000E+00
15	2	375.63	2.622E-03	4.118E+02	1.611E+03	1.136E+03	0.000E+00	0.000E+00
15	2	380.53	1.919E-03	4.066E+02	1.548E+03	1.126E+03	0.000E+00	0.000E+00
15	2	385.43	1.210E-03	3.106E+02	1.231E+03	8.553E+02	0.000E+00	0.000E+00
15	2	390.32	1.159E-03	3.056E+02	1.175E+03	8.450E+02	0.000E+00	0.000E+00
15	2	395.22	7.599E-04	2.299E+02	9.207E+02	6.321E+02	0.000E+00	0.000E+00
15	2	400.12	6.470E-04	2.127E+02	8.297E+02	5.868E+02	0.000E+00	0.000E+00
15		405.01	4.722E-04	1.302E+02	5.392E+02	3.559E+02	0.000E+00	0.000E+00
		409.91	3.519E-04	6.528E+01	2.627E+02	1.783E+02	0.000E+00	0.000E+00

THE CODE SYSTEM *COROUT*: RADIOACTIVE INVENTORY CALCULATIONS FOR DECOMMISSIONING STUDIES

A.A.RIMSKI-KORSAKOV, A.S.ROSCHIN, S.G.YAVSHITS
V.G.Khlopin Radium Institute, St.-Petersburg, Russia

INTRODUCTION

The code system COROUT is devoted to the evaluation of nuclear reactor out-of-core radioactive inventory for the sake of the nuclear power plant decommissioning problem. The code includes calculations of the neutron flux distributions and activation kinetics in the consistent way. Only thermal neutrons are taken into consideration in the present code version. Code is divided into three steps. The first step prepares the necessary data file containing data on reactor geometry, core flux, reactor operational history and data on elements in the out-of-core zones. The main part of calculations are performed during the second step. Here the thermal neutron flux distribution in the out-of-core area is calculated for two-dimensional cylindrical geometry and the system of gain-loss equations of the activation kinetics is solved for the elements in the different out-of-core shells. The Vladimirov's method of iterations on the spatial grid is used for the neutron flux calculations. The kinetic equations are solved by the operational method. The change of neutron field due to activation during reactor campaign is taken into account. The third part of COROUT code system allows to prepare plots of flux and activity distribution for different shells. All steps could be initiated independently using the results stored at the previous steps. The code is destined for the personal computers and has been written on the base of 32-bit FORTRAN language for IBM PC.

CALCULATION OF THERMAL FLUX DISTRIBUTION FOR THE AXIALLY SYMMETRIC SYSTEMS

The neutron flux distribution is calculated by means of numeric solution of the one-group 2-dimensional neutron transport equation. Under the condition of the isotropic neutron scattering which is approximately valid for thermal neutron case the transport equation is as follows:

$$\sqrt{1-\gamma^2}\left(\mu\frac{\partial\varphi}{\partial z}+\frac{1-\mu^2}{r}\frac{\partial\varphi}{\partial z}\right)+\gamma\frac{\partial\varphi}{\partial z}+\Sigma\varphi=\frac{1}{4\pi}\left(\Sigma_s\Phi+f\right) \qquad (1)$$

with initial condition $\varphi = 0$ at the external surface of reactor volume in question.

Here μ and γ are the direction cosines of neutron velocity, r and z are the cylindrical coordinates, $\Sigma_s(r,z)$ and $\Sigma(r,z)$ are the effective thermal macro cross-sections of elastic scattering and total (absorption + scattering) cross-section, correspondingly,

$$\Sigma(r,z) = \sum_{i=1}^{N_k} \left(\sigma^i_{abs} + \sigma^i_{el}\right) x_i(r,z), \quad \Sigma_s(r,z) = \sum_{i=1}^{N_k} \sigma^i_{el} x_i(r,z), \tag{2}$$

where $\sigma_{abs,el}$ are the values of absorption and elastic scattering of thermal neutrons, $x_i(r,z)$ is the atomic density of element i in the zone k, and N_k is the number of elements in the zone. The thermal neutron source f is the internal source localized in the core volume. The source flux value is considered as an external parameter and it has to be defined in input parameters. The flux Φ is obtained by the integration over the neutron velocity directions,

$$\Phi(r,z) = 4\int_0^1 d\gamma' \int_{-1}^{1} \frac{\varphi(r,z,\gamma',\mu')}{\sqrt{1-\mu'^2}} d\mu'. \tag{3}$$

According to Vladimirov [1] one can replace the variables r and μ by new variables x and y,

$$x = r\mu,$$
$$y = r\sqrt{\frac{1-\mu^2}{1-\gamma^2}}. \tag{4}$$

Then the equation (1) transforms to the equation as in the spherical case and the resulting 1-dimensional integro-differential equation can be solved by the iterations starting from some initial approximation for flux Φ (iterations over the number of neutron collisions with nuclei). Because the distance between neighboring nodes of the spatial grid must be less then the neutron free path length in the matter $\lambda = \Sigma^{-1}$, the necessary number of nodes is rather large (typically about 500×500 nodes are used). The convergence of iteration scheme is sufficiently high and it takes about 30-50 iterations to reach the accuracy less 1 %.

KINETICS OF RADIONUCLIDE TRANSFORMATION

The kinetics of radionuclide transformation in the zone k is described by the system of equations

$$\frac{dx_i(r,z,t)}{dt} = \sum_{j=1}^{N_k} A_{ij}(r,z,t) x_j(r,z,t) - A_i(r,z,t) x_i(r,z,t), \quad i = 1, \ldots, N_k \tag{5}$$

where the reaction rats A have the form: $A_{ij} = \lambda_{ij} + \sigma_{ij}^{abs}\Phi$, $A_i = \sum_{j=1}^{N_k} A_{ij}$, λ_{ij} is the rate of transformation of nuclide j to nuclide i due to radioactive decay and $\sigma\Phi$ is the rate due to neutron absorption. Using Laplace transformation the equations (5) can be solved in the analytical form,

$$x_i = \sum_{j \le i} c_{ji} e^{-A_j t}, \tag{6}$$

where coefficients can be found from recurrent expressions

$$\begin{aligned} c_{ji} &= \frac{i}{A_i - A_j} \sum_{k=j}^{i-1} A_{ki} c_{jk}, \quad i \neq j \\ c_{ii} &= x_i^0 - \sum_{k=1}^{i-1} c_{ki}, \qquad x_i^0 = x_i(t=0) \end{aligned} \tag{7}$$

These equations allow to define all coefficients starting from c_{11}. The method of solution (6), (7) is more preferable than numeric methods because in the eq. (5) the problem of equations rigidity may arise.

BENCHMARK CALCULATIONS

The benchmark calculations of radioactive inventory were performed for the Japan Power Demonstration Reactor (JPDR) of the Japan Atomic Energy Research Institute where the detailed information on the radionuclide distribution in the out-of-core reactor components and biological concrete shield is available [2]. The two-dimensional cylindrical geometry was chosen for the JPDR configuration. In order to diminish the calculation consumption the external boundary condition of (1) was transformed to the internal one. The 1-dimensional flux calculations has been performed in the vertical and horizontal reactor midplane which were used further as a boundary conditions for the 2-dimensional flux calculations. The JPDR model used in calculations is shown in Fig. 1.

No efforts have been performed in this version for the calculation of core region. The core was observed as a source of thermal neutrons with radial and axial flux variation over the core boundaries taken from Ref. 2. The maximal flux value of source was chosen equal 10^{12} n/cm²sec.

The total JPDR operational history has been taken into account and the following relation between reactor power and neutron flux was used: $\Phi = 4.2\ P$, where Φ is thermal neutron flux in 10^{12} n/cm²sec and P is the thermal power in MW.

The thermal cross-sections data were obtained from ENDF/B-VI file. The cross-sections values used in the calculations of both neutron transport and activation are presented in Table 1. The initial parent concentration in Table 2 were taken from Table A.2. of ref. 2.

Table 1. Thermal cross-sections used

Element	Elastic Cross Section (n,n), barn	Capture Cross Section (n,γ), barn
1-H	0.30153E+02	0.33231E+00
14-N	0.10316E+02	0.75064E-01
15-N	0.47487E+01	0.24281E-04
16-O	0.40145E+01	0.19021E-03
17-O	0.38513E+01	0.38330E-02
52-Cr	0.29913E+01	0.76392E+00
53-Cr	0.78540E+01	0.18236E+02
55-Mn	0.17682E+01	0.13313E+02
54-Fe	0.21920E+01	0.25928E+01
56-Fe	0.12199E+02	0.25930E+01
57-Fe	0.66795E+00	0.24887E+01
58-Fe	0.21999E+01	0.12749E+01
59-Co	0.60076E+01	0.37226E+02
58-Ni	0.25034E+02	0.46244E+01
59-Ni	0.23557E+01	0.80818E+02
151-Eu	0.33916E+01	0.91765E+04
152-Eu	0.53613E+01	0.23099E+04
153-Eu	0.67780E+01	0.29995E+03
155-Eu	0.35198E+01	0.36416E+04

Inventory in Core Shroud and Reactor Vessel

The results of our calculations for the vertical distributions of ^{60}Co and ^{55}Fe activities at the inner surface of shroud (79.0 cm) are presented in Fig. 2 in comparison with the measured data. The same comparison for the vertical (radius 103.7 cm) and radial (h=55 cm from core midplane) distribution of ^{60}Co activity in the reactor vessel are shown in Figs. 3 and 4. As it can be seen from this comparison rather good agreement between calculated and measured data takes place.

Inventory in the Biological Concrete Shield

The radial activity distribution of ^{60}Co at the height= 55 cm from core midplane in the biological shield is presented in Fig. 5. The profile of the vertical activity for the case of ^{152}Eu at the inner surface of the concrete shield (136.3 cm) is shown in Fig. 6. The significant discrepancy between the calculations (solid line in the figures) and measurements (dotes) is observed for the shielding region, the errors reaches up to 100% on the end of shield.

DISCUSSION OF RESULTS

Our results show that the description of radioactive inventory distributions within the reactor shroud and pressure vessel may be obtained with the errors less then 30 % , the error being defined mainly by the inaccuracy in the reactor geometry model. This rather good agreement between our results and experimental data as well as results of other multigroup calculations [3,4] indicates the adequacy of used one-group approach restricted by the thermal neutron case only. Such a restriction allows us to decrease sufficiently the computation time and use the same nuclear data in both transport and activation calculations.

The discrepancies in the description of the radioactive inventory distribution in the shielding region is the common feature of all calculations where JPDR data were analysed. There are a number of reasons which can lead to this disagreement. The first one is the inaccuracy of calculation approach used, the second one can be connected with the geometrical model of reactor, and the third group is connected with chosen nuclear data and contents of elements in construction materials of reactor. The good accordance between all data obtained by different authors for the shroud and vessel region probably indicates that the main reason of disagreement in the shielding region lies in the bad definition of elements composition in the shielding concrete. One could ascribe this, for instance, to inaccurate description of rebar distribution within the concrete shield. Other factors show this clearly. Our calculations as well as results of other works show the crucial difference between results for the vertical distribution of Eu activity at the inner surface of concrete and the radial dependence of Co activity into the concrete depth. If the vertical activity is described sufficiently well then the radial distribution is quite different from the measured one and the more depth is tested the more error is observed. The estimation of total macroscopic absorption cross-section Σ_{abs} from the experimental data on the radial activity distribution in the concrete gives the value about 0.1 cm^{-1}. The value of Σ_{abs} obtained from the Table A.2 [2] is on the order of value less or with the additional account of steel construction within shielding region may be increased up to 0.05 - 0.06 cm^{-1} which is still insufficient. So, the additional analysis of material composition in the shielding region is necessary.

CONCLUSIONS

The new code system for the evaluation of radioactive inventory in the decommissioning studies is presented. The code is based on the 2-dimensional neutron flux distribution calculations for the case of thermal neutrons only which is further used in the accurate calculation of activation kinetics. The advantage of the approach is the consuming of real computation time and the using of the same nuclear data for both neutron transport and activation calculation. The detailed calculations of radioactive inventory for the case of Japan Power Demonstration Reactor were performed. The results show that as well as in other works the quite good agreement with the measured data in the reactor shroud and pressure vessel takes place. The failure in the description of

radioactive inventory in the shielding region indicates insufficient data on the element composition in the shielding concrete. The new data are necessary for the shielding region analysis.

The close accordance of our results with the results of other approaches indicates that the thermal neutron activation takes the main part in the out-of-core activation processes. For the detailed intercomparison of different codes based on different approaches it seems to be important to perform the new round of benchmark calculations for some reactor model with simplified geometry and material composition in order to exclude the errors connected with the choice of these parameters and to compare the difference on the approaches only.

References

1. G.I. Marchuk - The methods of calculations for nuclear reactors. Moskow, Atomizdat,1961.

2.T.Sukegama, et.al.- Accuracy Verification for Calculation of Inventory in JPDR Due to Neutron Activation. IAEA,INDC(JPN)-164(1993).

3. S.J.Wall, N.J.France, M.H.Dean - Current Status of decommissioning Calculations for IAEA Benchmark (JPDR) . AEA-TSD-0259 NCS/R(94)32

4. J.R.White, A.P.Fyte - Preliminary UMass-Lowell Results of the IAEA Benchmark Calculation of Radioactive Inventory for Fission Reactor Decommissioning. Paper prepared for IAEA Consultant's Meeting, IAEA, Vienna, Austria, December 5-7, 1994.

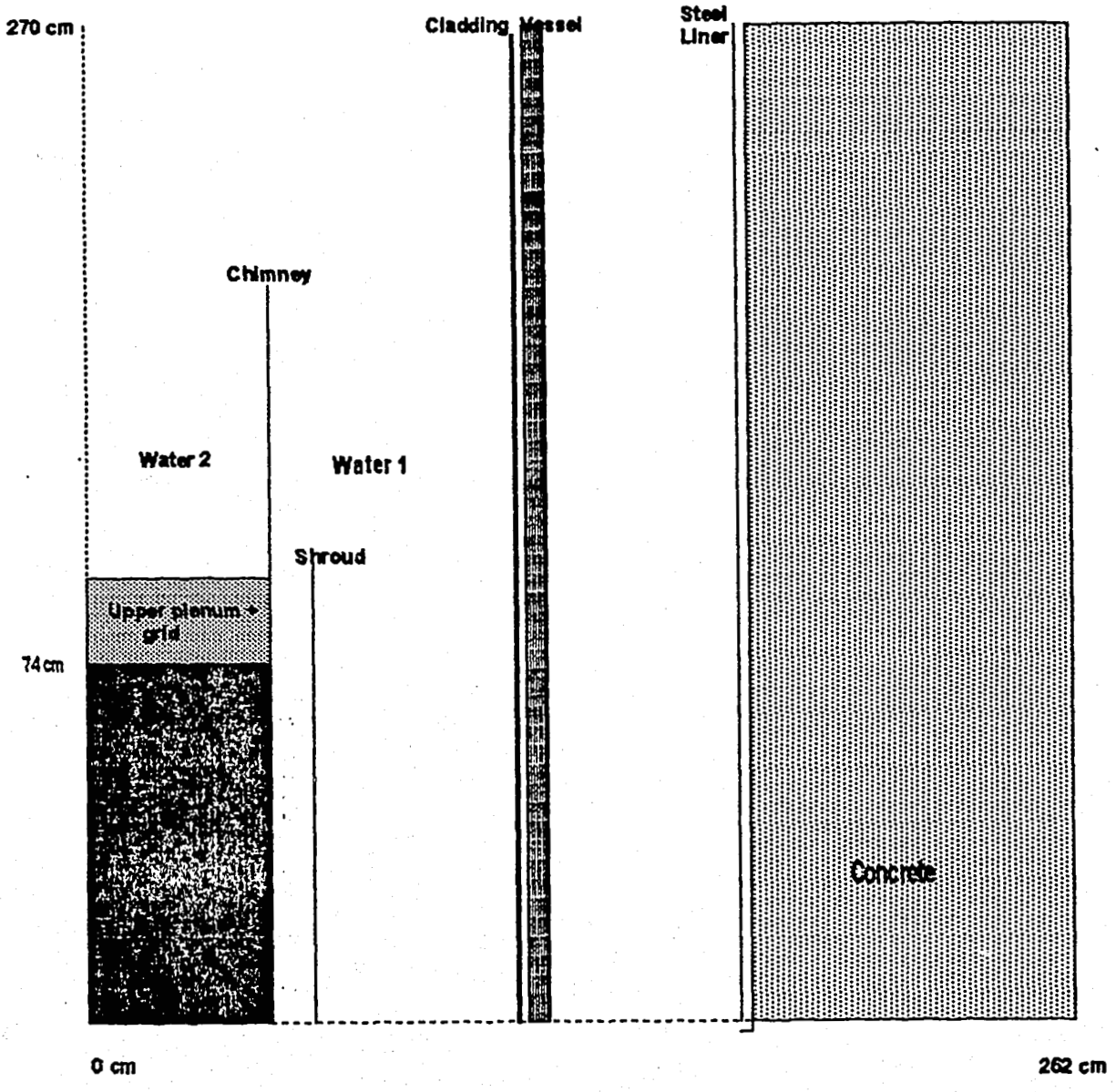

Figure 1. Two-dimensional cylindrical geometry model of JPDR beginning from core midplane level.

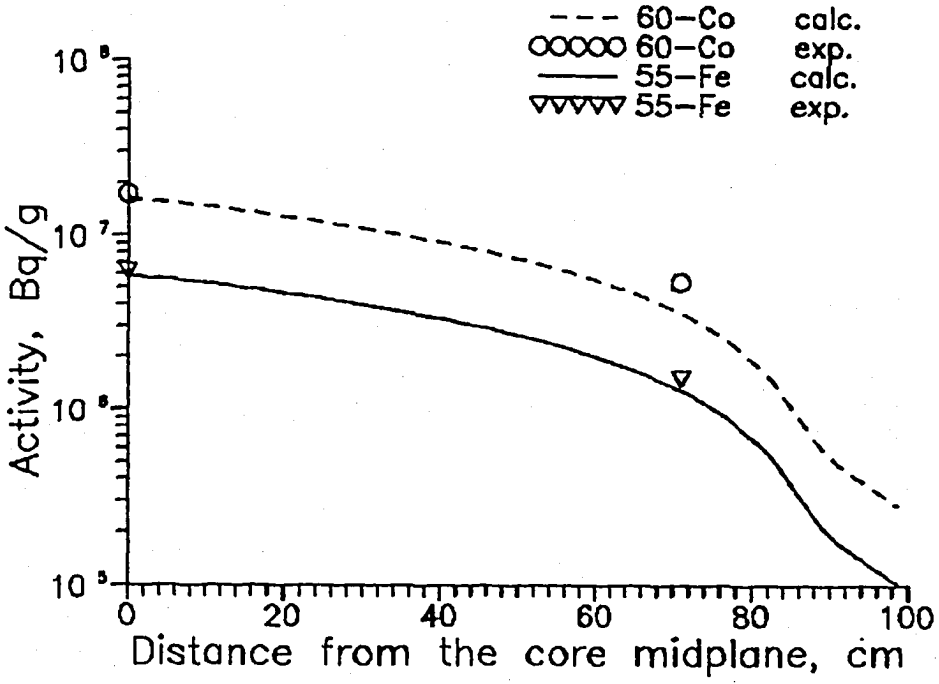

Figure 2. Vertical activity distribution of ^{60}Co and ^{55}Fe at the inner surface of shroud.

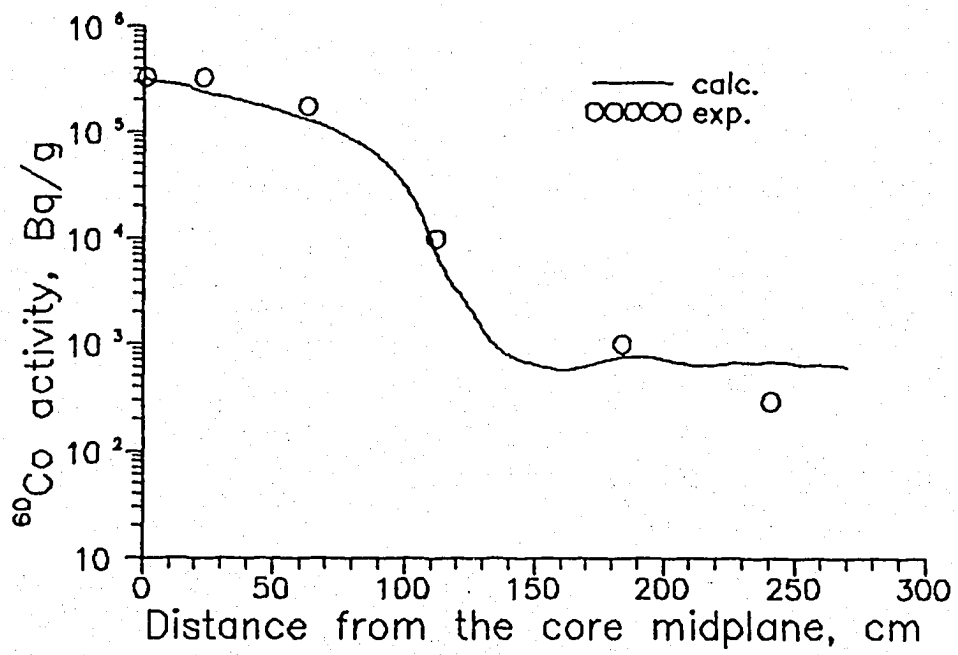

Figure 3. Vertical activity distribution of ^{60}Co at the reactor vessel.

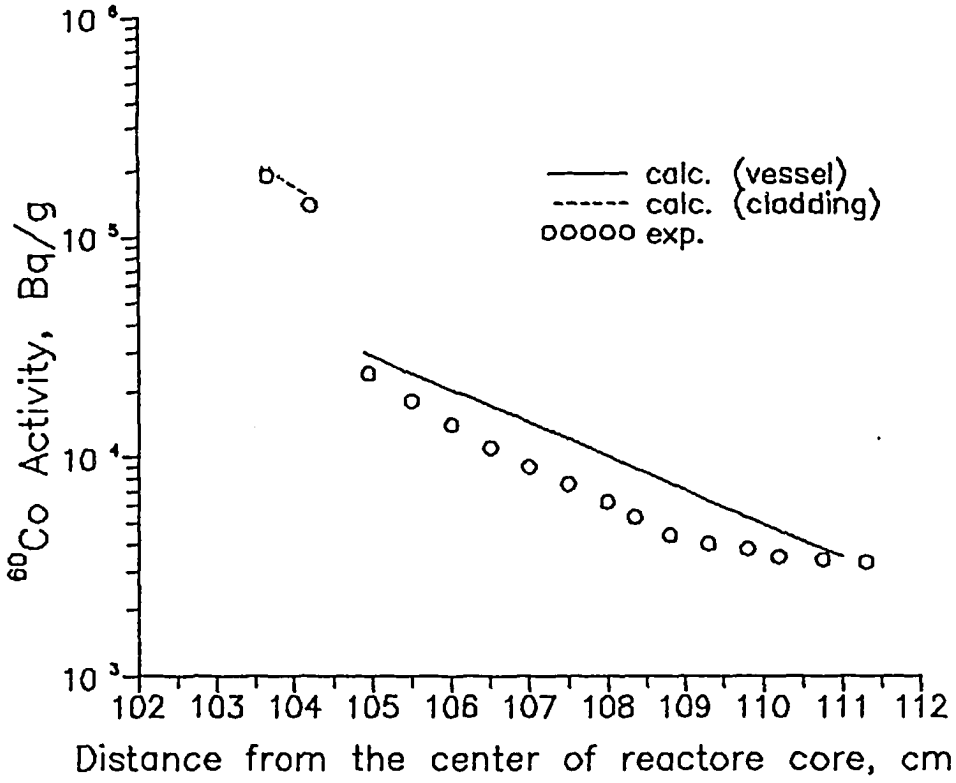

Figure 4. Radial activity distribution of ^{60}Co within the reactor vessel (inner surface at 103.7 cm).

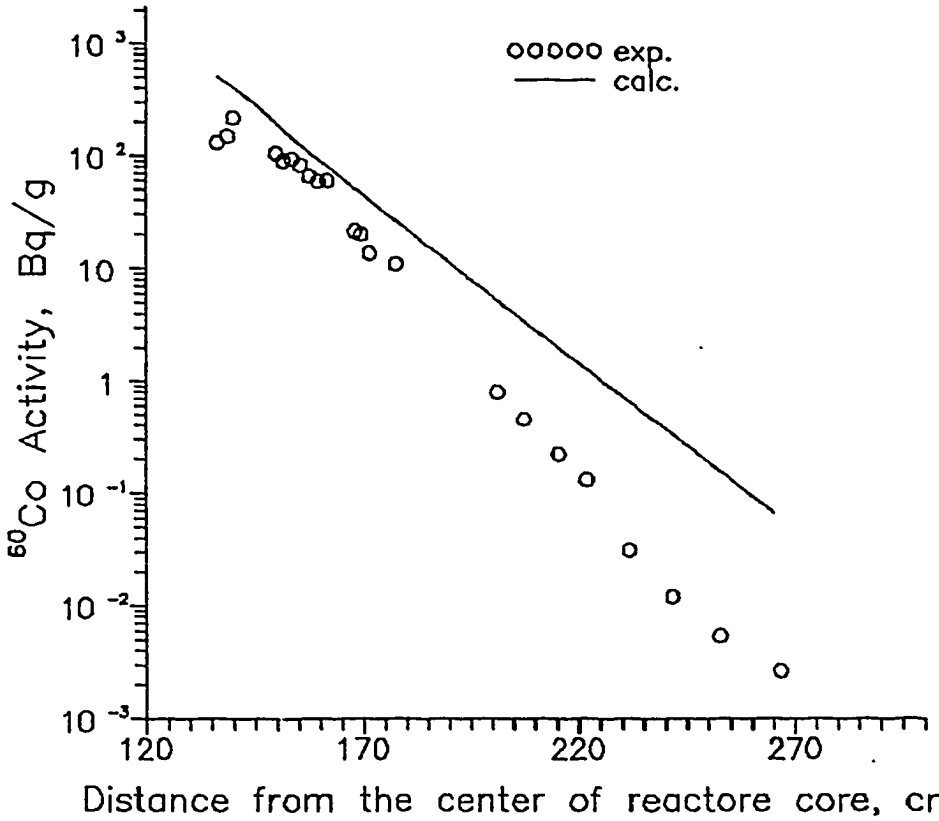

Figure 5. Radial activity distribution of ^{60}Co within the biological shield.
(inner surface at 135 cm, h=55 cm)

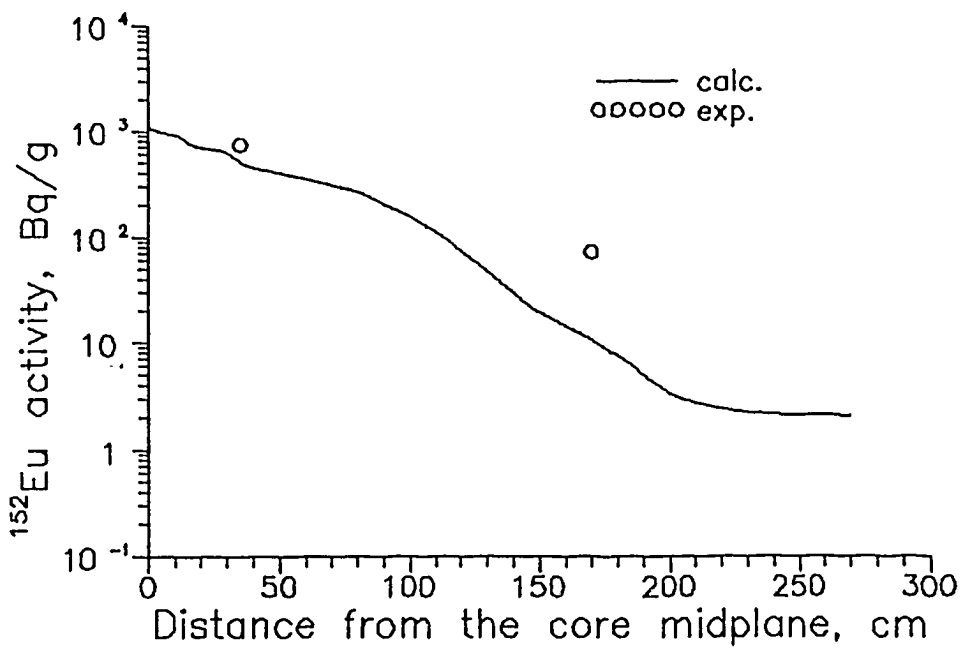

Figure 6. Vertical activity distribution of ^{152}Eu at the inner surface of biological shield.

MS. MAGRIN AVEDIKIAN
INIS.ROOM: A2418
INTERNATIONAL ATOMIC
ENERGY AGENCY
P.O.BOX 100
A-1400 VIENNA
AUSTRIA - IAEA

Nuclear Data Section
International Atomic Energy Agency
P.O. Box 100
A-1400 Vienna
Austria

e-mail, INTERNET: SERVICES@IAEAND.IAEA.OR.AT
e-mail, BITNET: RNDS@IAEA1
fax: (43-1) 20607
cable: INATOM VIENNA
telex: 1-12645 atom a
telephone: (43-1) 2060-21710

online: TELNET or FTP: IAEAND.IAEA.OR.AT
username: IAEANDS for interactive Nuclear Data Information System
username: ANONYMOUS for FTP file transfer
username: FENDL for FTP file transfer of FENDL files
for users with web-browsers: http://www.IAEA.OR.AT/programs/RI/NDS/ndsstart.htm